UNIVERSIDADE
BEIRA INTERIOR

The Influence Of Temperature In Regime Transition Boundaries For Single Droplet Impact Upon Heated Liquid Films

(Versão final após defesa)

André Filipe Serra Ferreira Mendes

Dissertação para obtenção do Grau de Mestre em
Engenharia Aeronáutica
(ciclo de estudos integrado)

Orientador: Prof. Doutor André Resende Rodrigues da Silva

abril de 2023

Declaração de Integridade

Eu, André Filipe Serra Ferreira Mendes, que abaixo assino, estudante com o número de inscrição 39455 do Curso de Engenharia Aeronáutica da Faculdade de Engenharias, declaro ter desenvolvido o presente trabalho e elaborado o presente texto em total consonância com o **Código de Integridades da Universidade da Beira Interior**.

Mais concretamente afirmo não ter incorrido em qualquer das variedades de Fraude Académica, e que aqui declaro conhecer, que em particular atendi à exigida referenciação de frases, extratos, imagens e outras formas de trabalho intelectual, e assumindo assim na íntegra as responsabilidades da autoria.

Universidade da Beira Interior, Covilhã 05 / 04 / 2023

Assinado por: **André Filipe Serra Ferreira Mendes**
Num. de Identificação: 14378814
Data: 2023.04.05 13:16:54+01'00'

Agradecimentos

Em primeiro lugar, gostaria de agradecer ao meu orientador Professor André Resende Rodrigues da Silva pela oportunidade que me deu de desenvolver este trabalho na área da propulsão. Agradeço o apoio, o conhecimento e a orientação proporcionados.

Gostaria de agradecer a oportunidade de ser membro do AEROG — Aeronautics and Astronautics Research Center, supervisionado pelo Professor Jorge Manuel Martins Barata, que sempre encorajou a investigação científica. Este trabalho não seria possível sem os recursos disponibilizados pelo AEROG. Gostaria de agradecer ao técnico de laboratório Sr. Rui Manuel Tomé Paulo que ajudou a adaptar a estrutura experimental e prestou assistência no laboratório quando necessário. Para aqueles que trabalharam ao meu lado na AEROG, gostaria de agradecer por todo o apoio e grandes momentos juntos. Entre estes amigos, destaco dois, em particular, os alunos de PhD Daniela Ribeiro e Daniel Rodrigues. Quero agradecer a ambos por toda a ajuda, orientação, amizade e paciência. Estarei eternamente em dívida com eles, e nunca esquecerei os grandes momentos que tivemos juntos.

Gostaria de agradecer aos meus amigos que fizeram parte da minha vida durante estes 5 anos. Aos meus melhores amigos, vocês estiveram sempre lá durante os altos e baixos e, por isso, estou mais do que grato. Obrigado por todos os bons momentos durante estes anos e pelos muitos que virão. Tenho de vos agradecer especialmente por terem estado ao meu lado durante este último ano, que se revelou um desafio em diferentes formas.

Por último, mas não menos importante, tenho de estar grato à minha família, pelo apoio que deram durante este tempo. Gostaria de agradecer aos meus avós por estes anos, pelas suas palavras amáveis e por sempre tentarem aprender mais sobre o meu trabalho, apesar de não o compreenderem completamente. Aos meus pais, obrigado por todo o apoio, paciência, dedicação e incentivo ao longo da minha vida académica.

Acknowledgements

Firstly, I would like to thank my supervisor Professor André Resende Rodrigues da Silva for the opportunity given to develop this work in the area of propulsion. I am grateful for the support, knowledge, and guidance apportioned.

I would like to acknowledge the opportunity to be a member of the AEROG — Aeronautics and Astronautics Research Center, overseen by Professor Jorge Manuel Martins Barata who always bolstered scientific research. This work would not be possible without the resources provided by AEROG.

I would like to thank the laboratory technician Mr Rui Manuel Tomé Paulo who helped adapt the experimental structure and provided assistance in the laboratory when needed.

For those who worked along my side in AEROG, I would like to thank you for all the support and great moments together. Between these friends, I have to highlight two, in particular, PhD students Daniela Ribeiro and Daniel Rodrigues. I want to thank both of them for all the help, guidance, friendship, and patience. I will forever be in their debt, and I will never forget the great moments we had together.

I would like to thank my friends who were a part of my life during these 5 years. To my best friends, you were always there through the ups and downs and, for that, I am more than thankful. Thank you for all the good times during these years and for the many that will come. I have to thank you especially for standing by my side during this last year, which proved to be a challenge in different ways.

Last but not least, I have to be grateful to my family, for the support that they gave during this time. I would like to thank my grandparents for these years, their kind words and for always trying to learn more about my work, even though they did not fully understand it. To my parents, thank you for all the support, patience, dedication, and encouragement throughout my academic life.

Resumo

A crescente preocupação com a taxa atual de consumo de combustíveis fósseis, as emissões poluentes e a limitação das reservas conduziu a uma busca do desenvolvimento de motores mais eficientes com emissões e consumo de combustível mais baixos. No entanto, são necessários estudos experimentais de impacto de gotas em filmes líquidos em condições semelhantes às que seriam esperadas dentro de uma câmara de combustão, ou seja, simulado o efeito de aquecimento provocado pelas paredes no filme líquido. O tema do impacto de gotas é relevante para diferentes indústrias, tais como a pintura a spray, impressão de jato de tinta, dispersão de pesticidas nas culturas, arrefecimento de superfícies quentes como dispositivos eletrónicos e pás de turbina, e claro, injeção de combustível em motores de combustão interna.

O principal objetivo desta dissertação é avaliar o efeito da temperatura do filme líquido na dinâmica do impacto de uma única gota. O estudo focou-se na avaliação da validade e aplicabilidade dos critérios atuais de splash e encapsulamento duma bolha, uma vez que estes dois fenómenos resultam numa maior atomização da mistura. Os combustíveis de aviação atuais como o Jet A-1 e o NExBTL são combustíveis multicomponente, resultando em taxas de evaporação não lineares uma vez que os diferentes fluidos que os constituem têm diferentes temperaturas de saturação. Como um passo intermédio, antes dos combustíveis multicomponentes, foram selecionados cadeias de carbono simples como N-Heptane e N-Decane.

A instalação experimental necessária foi concebida e adaptada para que a presente no laboratório satisfizesse esses requisitos. A configuração incluía uma câmara de alta velocidade, uma matriz LED, e uma bomba infusora ligada a uma agulha de cabeça plana, para conter o filme líquido um recipiente borossilicato foi usado e para aquecer o filme líquido um bloco de alumínio com resistência de aquecimento embutidas.

As experiências foram realizadas em diferentes alturas, a fim de avaliar o efeito da temperatura em torno dos limites selecionados. Ambos os fenómenos revelaram que eram afetados pela temperatura do filme líquido. O fenómeno de encapsulamento duma bolha, para a mesma altura, revelou que ocorria para temperaturas mais elevadas, mas não à temperatura ambiente. Embora o fenómeno de splash tenha sido igualmente afetado, também demonstrou resultados interessantes perto da zona de transição, onde numa gama específica de temperatura foi detetado um efeito de supressão. Verificou-se que nenhum dos limites selecionados poderia corroborar os resultados experimentais obtidos. Utilizando estes dados, foi proposta uma adaptação à correlação de encapsulamento de bolhas, embora não fosse possível o mesmo para a correlação de splash.

Palavras-chave

Impacto De Gotas, Filmes Líquidos Aquecidos, Estudo Experimental, Encapsulamento Duma Bolha, Splash, Limite De Transição

Abstract

The growing concern with the current rate of consumption of fossil fuels, pollutant emissions and the limitations of the reserves lead to a pursuit of developing more efficient engines with lower emissions and fuel consumption. However, experimental studies of droplets impinging upon a liquid film in similar conditions that would be expected inside a combustion chamber, i.e., simulation of the heating effect by the walls on the liquid film, are required. The subject of droplet impact is relevant to different industries, such as in spray painting, inkjet printing, pesticide dispersion on crops, cooling of hot surfaces such as electronic devices and turbine blades, and of course fuel injection in internal combustion engines.

The main goal of this thesis is to evaluate the effect of the temperature of the liquid film on single droplet impact dynamics. The study was focused on assessing the validity and applicability of the current criteria for spread/splash and bubble encapsulation on account that these two phenomena result in greater atomisation of the mixture. The current aviation fuels such as Jet A-1 and NExBTL are multi-component substances, resulting in non-linear evaporation rates since the different fluids that constitute them have different saturation temperatures. As an intermediate step, before the multi-components fuels, simple carbon chains equivalents like N-Heptane and N-Decane were selected.

The experimental facility necessary was designed and adapted for the one present in the laboratory to comply with such requirements. The setup included a high-speed camera, a LED array, and a syringe pump connected to a flathead needle, to hold the liquid film a borosilicate container was used and to heat the liquid film an aluminium block with embedded heating cartages.

The experiments were conducted at different heights in order to evaluate the effect of the temperature around the selected thresholds. Both phenomena revealed to be affected by the temperature of the liquid film. The phenomenon of bubble encapsulation, for the same height, revealed to happen at higher temperatures but not at room temperature. Although the phenomenon of splash revealed to be similarly affected, it also lead to interesting results near the transition zone, where in a specific range of temperature it was detected a suppressing effect. It was verified that neither of the selected thresholds could corroborate the experimental results obtained. Using this data, an adaptation to the correlation of bubble encapsulation was proposed, although, the same for the spread/splash correlation was not possible.

Keywords

Droplet Impact, Heated Liquid Film, Experimental Study, Bubble Encapsulation, Splash, Transition Threshold

Contents

List of Figures

List of Tables

Nomenclature

a	Correlation Parameter	$[-]$
D	Crown diameter	$[mm]$
$d_{cylinder}$	Cylinder diameter	$[mm]$
d_{drop}	Droplet diameter	$[mm]$
D_{in}	Needle inner diameter	$[mm]$
D_{out}	Needle outer diameter	$[mm]$
D_b	Crown base diameter	$[mm]$
D_e	Ejecta sheet diameter	$[mm]$
D_r	Crown rim diameter	$[mm]$
F_μ	Viscous forces	$[-]$
F_σ	Surface tension forces	$[N]$
F_I	Inertial forces	$[N]$
F_g	Gravitational forces	$[N]$
Fr_{drop}	Droplet Froude number	$[-]$
g	gravity	$[m/s^2]$
H	Crown height	$[mm]$
h	Liquid film thickness	$[mm]$
H^*	Non-dimensional crown height	$[-]$
h^*	Non-dimensional film thickness; Relative film thickness	$[-]$
h_1	Liquid film thickness in the impact region	$[mm]$
h_2	Liquid film thickness in the static film region	$[mm]$
h_b	Crown thickness	$[mm]$
K	Criterion between spread and splash	$[-]$
K_c	Critical threshold between spread and splash	$[-]$
L_{nd}	Non-dimensional length scale of the wall roughness	$[-]$
L_a	Length scale of the wall roughness	$[mm]$
m	Mass	$[g]$
Oh	Ohnesorge number	$[-]$
Oh_{drop}	Droplet Ohnesorge number	$[-]$
$\widetilde{Oh}_{film,drop}$	Alternative Ohnesorge number using a relation between the liquid film and droplet	$[-]$
Oh_{film}	Ohnesorge number of the liquid film	$[-]$
p	Probability of occurrence	$[-]$
P_g	Surrounding gas pressure	$[Pa]$
R_{nd}	Non-dimensional wall roughness	$[-]$
R_a	Wall roughness	$[\mu m]$

Re	Reynolds number	$[-]$
Re_{drop}	Droplet Reynolds number	$[-]$
$Re_{film,drop}$	Reynolds number using properties of the droplet and of the liquid film	$[-]$
T	Temperature	$[°C]$
t	Time	$[s]$
T_{CHF}	Critical heat flux temperature	$[°C]$
T_{drop}	Droplet temperature	$[°C]$
T_{film}	Liquid film temperature	$[°C]$
T_{Leid}	Leidenfrost temperature	$[°C]$
T_{sat}	Saturation temperature	$[°C]$
T_0	Ambient temperature	$[°C]$
T_g	Surrounding gas temperature	$[°C]$
T_w	Temperature of the surface/Temperature of the wall	$[°C]$
V	Volume	$[ml]$
v_{film}	Liquid film velocity	$[m/s]$
v^*_{film}	Unidirectional velocity	$[-]$
v_{drop}	Droplet impact velocity	$[m/s]$
v_1	Liquid film velocity in the impact region	$[m/s]$
v_2	Liquid film velocity in the static film region	$[m/s]$
v_g	Surrounding gas velocity	$[m/s]$
We	Weber number	$[-]$
We_{drop}	Droplet Weber number	$[-]$
y	Impact height	$[mm]$

Greek Symbols

α	Crown angle	$[^\circ]$
β	Cylinder-drop curvature ratio	$[-]$
μ^*	Viscosity ratio	$[-]$
μ_{drop}	Droplet viscosity	$[mPa\ s]$
μ_{film}	Liquid film viscosity	$[mPa\ s]$
μ_g	Surrounding gas viscosity	$[mPa\ s]$
ρ^*	Density ratio	$[-]$
ρ_{drop}	Droplet density	$[kg/m^3]$
ρ_{film}	Liquid film density	$[kg/m^3]$
ρ_g	Surrounding gas density	$[kg/m^3]$
σ_{drop}	Droplet surface tension	$[mN/m]$
σ_{film}	Liquid film surface tension	$[mN/m]$
τ	Non-dimensional time	$[-]$
θ	Non-dimensional temperature	$[-]$
θ_c	Critical contact angle	$[^\circ]$

List of Acronyms

CHF	Critical Heat Flux
fps	Frame Per Second
HVO	Hydroprocessed Vegetable Oil
IC	Internal Combustion
IR	Infrared
LED	Light Emitting Diode
MATLAB	MATrix LABoratory
NExBTL	Neste Renewable Diesel
PIV	Particle Image Velocimetry
POV	Point-Of-View
TC	Thermocouple

Chapter 1

Introduction

This thesis is devoted to the experimental study of the dynamic behaviour of a single droplet impinging onto a heated liquid film. This study main focus is to analyse the influence of the temperature of the liquid in single droplet impact dynamics. Considering the current pursuit for more environmentally friendly engines, the experiments were aimed at a comparison of the isothermal experiments of spread/splash and bubble encapsulation with the ones obtained with a heated liquid film. These two outcomes promote the atomisation of the mixture, and as a consequence, the reduction of pollutant emissions, therefore, becoming the focus of this study.

This first chapter is divided into three sections. The first section consists of the motivation followed by the objectives underlying this study, and finally, a summary of the work structure.

1.1 Motivation

In the last three decades, the consumption of fossil fuels has been increasing rapidly, resulting also in a rapid depletion of its reserves. Moreover, at the same time, the emissions of pollutant gases, e.g., carbon dioxide (CO_2), have grown exponentially. In an effort to avoid a critical point, the current internal combustion (IC) industry, both automotive and aerospace, pursue alternatives to fossil fuels. Finding alternatives that can replace effectively the current fuels in use is an extensive process. Thus, in the meantime, the industry evaluates ways to reduce the consumption of fossil fuels and pollutant emissions [1] while maintaining the efficiency of the engines or even trying to improve it.

The study of the physical and chemical phenomena that occur inside an engine, when the fuel mixture is injected into the combustion chamber, is not a novelty. However, assessing the dynamics of the impinging droplets while simulating the heating effect of the surface of the combustion chamber in the liquid film, remains a less studied matter at the time of writing this thesis. This experimental work has the objective of studying these effects, for that, the idea would be to use current aviation fuels, although that was not possible as will be explained later in this work.

1.2 Objectives

As previously mentioned, this work has the goal of evaluating the effects of the liquid film temperature in single droplet impact, more precisely, how it compares with the current isother-

mal results of spread/splash and bubble encapsulation. In order to achieve this a goal, a few objectives were devised for this thesis.

- Design and adapt the experimental facility to evaluate these phenomena;
- Characterization of the liquid film and posterior impact phenomena visualisation;
- Recurring to the selected criteria, evaluate how the results obtained fit previously developed correlations. If necessary and possible, with the data obtained, evaluate possible improvements to the correlations to fit the results of this work.

1.3 Work Structure

This thesis is divided into five chapters: Introduction, Literature Review, Experimental Procedure, Results and Discussion, and Conclusion and Future Work.

This first chapter contains the motivation behind the development of this work, followed by its objectives and a summary of the thesis structure.

The second chapter consists of the literature review, introducing important non-dimensional numbers used in the study of droplet impact and other relevant knowledge for this thesis regarding outcomes, transition thresholds, splash mechanism and bubble encapsulation.

The third chapter will explain the experimental procedure, and how the experimental facility was adapted and designed. Followed by the specifications of the components, the properties of the fluids, the methodology, and the methods and measurement techniques used for the experiments.

Chapter four contains the liquid film temperature results, evaporation rates of the fluids, droplet diameter, impact velocity and non-dimensional numbers. Furthermore, the outcomes that were visualised are presented, followed by the criteria and possible adaptations for the phenomena of splash and bubble encapsulation.

The last chapter is composed of the conclusion regarding the experiment work developed and future work in this subject.

Chapter 2

Literature Review

In the vast literature found, droplet impact was investigated in dry and wetted surfaces [2]. When the impact is on a dry surface [3], the surface topography can be smooth or rough [4], it can also be, heated [5], angled [6, 7], and influenced by a cross-flow [8, 6, 9, 10, 11]. When the impact is on a wetted surface, i.e., on a liquid film [12] or a deep liquid pool, the underlying surface can either be smooth or rough and as studied in this thesis, heat can also be applied to the surface [13] and consequently to the liquid film. Several criteria were created in order to prevent or help achieve certain outcomes that could be beneficial or detrimental in specific applications. This chapter will be dedicated to explaining the fundamentals of droplet impact and focused on the impact on liquid films since that is the objective of this work. This will be followed by the possible outcomes, the presence of a liquid film, crown evolution, splash mechanisms and bubble encapsulation. Closing the chapter is a small overview of the impact on heated surfaces.

2.1 Fundamentals Of Droplets Impact

When examining the different types of droplet impact, the factors that affect the dynamics of the impact are either related to the droplet parameters such as droplet diameter (d_{drop}), droplet impact velocity (v_{drop}), temperature (T_{drop}), viscosity (μ_{drop}), density (ρ_{drop}), surface tension (σ_{drop}) and the properties of the surrounding gas such as temperature (T_g), velocity (v_g), pressure (P_g), viscosity (μ_g), density (ρ_g), and flow regime. Specifically, on wetted surfaces, the liquid film parameters such as thickness (h), velocity (v_{film}), composition, temperature (T_{film}) viscosity (μ_{film}), density (ρ_{film}) and surface tension (σ_{film}) are essential to describe the dynamics of the impact. For both dry and wet surfaces (thin film), surface topography also represents a significant factor [14].

When analysing the results of the experiments, a set of non-dimensional parameters are essential to describe the relative importance of surface tension ($F_\sigma = \sigma_{drop}\, d_{drop}$), inertial ($F_I = \rho_{drop}\, v_{drop}^2\, d_{drop}^2$), viscous ($F_\mu = \mu_{drop}\, v_{drop}\, d_{drop}$) and gravitational ($F_g = g\, \rho_{drop}\, d_{drop}^3$) forces acting on the hydrodynamic structures formed after:

1. **Droplet Weber number**

$$We_{drop} = \frac{\rho_{drop}\, v_{drop}^2\, d_{drop}}{\sigma_{drop}} = \frac{\text{Inertial forces}}{\text{Surface tension forces}} \quad (2.1)$$

The Weber number represents the ratio between the inertial and the surface tension

forces. As demonstrated in equation 2.1, it is the ratio between the droplet kinetic and surface energy.

2. **Droplet Reynolds number**

$$Re_{drop} = \frac{\rho_{drop}\, v_{drop}\, d_{drop}}{\mu_{drop}} = \frac{\text{Inertial forces}}{\text{Viscous forces}} \quad (2.2)$$

The Reynolds number is the ratio between the inertial and the viscous forces.

3. **Droplet Ohnesorge number**

$$Oh_{drop} = \frac{\mu_{drop}}{\sqrt{\rho_{drop}\, \sigma_{drop}\, d_{drop}}} = \frac{\sqrt{We_{drop}}}{Re_{drop}} = \frac{\text{Viscous forces}}{\sqrt{\text{Surface tension forces} \times \text{Inertial forces}}} \quad (2.3)$$

The Ohnesorge number describes the relation between viscous, surface tension and inertial forces. It is an important factor in the characterisation of the disintegration process.

4. **Droplet Froude number**

$$Fr_{drop} = \frac{v_{drop}^2}{g\, d_{drop}} = \frac{\text{Inertial forces}}{\text{Gravitational forces}} \quad (2.4)$$

The Froude number represents the effects of gravity on the drop. This parameter will not be used during this thesis, considering that the effects of gravity can be neglected for $Fr_{drop} \geq 10^2$, as explained by Deegan et al. [15].

Besides these parameters, a dimensionless time is also introduced, equation (2.5).

$$\tau = \frac{v_{drop}\, t}{d_{drop}} \quad (2.5)$$

Although the droplet diameter and impact velocity have a great influence on the dynamics of the impact, as shown by equations (2.1), (2.2) and (2.3), the remaining parameters, such as the relative film thickness (h^*) (section2.3, cannot be undervalued.

$$h^* = \frac{h}{d_{drop}} \quad (2.6)$$

2.2 Droplet Impact Outcomes

Although the non-dimensional parameters are used to analyse and describe impacting phenomena, the remaining parameters of the liquid film and properties of the surrounding gas must also have to be taken into account, as they also play a crucial role. This section will explain the different outcomes that can be expected when a droplet impacts a dry or wetted

surface and the parameters/properties that affect them.

2.2.1 Spreading

Spread, according to Bai and Gosman [16], is when the droplet impacts with a moderate velocity onto a dry or wetted surface and spreads out to form a wall film, for a dry surface, or merges with the pre-existing liquid film, for a wetted surface. It is also referred to as deposition regime, by Rioboo et al. [17], where a drop deforms and remains attached to the surface, without any breakups, during the entire impact process (Fig. 2.1).

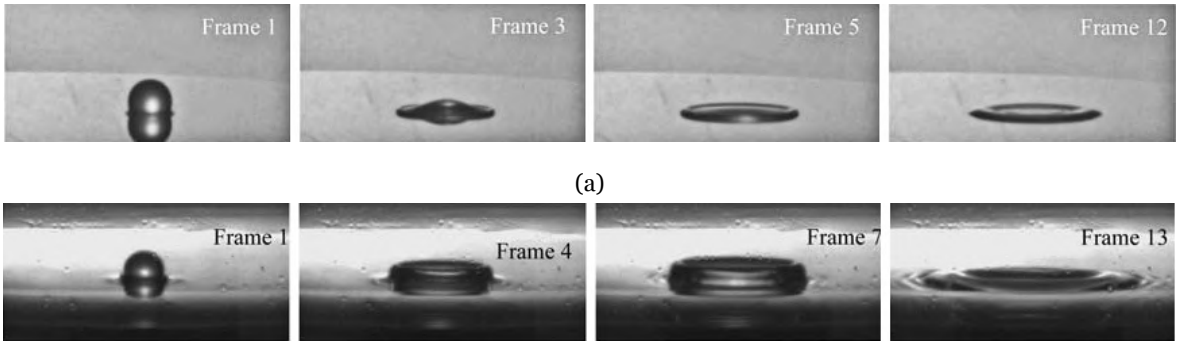

Figure 2.1: Spreading of a hexadecane droplet: (a) Smooth aluminium surface; (b) Liquid film. Adapted from Vander Wal et al. [18].

2.2.2 Prompt splash

According to Cossali et al. [19] and Liang et al. [20], on wetted surfaces, prompt splashing takes place at low Oh numbers and is associated with the ejection of droplets from the rim while the crown is still growing. They also referred that it only happens on rough surfaces, but this does not concur with the rest of the literature [18, 21]. This phenomenon can also be observed when a drop impacts a smooth surface, as shown in figure 2.2a, where Vander Wal et al. [18] impacted a hexadecane droplet on a smooth aluminium surface.

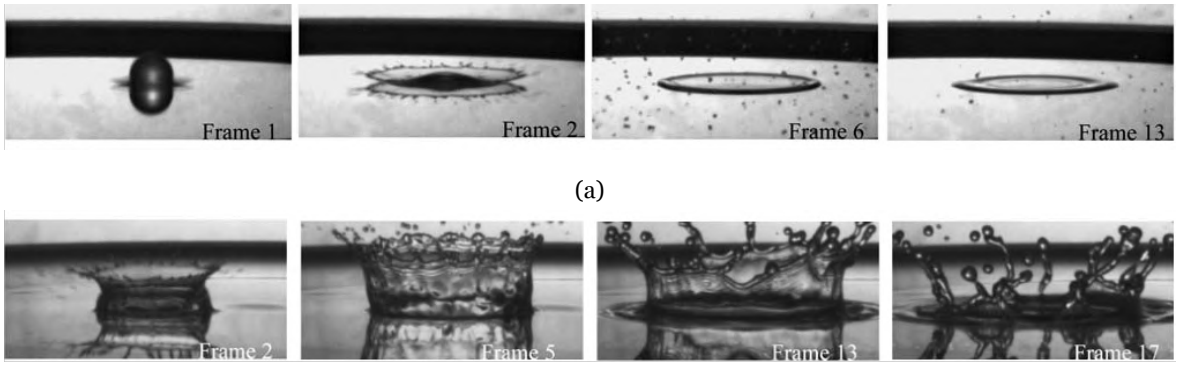

Figure 2.2: Formation of prompt splash: (a) Hexadecane droplet on a smooth aluminium surface; (b) Methanol droplet on a liquid film. Adapted from Vander Wal et al. [18].

2.2.3 Delayed splash

The delayed splash, as explained by Vander Wal et al. [18], occurs near or after the stage of maximum expansion of the crown. It is associated with the breakup of the fluid sheet forming the crown, and it is affected by both viscosity and surface tension. For Rioboo et al. [17], it is referred to as corona splash, and it is considered a characteristic of drop impacts on liquid films (Fig. 2.3).

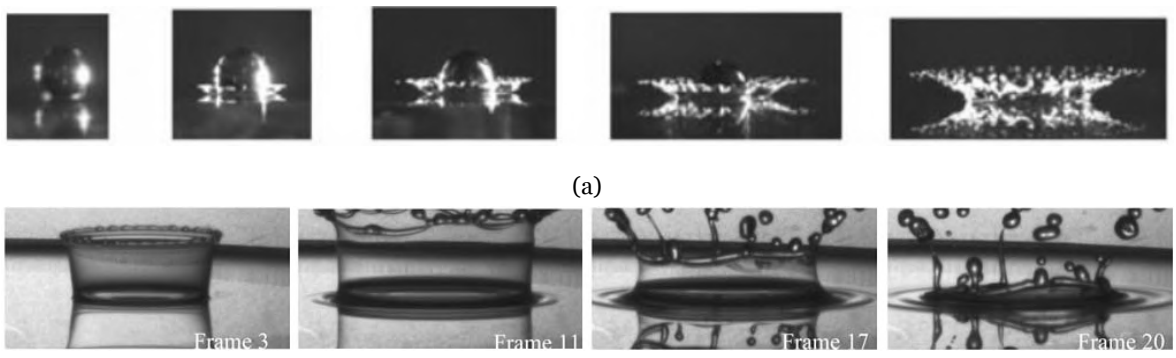

(a)

(b)

Figure 2.3: Formation of delayed splash: (a) Ethanol droplet on a smooth glass surface [17]; (b) Butanol droplet on a liquid film [18].

2.2.4 Rebound

According to Liang et al. [22], the rebound phenomenon is closely related to a low-impact Weber number. They suggested that to develop rebound, the Weber number must be between a lower and upper threshold. When the impact We is above the upper threshold, shear upon impact will damage the air pocket between the drop and the surface. For an impact We below the lower limit, the kinetic energy may not be sufficient to make the drop bounce completely from the surface (Fig. 2.4).

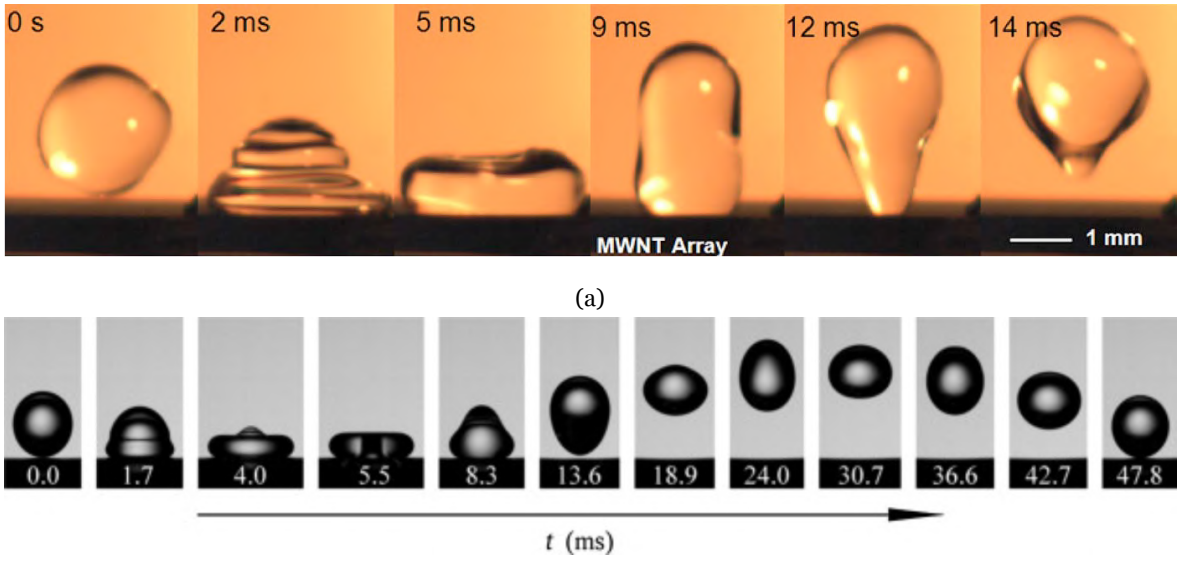

(a)

(b)

Figure 2.4: Rebound of a droplet: (a) Water on the surface of a carbon nanotube array [23]; (b) Butanol on a liquid film [22].

2.2.5 Partial rebound

Partial rebound has a principle similar to the rebound phenomenon, where the droplet rebounds, although the kinetic energy is above the upper threshold of the rebound. Since the droplet has more kinetic energy, this is enough to break the surface tension of the fluid, resulting in part of the droplet remaining stuck to the surface, either dry or wetted [24] (Fig. 2.5).

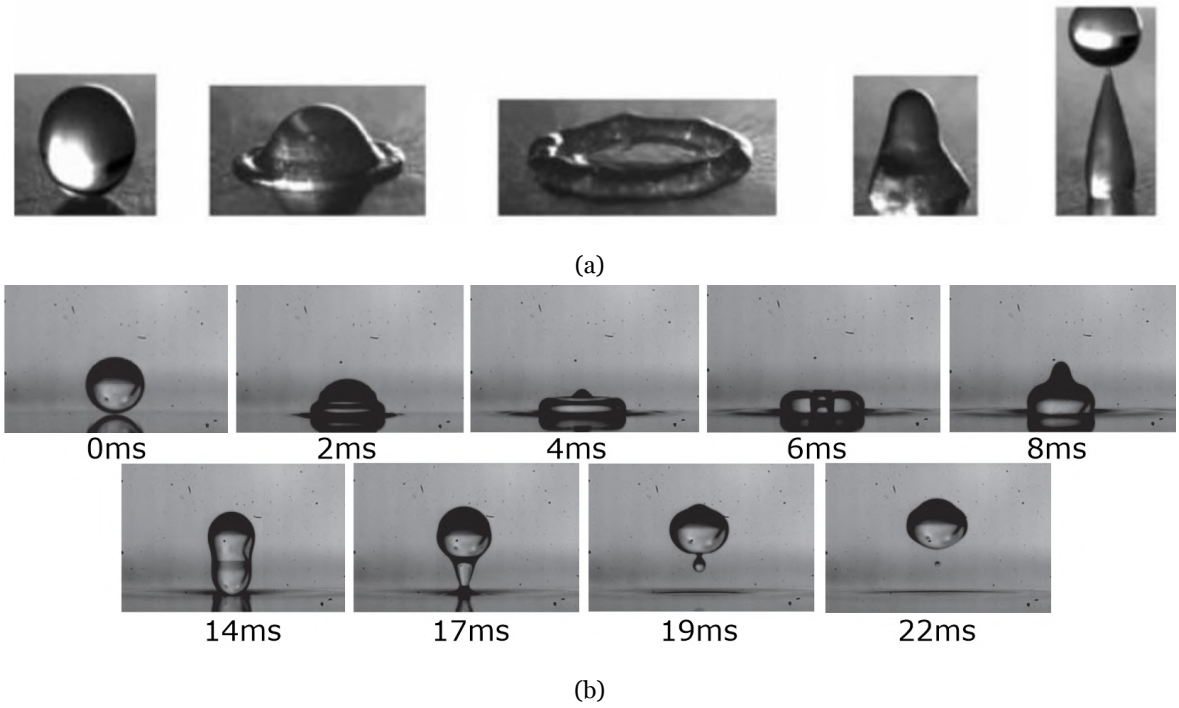

(a)

(b)

Figure 2.5: Partial rebound of a droplet: (a) Water on a rough dry surface [17]; (b) Ethanol drop on a liquid film [25].

2.2.6 Jetting

The morphology of the central jet primarily depends on the kinetic energy of the droplet and the properties of the liquid film. If the kinetic energy, expressed by We, is relatively small, the liquid viscous forces eventually dissipate it, suppressing the emergence of the central jet (Fig. 2.6a. When We increases to a moderate value, the kinetic energy is dissipated in part by the viscous forces of the liquid, but also a small remaining part is converted into a central jet (Fig. 2.6b. At high We, the energy is sufficient to make the jet rise rapidly and begins to pinch off and break up into droplets from the tip while rising (Fig. 2.6c) [26].

2.2.7 Bubble encapsulation

Bubble encapsulation is a phenomenon that can only be observed on wetted surfaces. It occurs when the crown enfolds, i.e., the crown starts to bend inwards, closing at the top and the process entraps air inside a dome shape of fluid (Fig. 2.7). According to Pan et al. [27], for thick films, the threshold for this transition occurs at $We \approx 2570$ and this value increases

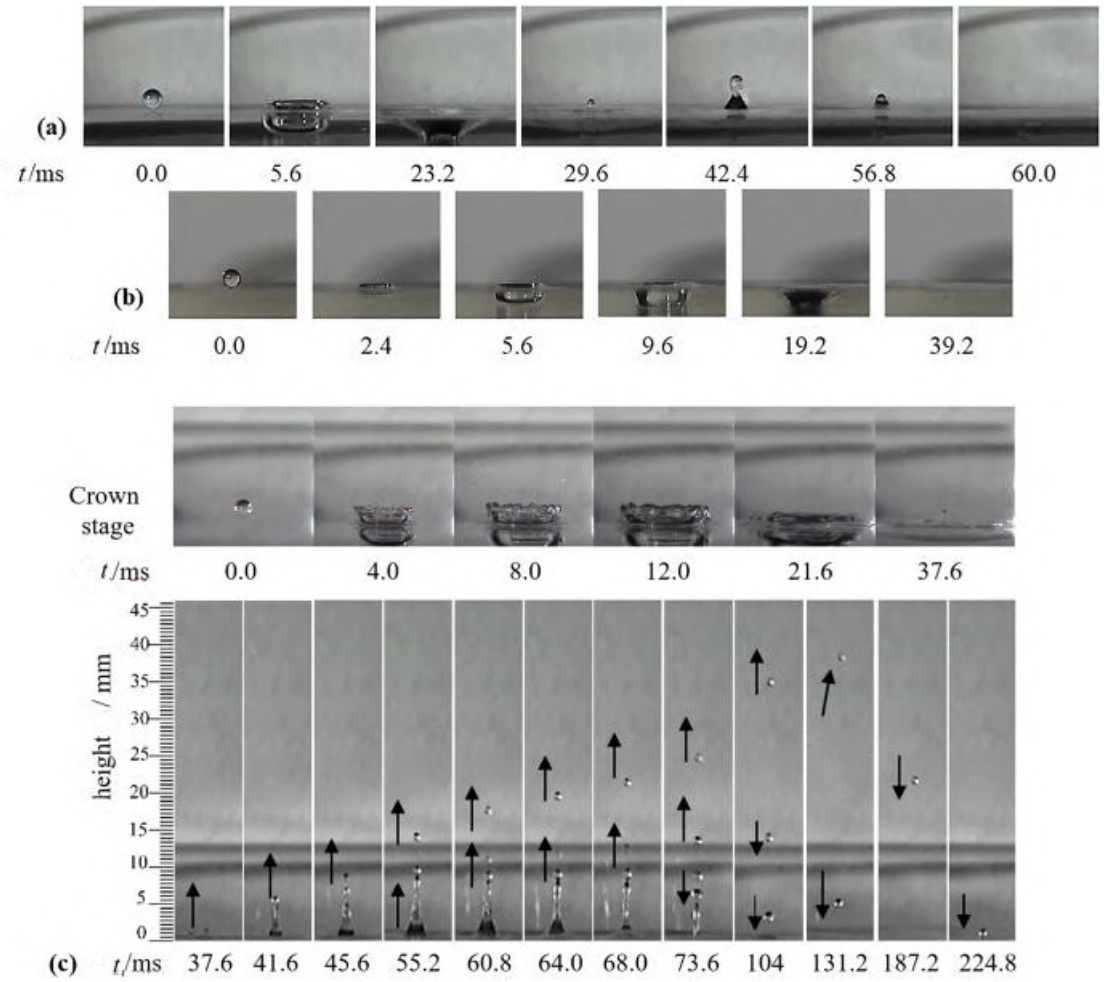

Figure 2.6: Water droplet impact onto an ethanol liquid film, followed by the evolution of jetting and its pinch-off ($d_{drop} = 2.56\ mm, h^* = 1.455$): (a) Formation of a small jet ($We = 159.64$); (b) No jet formation ($We = 88.69$); (c) Dynamic evolution of the jet and its pinch-off droplets ($We = 1596.5$) [26].

with decreasing film thickness ($h^* \leq 1$). With this information, it is possible to conclude, that the phenomenon depends both on the film thickness and on the impact velocity of the drop. Later, Ribeiro et al. [28, 29] presents a threshold for a film thickness between $0.4 \leq h^* \leq 1$ where the transition would occur for $We > 1500$. This phenomenon will be later explained in more detail in section 2.7.

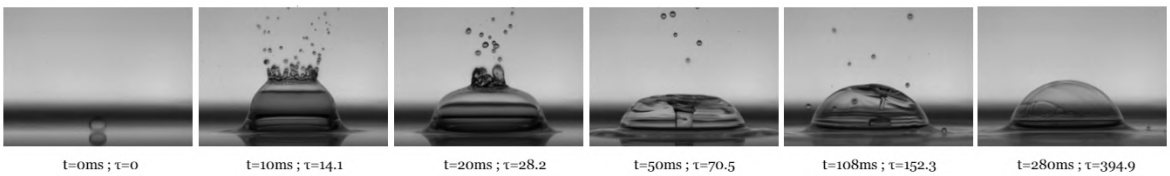

Figure 2.7: Bubble formation for a $2.9\ mm$ droplet of 75% Jet Fuel/25% HVO Mixture. Adapted from Ribeiro et al. [28].

2.3 Liquid Film Influence

When a drop impacts a liquid film, various stages of impact are to be expected. These are demonstrated in figure 2.8 accompanied by the nomenclature relative to structures that appear due to the impact.

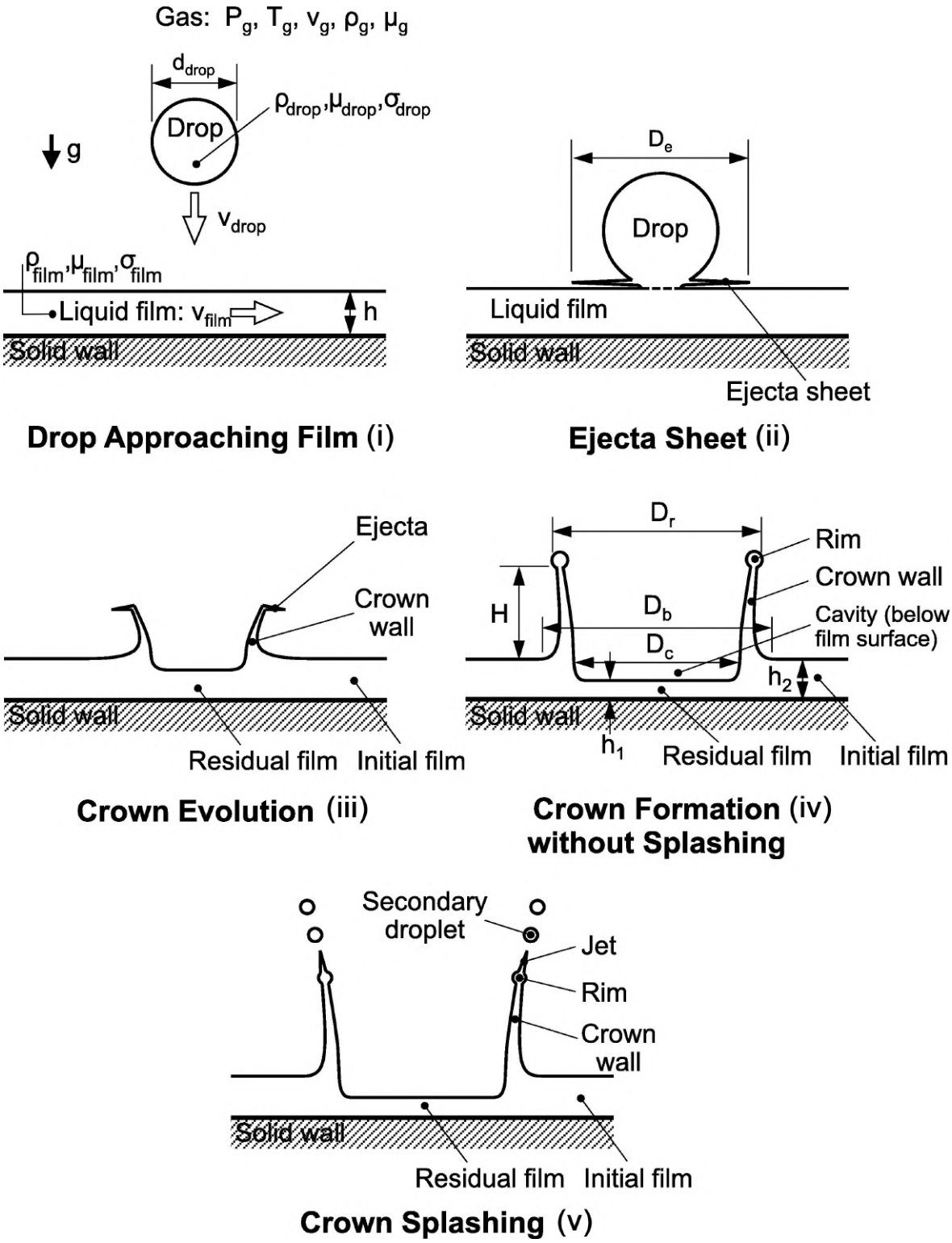

Figure 2.8: Schematics of drop impact on a liquid film and associated nomenclature. Adapted from Liang and Mudawar [24].

Figure 2.8 shows the following stages: (i) the drop prior to impact, (ii) formation of the ejecta sheet, (iii) transition from ejecta to liquid crown, (iv) formation of liquid crown following impact without splashing, and (v) formation of liquid crown following impact with splashing. The ejecta sheet is a very thin liquid sheet that forms in the first milliseconds of impact and results in the formation of the liquid crown. Splashing refers to the shattering of small secondary droplets from the crown's rim [24].

When analysing the impact on a wetted surface, a new factor must be considered when compared with dry surfaces. This factor is the relative film thickness, also denominated non-dimensional film thickness (h^*). This parameter is the ratio between the liquid film thickness (h) and the diameter of the droplet (d_{drop}):

$$h^* = \frac{h}{d_{drop}} \quad (2.7)$$

Other factors used to help define droplets impact on liquid film are the length scale of the wall roughness (L_a) and the wall roughness (R_a) [30]. Both these factors are non-dimensionalised by the droplet diameter, resulting, respectively, in the equations (2.8) and (2.9).

$$L_{nd} = \frac{L_a}{d_{drop}} \quad (2.8)$$

$$R_{nd} = \frac{R_a}{d_{drop}} \quad (2.9)$$

Across the literature, different classifications regarding the liquid film thickness are provided, making it difficult to find a universal definition for this particular subject. According to Tropea and Marengo [30], a liquid film can be classified into four categories. Based on table 2.1, liquid film and thin film are restricted to $h^* < 1.5$, although according to Vander Wal et al. [18] a different classification is proposed where thin films corresponded to $h^* \approx 0.1$, thick films corresponded to $0.1 \leq h^* \leq 10$ and deep pools corresponded $h^* \gg 10$.

Table 2.1: Liquid film classification [30].

Regime	Range	Characteristics
Thin film	$L_{nd} < h^* < 3R_{nd}^{0.16}$	Impact depends on wall features
Liquid film	$3R_{nd}^{0.16} < h^* < 1.5$	Impact is weakly dependent on wall
Shallow pool	$1.5 < h^* < 4$	Impact depends on film thickness but is independent of wall features
Deep pool	$h^* \gg 4$	Impact is independent of film thickness

2.4 Crown formation and evolution

When a droplet impacts vertically on a liquid film, the fluid that forms the drop experiences a drastic redirection of motion from vertical to radial. A theory for the formation and propagation of the crown was proposed by Yarin and Weiss [31], in which the authors explain

that a kinematic discontinuity is formed as the fast redirected liquid meets the static liquid film, which contributes to the crown's formation and propagation. This theory has been accepted widely by the scientific community, and even it is validated by simulations and by PIV measurements [24].

Later, Trujillo and Lee [32], besides adopting the concept of kinematic discontinuity presented by Yarin and Weiss [31], also had into consideration the film thickness and the effect of the viscous forces. These two theories were both later refuted by Roisman and Tropea [33], in an experiment where the authors did not have into consideration the viscous [32] or inviscid [31] effects. The authors compared their results with the previous two models [32, 31], where analysing the phenomenon without viscous or invisid effects showed negligible differences. This observation led them to suggest that the main factor for the formation of the crown at a high impact velocity would be the inertia of the liquid. Figure 2.9 shows the schematic of the kinematic discontinuity presented by Roisman and Tropea [33], where h_1 and v_1 represent the film thickness and film velocity in the impact region, and h_2 and v_2 the film thickness and film velocity in the static film region, respectively. They also define the crown thickness (h_b), equation (2.10) and angle α, equation (2.11)).

$$h_b = h_1 + h_2 \quad (2.10)$$

$$\alpha = \arccos\left(\frac{(h_1 - h_2)\,(v_1 - v_2)^2}{h_b\,(v_1 - v_2)^2 - \dfrac{8\,\sigma_{drop}}{\rho_{drop}}}\right) \quad (2.11)$$

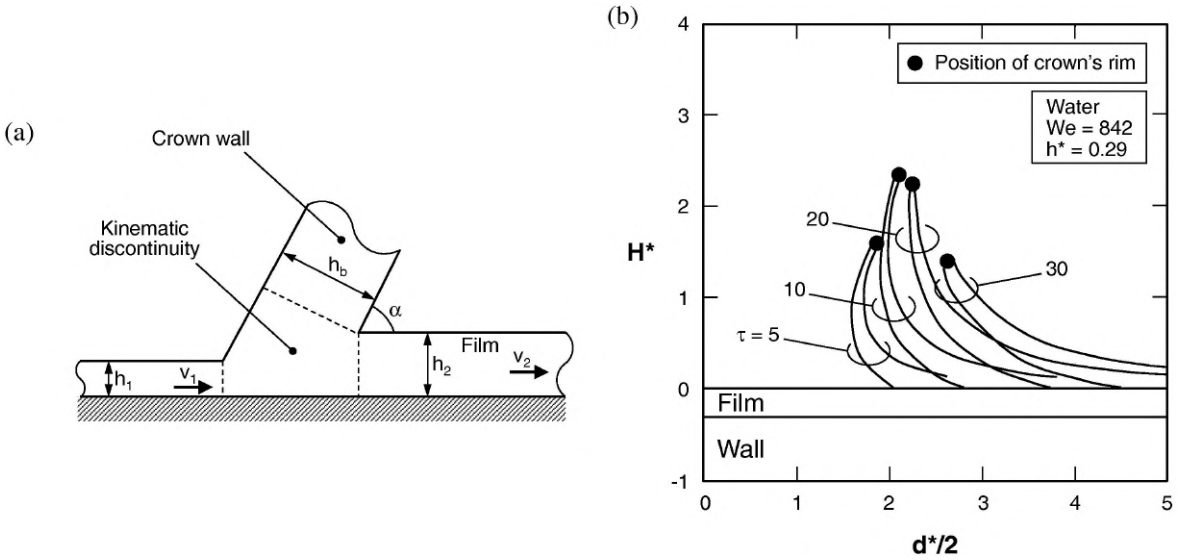

Figure 2.9: (a) Schematic of crown formation based on kinematic discontinuity. (b) Predicted shape of crown evaluation for water with $We = 842$ and $h^* = 0.29$ [24].

The main geometrical parameters of a developing crown are the crown diameter (D), crown

height (H), crown angle (α) and thickness. As shown in figure 2.8 the crown diameter can be measured in two ways, by the base (D_b) and by the rim (D_r). The crown height, as shown in figure 2.8, is measured from the base of the crown to the base of the rim, and the angle α is the angle between the base of the crown and the liquid film (Fig. 2.9).

Both the formation and propagation of the crown can be affected by external factors such as the surrounding gas viscosity (μ_g) and density (ρ_g), surface topography, the velocity of the flowing film (v_{film}) and the shape of the droplet before impact. Liang et al. [34] found that decreasing the density ratio ($\rho^* = \rho_{drop}/\rho_g$) caused the crown wall to curve inwards, especially for $\rho^* < 100$. The viscosity also plays an important role in the dynamics of the impact. According to Liang et al. [34], crown expansion can be suppressed when the viscosity ratio ($\mu^* = \mu_{drop}/\mu_g$) is lower than 0.5. Liang et al. [35] experimented with impacting a droplet onto a thin liquid film on cylindrical surfaces. From that, the authors discovered that increasing the curvature of the cylinder ($\beta = d_{drop}/d_{cylinder}$) caused the liquid sheet to almost bestride the surface, as seen in figure 2.10.

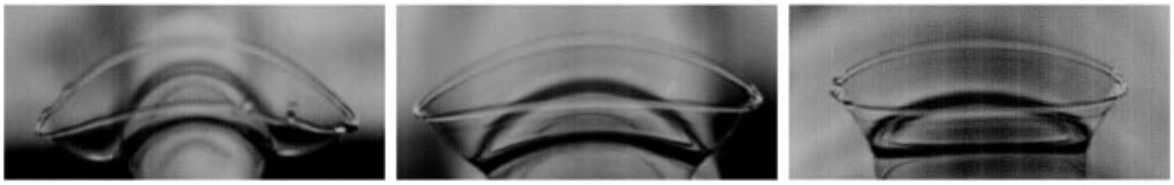

Figure 2.10: Effects of wall curvature for drop-cylinder impact on crown shape for butanol: (a) $\beta = 0.462$ with $We = 371$; (b) $\beta = 0.229$ with $We = 352$; (c) $\beta = 0.091$ with $We = 327$. Adapted from Liang et al. [35].

2.4.1 Crown diameter

Essays led by Liang et al. [36], Rieber and Frohn [37] and Agbaglah and Deegan [38] concluded that the crown diameter is independent of the drop We and Re. More recently, a new study performed by Wu et al. [39] shows a dependency of the crown diameter with We. They concluded that for $We > 172$, the diameter of the crown is not affected. Furthermore, for $We \leqslant 172$, the crown diameter tends to increase with We. This phenomenon is explained by Wu et al. [39], that for a $We > 172$, the film at the point of impact is completely pushed away, leaving the steel plate underneath exposed. Regarding the effect of the non-dimensional film thickness (h^*), Liang et al. [36] states that it plays an important role in the crown diameter. This results in a growth of the crown diameter as a consequence of the decreasing relative film thickness. Mukherjee and Abraham [40] presented a more precise definition regarding the influence of the non-dimensional film thickness on the crown, stating that the crown grows with the increase of h^* for thin films ($h^* < 0.25$) and decreases for thick films ($0.25 < h^* < 2$).

2.4.2 Crown height

Roisman and Tropea [33] presented a theoretical model where they showed that increasing h^* would result in a great increase of the non-dimensional crown height ($H^* = H/d_{drop}$).

Afterwards, Cossali et al. [41] also investigated the influence of the non-dimensional film thickness on H^* experimentally. The authors then compared their results with the theoretical model of Roisman and Tropea [33], as demonstrated by figure 2.11. Looking at the experimental results, represented by the squares, it is possible to see that the maximum non-dimensional crown height is $H^* \approx 1$, for $We = 296$. As the Weber number increases, H^* shows a growth, clearly observed when $We = 843$, where the crown non-dimensional height doubles its initial value. Although, the relation between the growth of H^* and the relative thickness expected according to the theoretical model, represented by the lines, was not verified. With these results, the experiment revealed a very weak influence of h^*, however, the results demonstrated a great dependence on We. They attribute the differences between the analytical model and the experimental results to the fact that Roisman and Tropea [33] did not consider the velocity component normal to the surface when varying the film thickness.

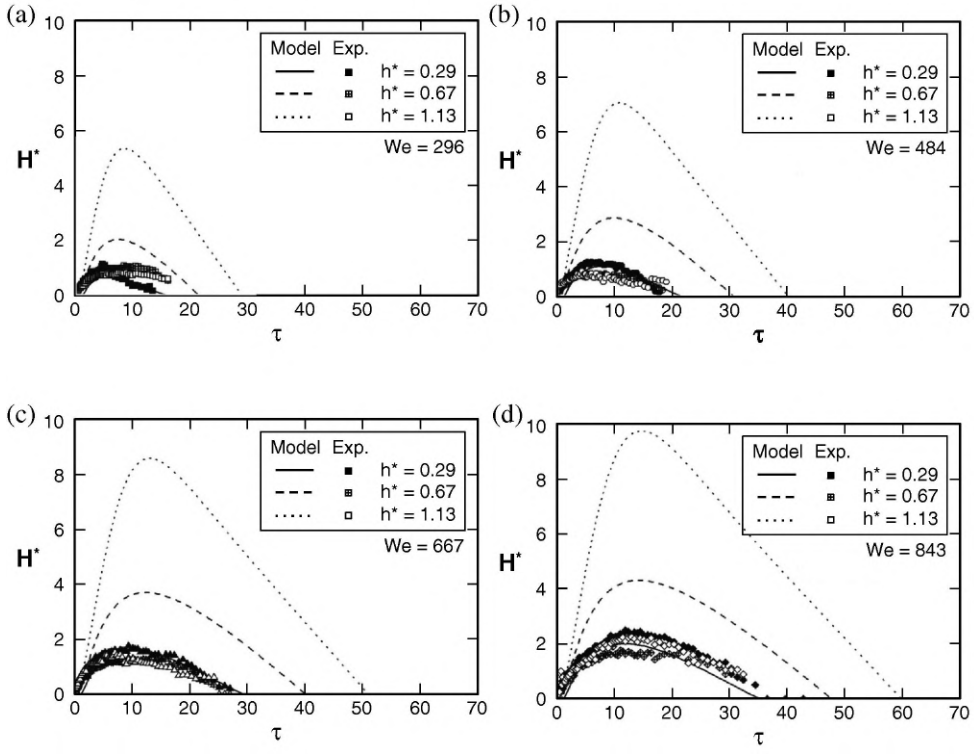

Figure 2.11: Non-dimensional crown height evolution relative to non-dimensional time for different film thicknesses according to measurements of Cossali et al. [41] and theoretical predictions of Roisman and Tropea [33] for (a) $We = 296$, (b) $We = 484$, (c) $We = 667$, and (d) $We = 843$ [24].

2.4.3 Crown angle

Wang and Chen [42] concluded that the crown wall is nearly perpendicular to the horizontal film, i.e. $\alpha = 90$ for $h^* = 0.5$. A later study performed by Fedorchenko and Wang [43] found that the crown angle was completely determined by the film thickness and independent of the impact velocity and/or properties of the fluid. Their study found that in the initial stages of crown emergence, the crown angle was $\alpha = 90$ for $h^* \geq 0.25$, but for very thin films, $h^* < 0.25$, the crown angle can be determined by equation (2.12).

$$\cos\alpha = 1 - 4\,h^* \quad (2.12)$$

More recently, Ribeiro et al. [44] studied the influence of the liquid film thickness on the crown angle, in the phenomenon of bubble encapsulation. The authors findings showed that for very thin films ($h^* < 0.2$), the crown was almost perpendicular to the liquid film, therefore, disagreeing with Fedorchenko and Wang [43].

2.4.4 Crown thickness

Determining the thickness of the crown is something highly searched by investigators, although, it is rather complicated. The reason behind this is related to the problem that after a droplet impacts a liquid film, the crown formed does not acquire a uniform thickness. A study performed by Fujimoto et al. [45] shows that a detailed temporal and spatial distribution of the crown thickness is only possible through a numerical simulation, where it was concluded that the crown thickness decreased with decreasing surface tension. Later, Cossali et al. [41] implemented a technique using light intensity in an attempt to measure the crown thickness. The authors were able to obtain approximate measurements of what was denominated in the article as normal thickness. The normal thickness is defined as half the difference between the outer and inner crown diameters.

2.4.5 Cavity beneath the crown

After a drop impacting on a deep pool, below the original free liquid film/interface level, a cavity begins to form. The cavity then continues to grow, enlarging, and soon takes the shape of a hemisphere, observed in figure 2.12c. The growth of the cavity starts to slow down, and it begins to collapse. At this moment, capillary waves begin to spread over the cavity and distort its shape figure 2.12e, exhibiting a shape with sharp edges between the different height levels formed, figure 2.12f. The cavity starts to close from the bottom, causing the depth of the cavity to decrease quickly, figure 2.12f and figure 2.12g. Meanwhile, the width of the crater does not change significantly because the liquid accelerates upwards within this period. Right before the central jet produced emerges, due to the closing of the cavity, the cavity shape assumes an almost cylindrical shape, figure 2.12g, immediately after this shape collapses we see a thick central jet rising out of the cavity, figure 2.12h [43]. As the film thickness decreases, the shape of the cavity is affected in the expansion phase of the cavity, this will collide with the surface below and prevent the formation of the hemisphere shape. In such cases, the cavity would assume an almost cylindrical shape.

2.5 Splashing

The splashing phenomenon is defined as the separation of fluid from the immediate impact site, associated with the formation of secondary droplets, and as explained by Vander Wal et al. [18], it tends to occur with high impact velocities. Splashing is a very important phenomenon in IC engines [46], where it is crucial to the atomization of the fuel, leading to complete combustion and a reduction of pollutant emissions. On the other hand, this phenomenon is detrimental to coating processes such as inkjet printing and pesticide delivery

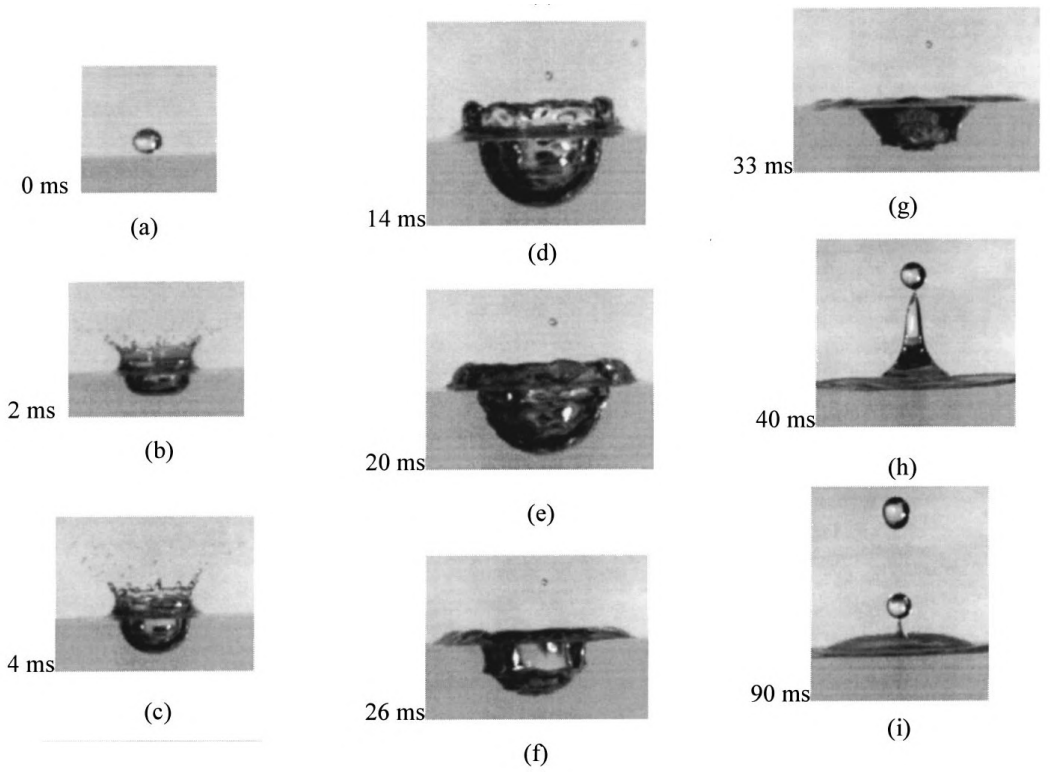

Figure 2.12: Sequence of images of a water drop impacting on a water target liquid. The impact conditions are $d_{drop} = 3.12$ mm, $v_{drop} = 3.47$ m/s, $h^* \approx 5$. Adapted from Fedorchenko and Wang [43].

[47], where the splash of the droplets would cause an uneven spreading of the fluid. As explained in section 2.2, there are two types of splashing, delayed splash and prompt splash. The former is associated with the breakup of the crown rim after it is fully formed, and the latter is related to the ejection of secondary droplets while the crown is still growing [17, 19, 18, 20].

According to Liang et al. [34], the increase in the viscosity of the surrounding gas (μ_g) would suppress splashing. Vander Wal et al. [18] concluded that viscosity promotes splashing on dry surfaces, but suppresses splashing when impacting on a thin film. Liang et al. [20] found that prompt splash takes place at low μ_{drop}, while high μ_{drop} result in a delayed splash. Vander Wal et al. [18] in their experiments found that high surface tension would suppress splashing, despite the impact being on a dry or wetted surface.

2.5.1 Splashing mechanism

One of the most important factors when investigating the splashing mechanism is to determine the so-called spread/splash threshold, where above this limit secondary drops start forming. This threshold is highly dependent on the surface tension and usually is represented in terms of We or a combination of We with other parameters. Several studies showed that the splashing threshold is significantly influenced by viscosity, surface tension and film thickness [19, 42]. A study conducted by Cossali et al. [19] shows that increasing h^* would also increase the We threshold. A later study performed by Rioboo et al. [48] obtained the same

conclusion for very thin films, $0.02 \leq h^* \leq 0.04$. However, other studies conducted by Wang and Chen [42] and Asadi and Passandideh-Fard [49] concluded that the non-dimensional film thickness had a low to none effect in the We threshold for thin films, $h^* < 0.1$.

Since the We threshold is influenced both by viscosity and film thickness and also by the surface tension, the common method to express the spread/splash threshold is a K-type correlation combining the droplet inertia with its surface tension (We), viscous forces $(Oh$ or $Re)$ and non-dimensional film thickness (h^*) [24]. Table 2.2 presents a summary of various papers regarding the critical K, K_c correlations to predict the onset of splashing.

Table 2.2: Correlations for critical K to predict the onset of splashing

Author(s)	**Fluids**	**Experimental conditions**	**Threshold(s)**
Vander Wal et al. [50]	heptane, nonane, decane, dodecane, tetradecane, DI water, 30% glycerol/water, methanol, ethanol, N-propanol and butanol	$d_{drop} = 2.0\ mm$ $h^* = 0.1$ $v_{drop} = 2.2 \pm 0.15\ m/s -$ $4.2 \pm 0.15\ m/s$ $We = 120 - 1400$ $Re = 9 \times 10^2 - 14 \times 10^3$ $Oh = 10^{-3} - 17 \times 10^{-3}$	thin films: $K = Oh\, Re^{1.17} = 63$ dry surface: $K = Oh\, Re^{0.609} = 0.85$
Cossali et al. [19]	water, glycerol/water mixes	$d_{drop} = 3.07 \pm 0.07\ mm -$ $3.51 \pm 0.06\ mm$ $h^* = 0 - 1$ $We = 2 \times 10^2 - 1.6 \times 10^3$ $Oh = 2.2 \times 10^{-3} - 0.141$	$K = We\, Oh^{-0.4} = 2100 + 5880\ {h^*}^{1.44}$
Gao and Li [51]	water, glycerin/water mixes	$d_{drop} = 2.6\ mm -$ $4.6\ mm$ $h = 0.17\ mm - 0.5\ mm$ $v_{drop} = 0.63\ m/s -$ $4.2\ m/s$ $\mu_{drop} = 1\ mPa\ s -$ $46.47\ mPa\ s$ $\sigma_{drop} = 0.0657\ N/m -$ $0.0714\ N/m$ $v_{film} \approx 1.745\ m/s -$ $3.316\ m/s$	$K = We\, Re^{0.5} =$ $= 3378\ \left(1 + h^*\ {v^*_{film}}^2\right)^{-1}\ \left(1 + h^*\ v^*_{film}\right)^{-0.5} =$ $= 3378\ \left(1 + h^*\ \frac{v_{film}}{v_{drop}}^2\right)^{-1}\ \left(1 + h^*\ \frac{v_{film}}{v_{drop}}\right)^{-0.5}$
Zhu et al. [52]	water	$d_{drop} = 1.95 \pm 0.2\ mm$ $h^* \approx 0.06 - 0.36$ $v_{drop} = 2.3 - 4.5\ m/s$	$K = We\, Oh^{-0.4} = 1880 + 156122\ {h^*}^{2.017}$
Motzkus et al. [53]	water, 50% water/ethanol, 45% water/ 55% glycerol	$d_{drop} = 1.90 \pm 0.025\ mm$ $-4.30 \pm 0.025\ mm$ $h^* = 1.2 - 3.9\ mm$ $v_{drop} = 1.4\ m/s - 4.5\ m/s$ $We = 62 - 1754$ $Oh = 2.0 \times 10^{-3} - 15.4 \times 10^{-3}$	$K = We\, Oh^{-0.4} = 2100 + 2000\ {h^*}^{1.44}$
Okawa et al. [54]	water	$d_{drop} = 0.15\ mm - 4.7\ mm$ $h^* = 0.43 - 68$ $We = 2.5 - 980$ $Oh = 1.5 \times 10^{-3} - 8.4 \times 10^{-3}$	$K = We\, Oh^{-0.4} = 2100$
Terzis et al. [55]	AdBlue, 50% urea/water	$d_{drop} = 2.1 \pm 1\%\ mm$ $h^* = 0.1 - 0.65$ $v_{drop} = 4.4 \pm 6\%\ m/s$ $We = 100 - 660$ *Depending on which fluid is used for the film and the drop:* $\mu = 1.37\ mPa\ s$ *or* $1.89\ mPa\ s$ $\sigma = 0.07362\ N/m$ *or* $0.07499\ N/m$	$K = We_{drop}\ \widetilde{Oh}^{-0.4}_{film,drop} =$ $= We_{drop}\left[\frac{1}{2}\ Oh_{drop}\left(1 + \frac{\mu_{film}}{\mu_{drop}}\right)\right]^{-0.4} =$ $= 1413 + 9347\ {h^*}^{1.2}$ (only appliable for delayed splash)

2.5.2 Secondary droplets

According to Tropea and Marengo [30], there are at least three types of secondary droplets sources:

1. A prompt instability of the ejecta sheet that occurs immediately upon impact and produces very small droplets;

2. Rim instability of the ejecta sheet that produces medium size droplets;

3. Rim instability of the crown sheet that produces jets and large droplets.

Studies performed by Yarin and Weiss [31] and Cossali et al. [41] showed that the number of jets on the crown rim tends to decrease with time for $0 < \tau < 8$, reaching an approximate asymptotic value of about 10 for $\tau > 8$. The study carried out by Cossali et al. [41], also states that the number of secondary droplets tends to have its maximum value around $1 < \tau < 3$, during the beginning of the crown evolution, independently of the experimental conditions, i.e., independent of We and h^* (Fig. 2.13).

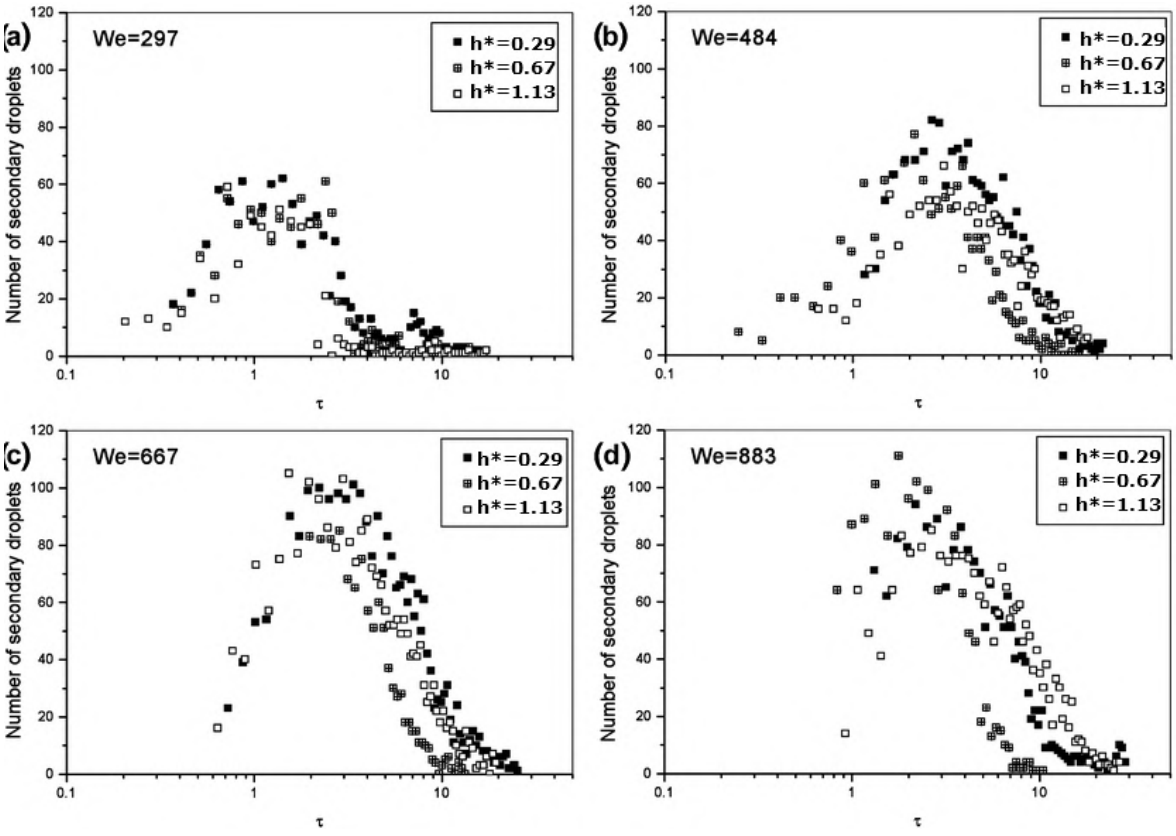

Figure 2.13: Time evolution of secondary droplet number for different impact velocities and different film thicknesses. Adapted from Cossali et al. [41]

2.6 Ejecta and Lamella Sheets

The ejecta sheet is produced almost immediately at the moment of impact. As the drop touches the surface with a finite speed, it produces a localized pressure singularity, pushing the fluid outwards as shown in figure 2.14 [15].

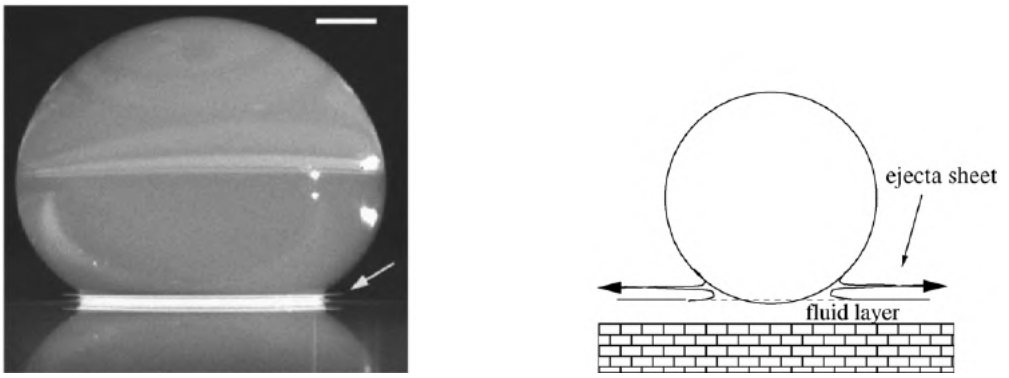

(a) (b)

Figure 2.14: (a) Experimental snapshot of a drop directly after impact at $Re = 1080$ and $We = 4170$; (b) Diagram of the same process. An ejecta sheet shoots out horizontally from underneath the drop. Adapted from Deegan et al. [15].

According to Deegan et al. [15], the evolution of the ejecta sheet and the consequent combination with the crown sheet is divided into three possible outcomes:

1. The ejecta sheet becomes the leading edge of the crown sheet, as the latter grows underneath the former;

2. The ejecta sheet collides with the liquid film to produce bubble rings;

3. The ejecta sheet breaks up immediately for prompt splashing conditions.

A study made by Josserand and Zaleski [56] showed that viscosity influences the liquid motion in the neck region and dictates the width of the ejecta sheet. A later study made by Agbaglah and Deegan [38] found that the surface tension either allows or prevents the formation of the ejecta sheet, i.e, when the fluid has a high surface tension, the leading edge of the ejecta sheet is pulled back and forms the rim as it folds backwards.

The majority of the investigators do not distinguish between the ejecta and the lamella sheet. The ejecta sheet, as explained before, is formed almost immediately ($\approx 100\,\mu s$) upon impact, while the lamella is a slower sheet that emerges after the ejecta, normally $500 - 1000\,\mu s$ after impact. In order to resolve the ambiguity related to the two sheets, Zhang et al. [57] analysed several impacts by resorting to an X-ray technique providing evidence for the existence of both sheets. According to their results, when only one sheet emerges, the authors do not specify which sheet it is. This can lead to the conclusion that in such a situation, it is not possible to detect the formation of each individual sheet and both of them end up merging in a fraction of a second, resulting in the observation of the combined sheet that emerges.

Regarding the two sheets emergence, it is possible to have the disintegration of the ejecta resulting in prompt splashing or the absorption of the ejecta sheet by the lamella. Figure 2.15a and figure 2.15b show a thin ejecta sheet and a thicker lamella sheet while figure 2.15c shows the ejecta and lamella sheets combined into a single sheet. Figure 2.15 (d) shows a $We - Re$ regime diagram indicating the number and type of sheets resulting from the drop impact [57].

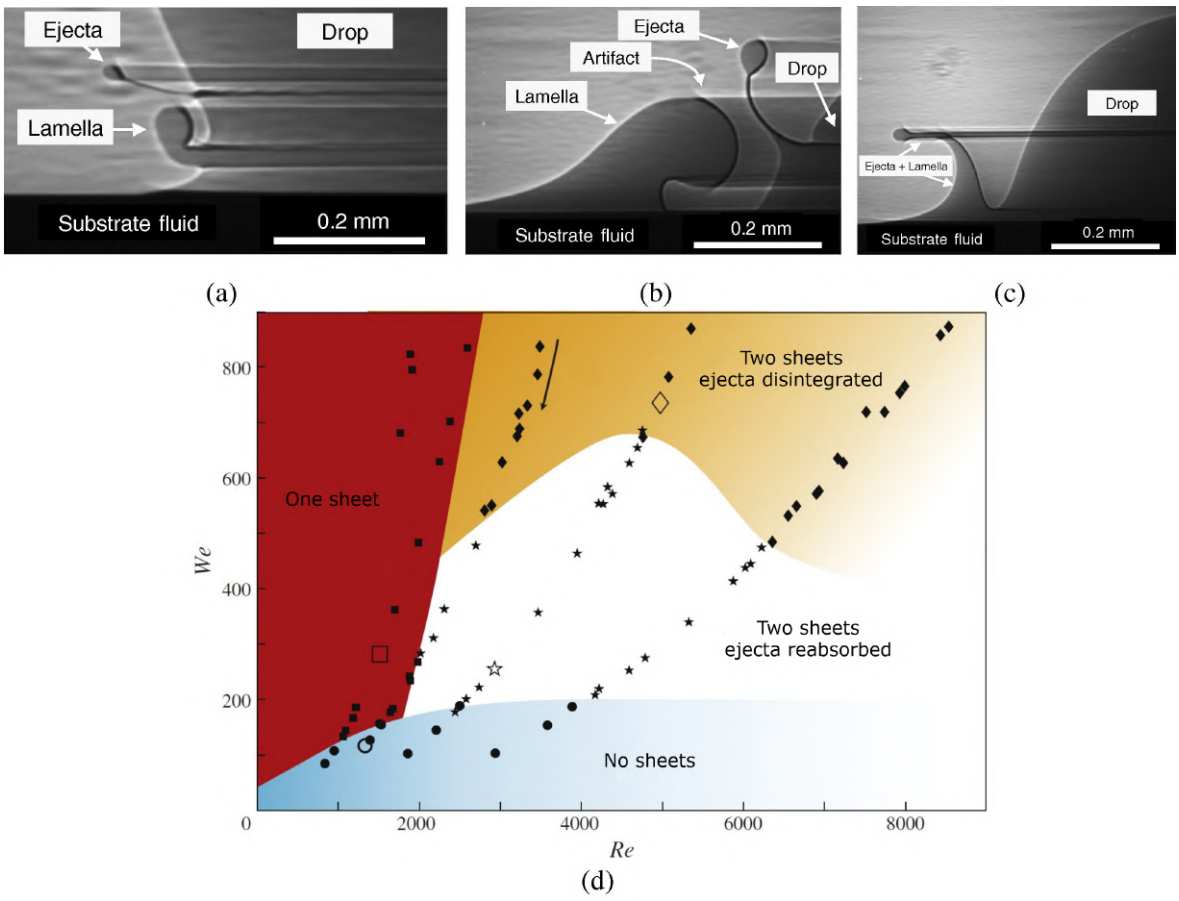

Figure 2.15: Distinguishing ejecta and lamella sheets for silicone oil: (a) $We = 396$ and $Re = 5703$; (b) $We = 324$ and $Re = 2191$; and (c) $We = 451$ and $Re = 710$; (d) Number of sheets resulting from drop impact. Adapted from Zhang et al. [57].

2.7 Bubble Encapsulation

The phenomenon of bubble encapsulation (Fig. 2.16) was observed over the years, although a more in-depth study is still absent in the current literature. Engel [58] compared the impact of meteorites with the impact of a liquid drop onto a deep pool, presenting a morphology similar to the one observed for bubble encapsulation. This was later confirmed even in relatively thin films $(0.2 < h^* < 1)$, as reported by Ribeiro et al. [28, 29]. However, this work focuses on the dynamics of the crater rather than on the crown enfolding at the top and encapsulation of a bubble. In the experiments performed by Pan et al. [27], they claim that the transition boundary is highly dependent on the thickness of the liquid film. They present only a transition point of $We \approx 2570$ for large thicknesses and this Weber number would increase for

$h^* \leq 1$. Motzkus et al. [59] focused their study on the disintegration of the bubble and the subsequent microdroplets formation. The authors correlated bubble bursting with the decreasing hemispherical thickness caused by the effect of the rising bubble and the drainage of liquid at its base. In a study with the goal of simulating the impact of diesel droplets in the combustion chamber walls while covered by lubricant oil, Geppert et al. [60] spotted bubble formation regularly. In these experiments, the phenomenon occurred for $h^* \geq 0.2$ and $We > 1000$.

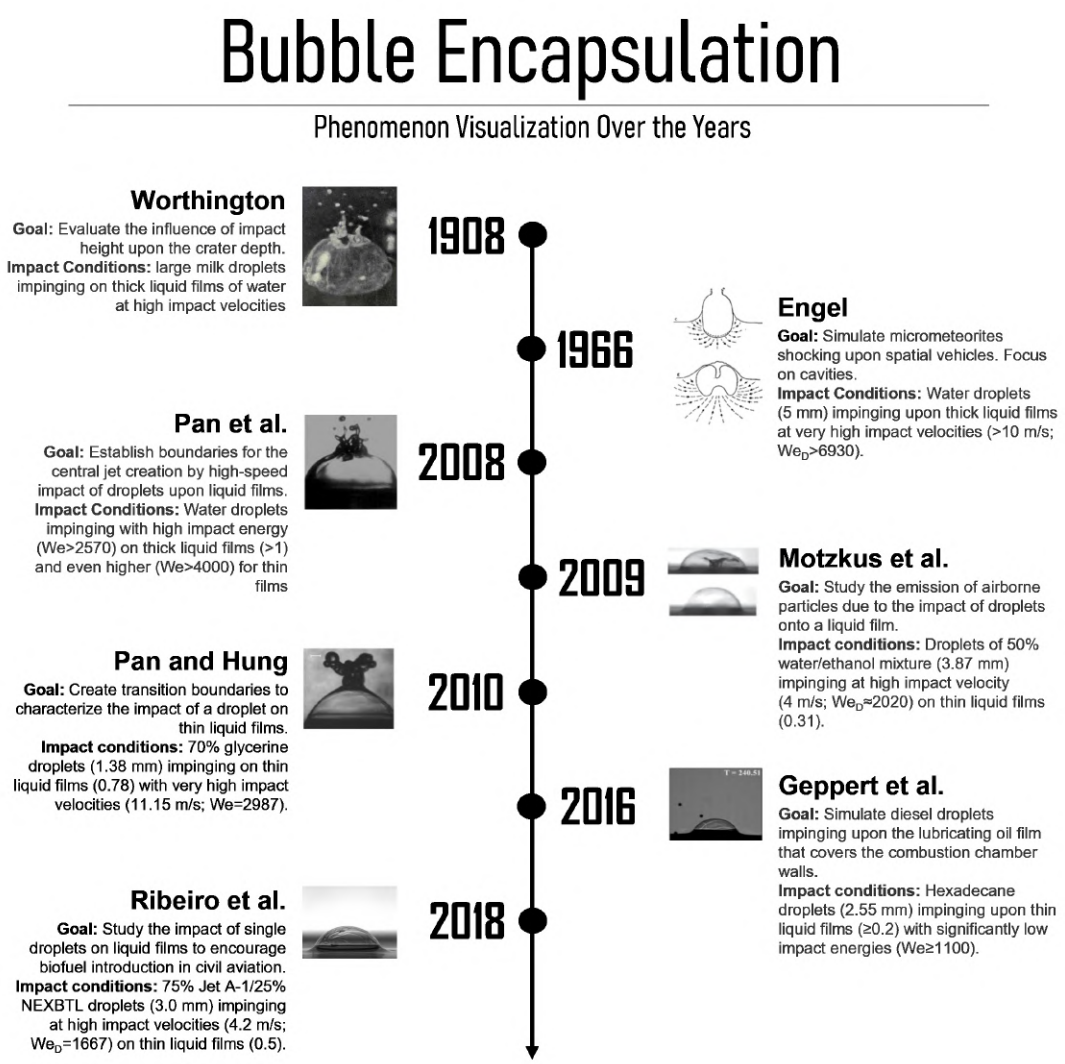

Figure 2.16: Bubble Encapsulation Visualization over the years [29].

More recently, this phenomenon was unexpectedly found by Ribeiro et al. [28, 61, 29] while studying the implementation of biofuels in civil aviation. After these findings, Ribeiro et al. [28, 62, 63, 29] investigated in deepened what were the main parameters that influence this phenomenon, in addition to if it is something to be avoided or encouraged in IC engines. Bubble encapsulation was found to be a phenomenon that occurs within a specific set of initial impact conditions. When a droplet impacts a liquid film it can result in a prompt or delayed splash. This can be followed by an enfolding of the crown which eventually, results in the encapsulation of a bubble while remaining at the top of the liquid film. In case sec-

ondary droplets fall on the dome or if the bubble reaches the critical thickness due to the liquid drainage, it may burst. For the first time in the literature, a criterion for bubble encapsulation, defined in equation (2.13), was proposed by Ribeiro et al. [62, 63]. This criterion was based on and deduced considering the spread/splash criterion presented by Vander Wal et al. [50], see table 2.2.

$$Re_{drop}\, Oh_{film}^{a} = 34.5 \iff a = \frac{ln(34.5/Re_{drop})}{ln(Oh_{film})}\ ,\ \forall\, a \in [1.022, 1.142] \quad (2.13)$$

The novelty in the criterion presented by Ribeiro et al. [62, 63] was the use of an Ohnesorge number with a characteristic length scale based on the liquid film thickness h, Oh_{film}, and the correlation includes the conditions where bubble encapsulation has a probability of occurrence of $p \geq 0.5$. Both the Ribeiro et al. [62, 63] and Vander Wal et al. [50] correlations, considered experiments with a thermal equilibrium between the droplet and the liquid film, i.e., for a liquid drop and film at isothermal conditions.

2.8 Impact on a heated surface

The majority of the studies researched on droplets impacting on heated surfaces are performed without a liquid film, i.e., on dry surfaces [64, 65]. This is one of the reasons for the more in-depth exploration and development of this work.

Analysing the impact on heated surfaces represents an added challenge, not only due to the dynamic interactions of the fluids but also by taking into account the thermodynamics and how these thermodynamic interactions can influence the fluid dynamics and vice-versa. Having into account the parameters and properties presented in section 2.1, the temperature of the droplet and of the liquid film has their utmost importance. Besides the previously mentioned temperatures, the temperature of the surface (T_w) and the saturation temperature of the fluid (T_{sat}), the temperature at which the fluid at a given pressure begins to boil, are also important factors that are needed to define our heat transfer regime.

2.8.1 Heat transfer regimes

According to Naber and Farrell [66] and Ko and Chung [67], there are four different regimes, which are based on the drop evaporation lifetime, as can be seen in figure 2.16.

According to Bernardin et al. [69], the film evaporation regime is where the heat from the surface is conducted through the liquid film and dissipated by evaporation at the liquid-gas interface. It is characterized by long evaporation times, existing several degrees below the T_{sat}, depending on the surface roughness and the properties of the fluid. Increasing the temperature $(T_{sat} < T_w < T_{CHF})$, the next regime is the nucleate boiling, where the heat transfer rate increases and the evaporation time decreases due to the formation of bubbles. This regime lower boundary is defined by the minimum surface superheat required to sustain vapour bubble nucleation and growth within the impinging droplets while its top boundary

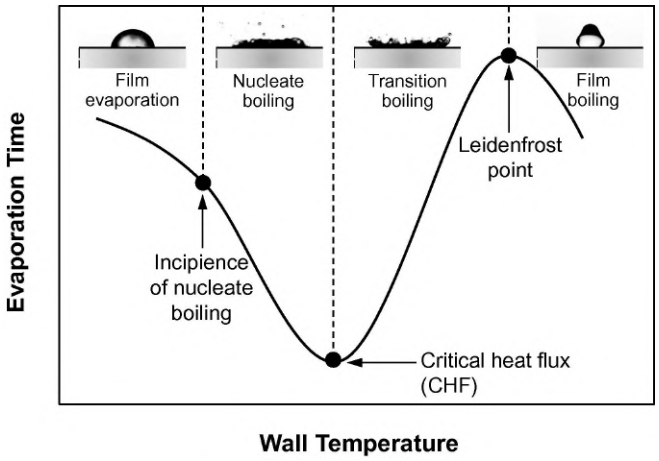

Figure 2.17: Heat transfer regimes associated with a drop impinging a hot wall [68]

is called the critical heat flux point (CHF). At this point, the surface is at the highest capacity and wettability, while also reaching the maximum point of heat transfer, resulting in the minimum possible evaporation time. Passing the CHF point it enters the transition boiling regime ($T_{CHF} < T_w < T_{Leid}$). As the surface temperature continues to increase in the transition boiling regime as it approaches the Leidenfrost point, the heat transfer rate starts to decrease as the surface wetting and boiling are less efficient. At this point due to the rapid development of a thin vapour layer that cushions the spray droplets from the surface upon impact, the heat transfer is at its minimum as also the evaporation time of the droplet. Above the Leidenfrost point, the droplet enters the regime of film boiling ($T_w > T_{Leid}$) characterise by the existence of a vapour layer due to the Leidenfrost effect.

As indicated by Naber and Farrell [66], and Panão and Moreira [70], during the evaporation regime and the nucleate boiling regime a liquid film is formed on the surface, therefore these two regimes are considered wetting regimes. During the transition regime, the fluid is only in intermittent contact with the surface due to the separation caused by vapour expelled from the liquid. The film boiling regime since it begins after the Leidenfrost point, where a thin vapour layer is formed between the liquid and the surface, is considered a non-wetting regime.

It is well established across the literature that the film evaporation regime can be divided into three stages: initial, fundamental and final (Fig. 2.18). The initial stage is during the drop impingement phase, where, after contact, the drop spreads and oscillates until it achieves an equilibrium stage consisting of a spherical cap. When the spherical cap begins to evaporate, it enters the fundamental stage, during which the wetted area is preserved, with the contact angle and drop height gradually abating. The final stage consists of a rapid succession of events, where the spherical cap evaporates until the contact angle reaches a critical value, denominated as critical contact angle (θ_c). Upon reaching θ_c, the cap cannot maintain the same wetted area, as it shrinks laterally into a cap with a smaller area. This process keeps repeating until the liquid is completely evaporated.

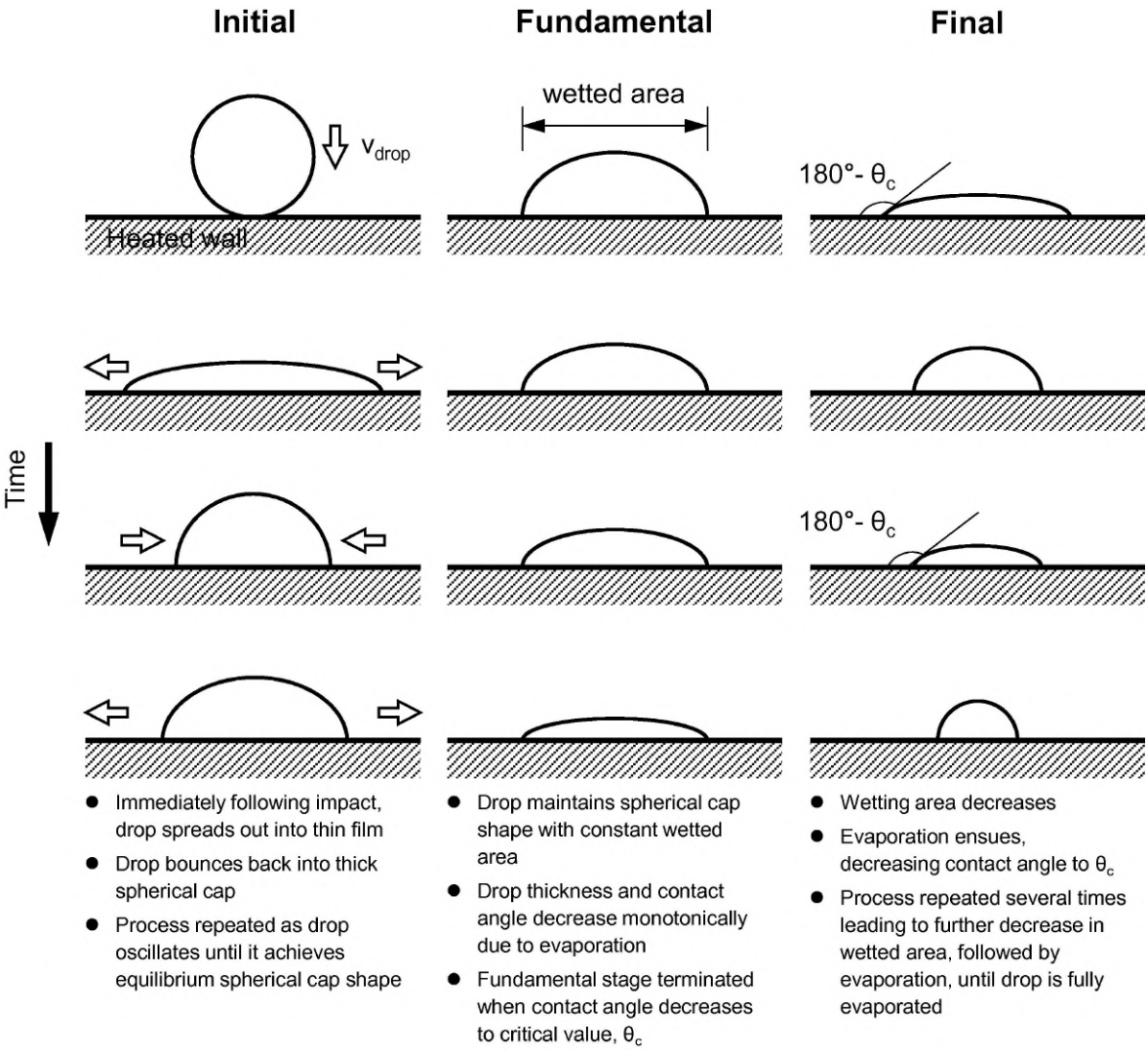

Figure 2.18: Schematic representation of three stages of drop impact with a heated wall during film evaporation regime [68].

2.8.2 Impact on a heated wet surface

As earlier mentioned, the majority of the studies related to droplets impacting heated surfaces are performed on dry surfaces or early numerical simulations [71]. Those that exist on wetted surfaces are more focused on the application for fire suppression or surface cooling and do not analyse how the properties of the fluids such as viscosity and surface tension affect the dynamics of the impact nor how the temperature affects the current thresholds for isothermal conditions. These studies, in most cases, only define their liquid films as a deep pool. An example of this is a study performed by Lan et al. [72], where they investigated the surface cooling mechanism on liquid pool fire suppression, with multi-component water spray/mist, with and without additives, impacting upon hot liquid fuel surfaces such as alcohol and molten ghee. With this study, they concluded that the presence of 5% $NaCl$ would enlarge the liquid column height and produce more secondary droplets. In addition to this, they also found that at $220°C$, pure water and the 5% $NaCl$ mixture, would cause a vapour explosion. Therefore, this type of fluids should be avoided during molten ghee fire suppres-

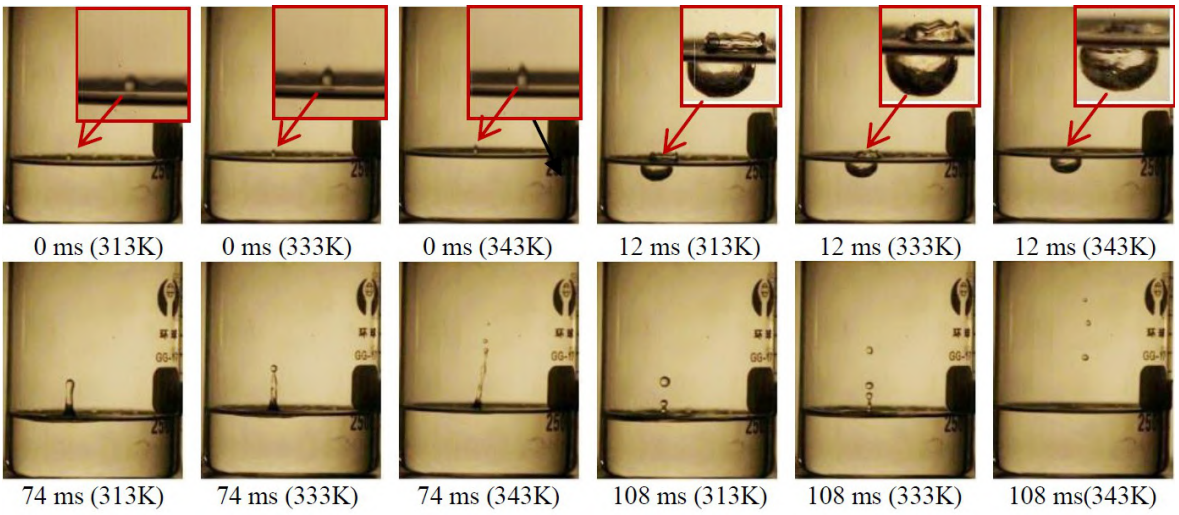

Figure 2.19: Water drops with 5% $NaCl$ impact on alcohol surfaces with different temperatures for $We = 299$ [72].

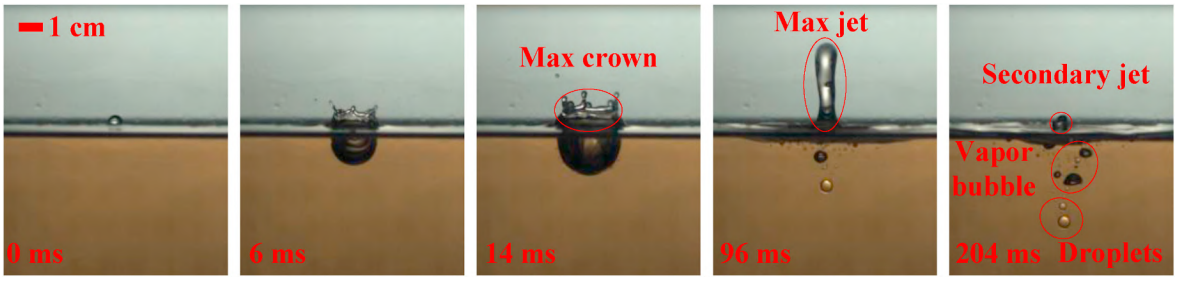

Figure 2.20: Secondary jet for the oil temperature of $213°C$ and the droplet diameter of $3.1\ mm$ for $We = 503$ [73].

sion with water-based technologies. The authors present the properties of the fluids used for the impact and as can be seen, by figure 2.19, the experiments were conducted in a deep pool regime.

The same situation is found in Fan et al. [73], where they explored the hazardous behaviours in cooking oil fires. The authors concluded that both the Weber number and oil temperature have significant effects on the formations of jets and bubbles, but only the oil temperature can affect the occurrence of vapour explosion significantly. Similar to the previously mentioned study, it is possible to deduct through the images that the experiments were performed in a deep pool scenario, figure 2.20.

Very recently a paper was presented by Wu et al. [39] with an experimental goal similar to the ones in heated dry surfaces or liquid film without temperature. The authors evaluate the effect of the We and the temperature of the liquid film on crown height and diameter, for a fixed film thickness of $h = 0.4\ mm$. The authors used two different fluids, ethanol for the droplet impacting and glycerol for the liquid film. One of the objectives was to evaluate the effect of the ethanol droplet impacting the glycerol liquid film when this one is at a higher temperature than the T_{sat} of the ethanol. With this study, Wu et al. [39], concluded that the crown diameter does not display a clear tendency to be affected by the temperature of the

liquid film. However, the crown height shows an increasing tendency with the liquid film temperature (Fig. 2.21b). The authors explain this crown effect as a result of reducing the energy necessary to overcome the viscosity and surface tension of the film while the crown is expanding and growing, therefore more energy is transferred for the growth of the crown in height.

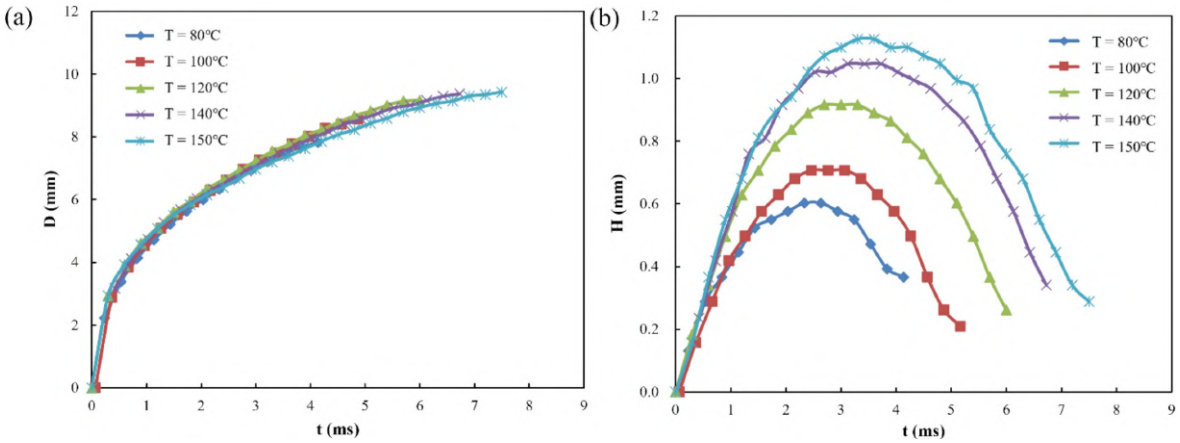

Figure 2.21: The effect of film temperature on the crown diameter (a) and height parameters (b) [39].

A phenomenon described by Wu et al. [39], is when the ethanol droplet impacts the glycerol film at a temperature above the T_{sat} of the ethanol. After impact, as the droplet starts to heat up at a certain point, due to the differences in the saturation temperatures, it can be observed what they call *sputtering*, where the ethanol reacts with the temperature violently, ejecting several droplets (Fig. 2.22).

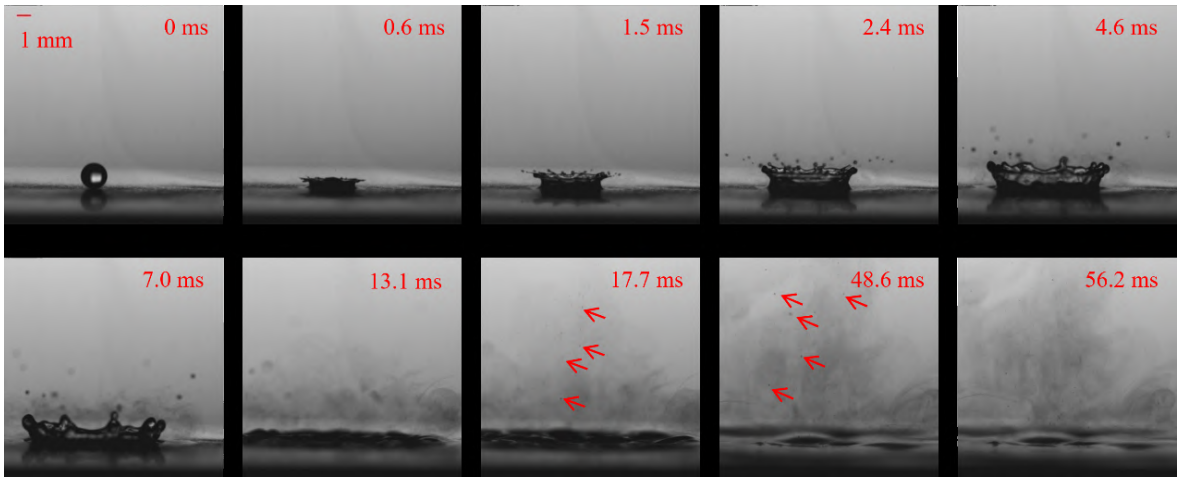

Figure 2.22: The phenomenon of Splash Crown-Sputtering [39].

Vasconcelos et al. [74] also presented recently an experimental study where they evaluate the effects of the liquid film temperature on the central jet height and crater formation, recuring to a non-dimensional temperature parameter $(\theta = (T_{film} - T_0)/(T_{sat} - T_0)$. Regarding the crater formation, the authors observed the formation of recirculation zones along with the alteration of the crater shape and local curvatures with the increase of the liquid film tem-

perature. Regarding the central jet height (Fig.2.23), the authors detected that for higher temperatures there is an increase in the maximum jet height for $h^* = 1.0$ and $h^* = 1.5$, whereas the tendency is unclear for lower thicknesses $(h^* = 0.5)$. In addition to this, it is also described that the number of secondary droplets originating from the central jet breakup is also promoted for increasing values of temperature.

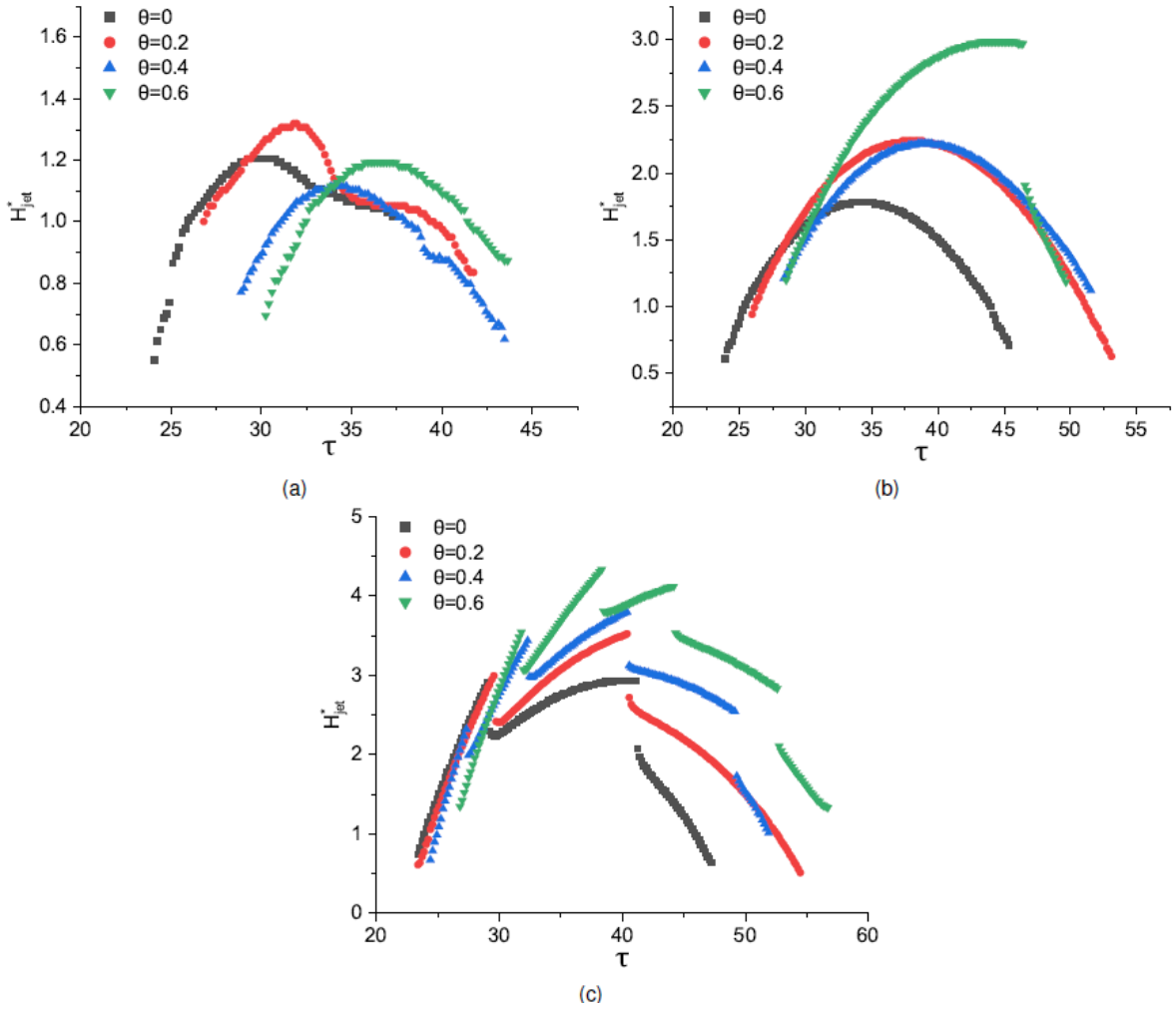

Figure 2.23: Central jet height measurements with n-decane for different dimensionless temperatures: (a) $h^* = 0.5$, (b) $h^* = 1.0$, and (c) $h^* = 1.5$ [74].

Chapter 3

Experimental Procedure

This chapter will exhibit, in detail, all the relevant data and features pertinent to the experimental procedure. A schematic of the experimental setup will be shown, including all the components, specifications, and thermophysical properties (density, surface tension, viscosity, saturation temperature) of the fluids used in the experiments. The chapter ends with details on the work methodology and measurement techniques.

3.1 Experimental Setup

In order to achieve the objectives formerly presented, an experimental facility was designed, represented in figure 3.1, allowing the experimental study of droplets impacting onto heated liquid films. For that, the existing facility in the laboratory was adapted, having into account the former design. For this experiment, it is fundamental to have an image acquisition system, the film container, the impact site illumination, the droplet dispensing system and the heating element.

In order to keep the laboratory temperature and relative humidity of the air approximately constant, these parameters were closely monitored. The image acquisition, provided by a high-speed camera, was manually triggered and positioned in front and aligned with the impact site, illuminated by a LED (light emitting diode) array through a diffusive glass placed there to provide uniform backlighting. The droplets were generated by a syringe pump connected to a needle and controlled by the computer, allowing the release of the fluid with a specific pump rate of $0.3\,ml/min$. The impact surface was a borosilicate container filled with a specific fluid thickness (h) defined in accordance with the droplet diameter and thermophysical properties of the fluid, due to the density of the fluids varying with the temperature. This thickness was calculated previously in volume and later translated to a mass. This mass would be measured later, recurring to a precision scale, in order to achieve the specific value needed for the film thickness. During the experiments, a second syringe pump was implemented in order to maintain a constant film thickness. The function of this pump was to compensate for the evaporation rate of the fluid at a specific temperature. For that, evaporation tests were performed for each fluid over a wide range of temperatures. With this analysis, it was possible to calculate the evaporation rate (ml/min) and then set the second syringe pump accordingly.

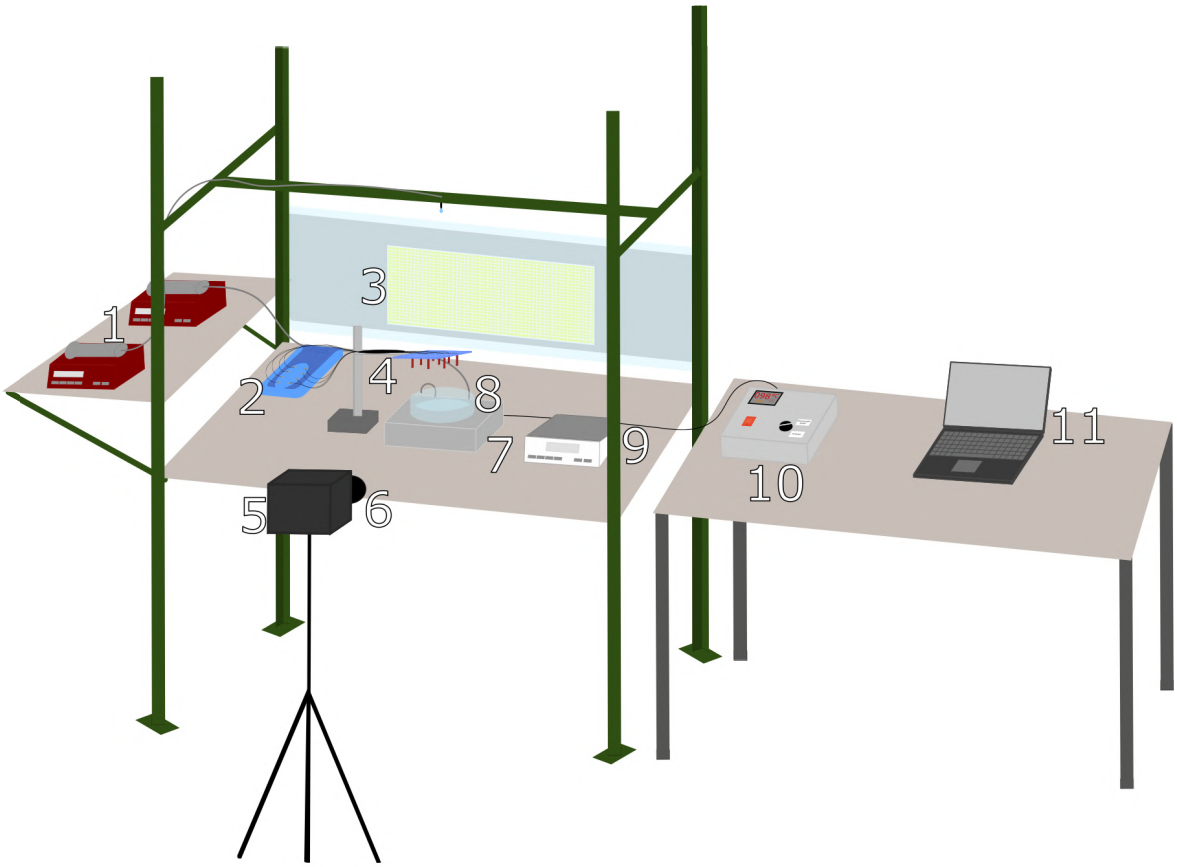

Figure 3.1: Schematic of the experimental setup: 1– Syringe pumps; 2– Thermocouple data logger; 3– Illumination; 4– Type-K thermocouples; 5– High-speed camera; 6– Macro lens; 7– Aluminium block; 8– Borosilicate container; 9– Precision Scale; 10– Aluminium block temperature control box; 11– Computer.

3.1.1 Image Acquisition System

As a standard for these studies, a great image acquisition system is necessary to acquire images with a certain degree of accuracy and quality. Keeping in mind the previous necessary features, the camera used was a Photron FASTCAM mini UX50, with an image resolution of 1.3 Megapixel at frame rates from 2 000 fps up to 160 000 fps at a reduced image resolution. In order to provide the optimal visualisation of the impact, the camera was equipped with a Macro Lens Tokina AT-X M100 AF PRO D with a minimum focus distance of $0.3\ m$, a focal length of $0.1\ m$, a macro ratio of $1:1$ and a filter size of $55\ mm$ (Fig. 3.2).

The high-speed camera was triggered manually, as explained previously in section 3.1. In order to get an optimal visualisation of the phenomena caused by the droplets impact, a frame rate of $4\,000\ fps$ and an exposure time of $1/8000\ s$ were used. This resulted in a time interval of $0.25\ ms$ between frames and resolution of 1280×512. While the camera was operated with an angle $(5° - 10°)$ the exposer time was increased to $1/6250\ s$. These parameters were used in the main experiments, with an angle due to the Marangoni effect. While for the impact velocity, the camera was positioned without any angle. There was an exception to these camera parameters in the impact velocity, for the maximum height of the setup it was necessary a frame rate of $10\,000\ fps$ to capture the droplet properly. The tests for determining

Figure 3.2: Photron FASTCAM mini UX50 and the Macro Lens Tokina AT-X M100 AF PRO D.

the droplet diameters were executed with a camera exposure of $1/5000 s$, a reduced frame rate of $2\,000\ fps$, which resulted in a time interval of $0.5\ ms$ between frames and a resolution of 1280×1024.

3.1.2 Droplet Dispensing System

For this experimental study, it was necessary to form and dispense droplets with precision and controllability. In order to provide that, it was used a medical syringe pump NE-1000, figure 3.3. This device has an operation capacity of $1.459 \mu l/h$ with a $1 ml$ syringe and $127.2 ml/min$ with a $60 ml$ syringe. Besides that, the pump can be programmed and controlled from a computer. In this case, a $50 ml$ syringe was used with a pumping rate of $0.300 ml/min$. A medical tube connected the syringe to a straight-tip stainless steel needle. A second pump was also applied to compensate for the fluid evaporation rate and help maintain the film thickness constant during the experiments.

Figure 3.3: Syringe pump NE-1000.

The droplets originated from a straight tip of a stainless steel needle and detached when

the gravitational effects exceeded the surface tension forces. The needle selected for this work had an internal diameter of $0.84\ mm$, figure 3.4. This provided similar diameters for the two fluids, which was important in order to evaluate how the temperature affected the dynamics of the impact, as a consequence of the variation of properties of the fluids with the temperature.

Figure 3.4: Stainless steel needle.

3.1.3 Impact Surface

In this experimental study, the droplets must impinge on a heated liquid film. For this reason, it was needed a container that could hold the liquid film and withstand the different range of temperatures used in this study. The container was made of borosilicate glass since it has a low coefficient of thermal expansion, it is more resistant to thermal shock than any other common type of glass. It also has a very precise optical surface that is practically unchangeable with temperature, making it, for these reasons, a good choice for optical access with the high-speed camera. The container is composed of a hollow cylinder with an internal diameter of $120\ mm$, an external diameter of $130\ mm$ and a height of $50\ mm$. The cylinder was then glued to a $150 \times 150\ mm$ flat borosilicate glass (Fig. 3.5). To assemble both pieces together, it was used acetoxy silicone because this type of adhesive can withstand a maximum temperature of $250°\mathrm{C}$, which is enough since in this work the temperature does not go beyond $120°\mathrm{C}$, and besides that, it is compatible with various types of glass. The reason for this type of assembly was to avoid the curvature present in "one-piece" containers, like Petri dishes, that distorted and made difficult the observation of the phenomena.

3.1.4 Illumination

Since it was needed to observe the different phenomena properly, an excellent illumination source was required. A $96\ W$ LED array was created by attaching LED ribbons to a wooden panel, as demonstrated in figure 3.6. This LED array was powered by a power supply, which functions as a transformer converting alternating current into direct current to achieve a more efficient and uniform illumination. In order to obtain the improved results of the illumination, the whole room was dark except for the LED array switched on. The LED array was placed parallel to the droplet falling plane and a diffusive glass was placed between the

Figure 3.5: Borosilicate container.

array and the impact site, once again to help provide a uniform light source.

(a)

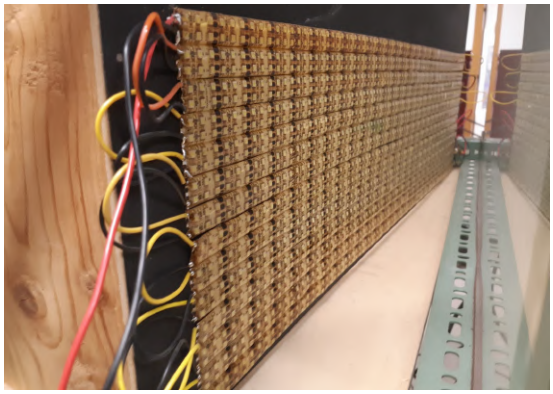

(b)

Figure 3.6: (a) Power supply; (b) LED array.

3.1.5 Heating Element

The heating element, figure 3.7a, is made of Aluminium 5083 which has an exceptional performance to withstand high temperatures. The dimensions of the block are $150 \times 150\ mm$. In order to heat the aluminium block, four cartridge heaters of $250\ W$ are embedded inside it and distance evenly in order to distribute uniformly the heat across the surface. Appendix A.1 shows the technical drawing of the aluminium block, which contains more information. Figure 3.7b shows the control box of the aluminium block. To measure the temperature of the block, there are two options, an IR (infrared) sensor or a type-K thermocouple. The last thermocouple is embedded in the middle of the aluminium block and was the one used to measure the temperature of the aluminium block during these experiments.

(a) (b)

Figure 3.7: Heating element: (a) Aluminium block with four 250W cartridge heaters and one embedded type-K thermocouple; (b) Aluminium block control box.

3.2 Fluids Thermophysical Properties

Since the temperature of the fluids varied, their properties also changed. The ideal would be to study aviation fuels in use, such as Jet A-1, a common aviation fuel, and Neste Renewable Diesel (NExBTL), a biofuel. Although, these are multi-component substances, resulting in non-linear evaporation rates since the different fluids that constitute them have different saturation temperatures. This also results in the variation of their thermophysical properties not only with the temperature but also with the current fluid present, since once one component evaporates the remaining liquid is a new multi-component fluid. In order to circumvent this problem, for this work two simple carbon chains substitutes, N-Heptane and N-Decane were selected. The reason behind the selection of these two fluids is connected with the fact that they are surrogate fuels, therefore acting like a good intermediate step before the experiments with multi-components fluids. In addition, the saturation temperature of these two fluids is distanced from their auto-ignition point, making it easy to work with them at higher temperatures. The variation of properties with the temperature of these single-component fluids is well-defined in the literature. For these reasons, the N-Heptane and N-Decane represent a good starting point in the pursuit of investigating the effect of the temperature of the liquid film when a droplet impacts it.

Knowing that the thermophysical properties of the fluids change with the temperature, it was necessary to define these variation curves. Defining this data was an important step, in order to be able to evaluate how outcomes were affected by the temperature. The equations for the

curves of variation were obtained from *Chemical properties handbook* by Yaws [75] and are present in appendix A.2.

3.2.1 Density

According to the *Handbook of Aviation Fuel Properties* [76], density (ρ) is defined in terms of mass per unit volume of a substance or object at a particular temperature. It is usually expressed in kg/m^3 and represented by equation (3.1):

$$\rho = \frac{m}{V} \quad (3.1)$$

where m is the mass and V is the volume occupied by the substance.

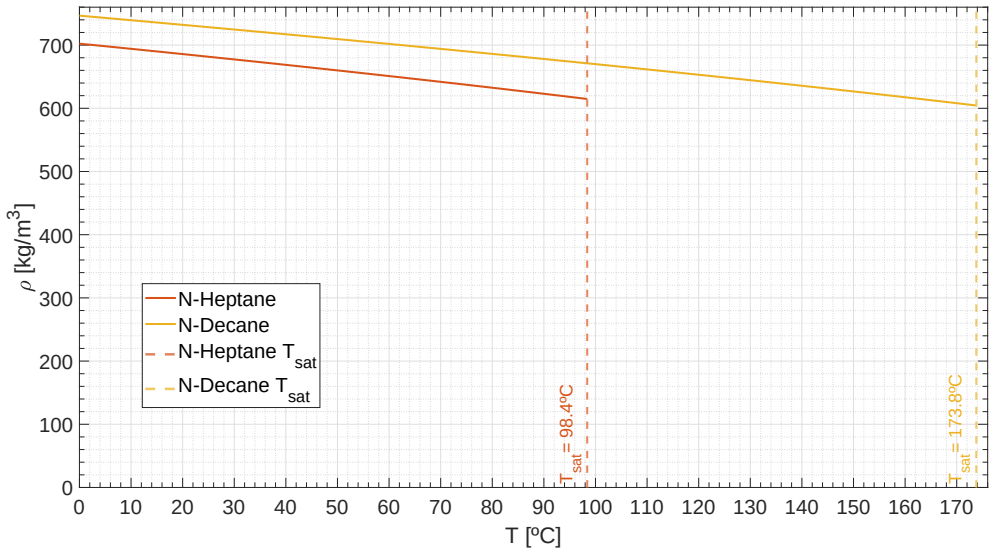

Figure 3.8: Fluids density variation with temperature.

Figure 3.8 shows the variation of the density of both fluids until their saturation temperature. This information is crucial in order to determine the correct mass of fluid, needed to create the volume of fluid necessary for a certain liquid film thickness at a specific temperature. It is possible to see that both fluids density decreases with the temperature. Moreover, both have a similar decreasing rate.

3.2.2 Surface Tension

The surface tension (σ) is defined, by the *Handbook of Aviation Fuel Properties* [76], as the specific free energy at the interface with another fluid. Generally, the surface tension values are reported when the fluid is in contact with air.

In figure 3.9 is represented the variation of the surface tension of both fluids with the temperature. As seen previously with density, the surface tension of both fluids decreases with the temperature and their decreasing rate is similar.

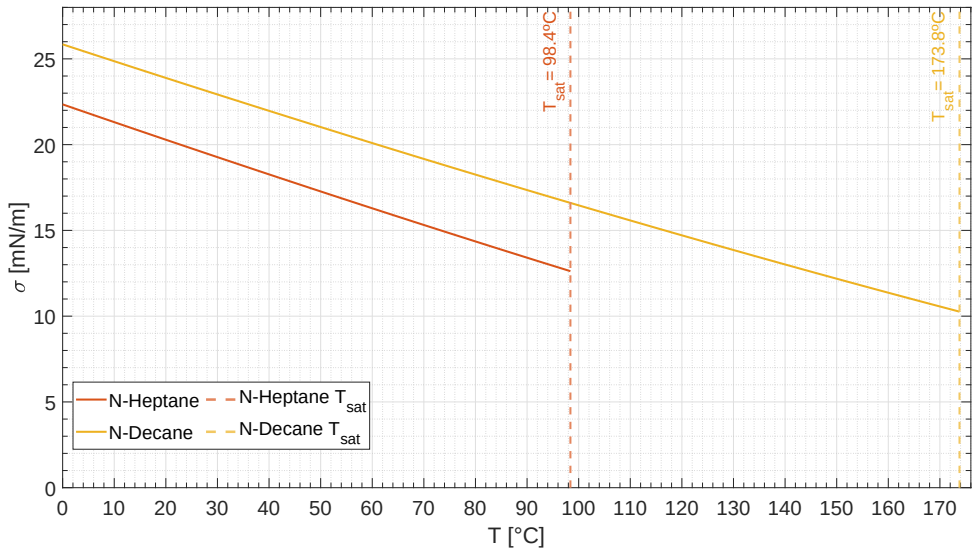

Figure 3.9: Fluids surface tension variation with temperature.

3.2.3 Viscosity

The viscosity (μ) of a fluid is a measure of its internal resistance to motion caused by cohesive forces among the fluid molecules, according to the *Handbook of Aviation Fuel Properties* [76].

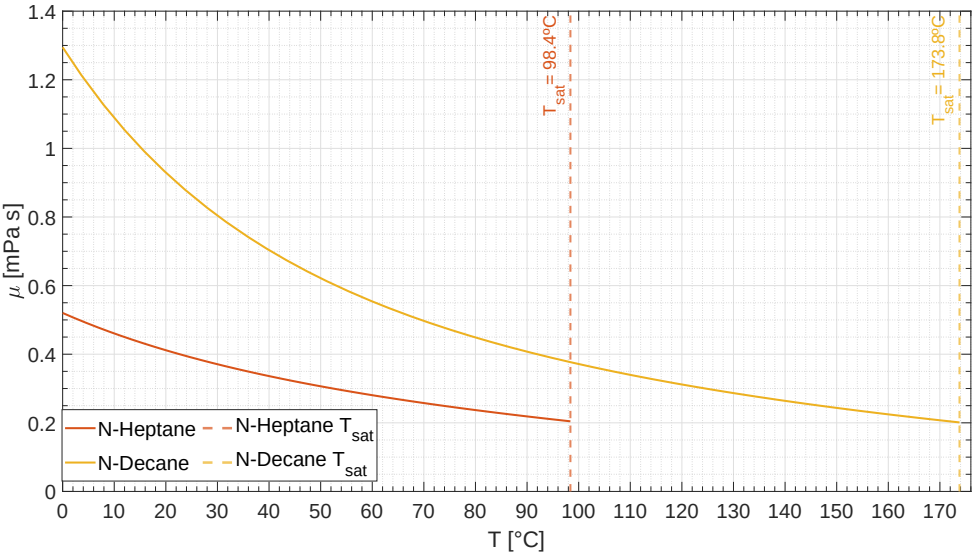

Figure 3.10: Fluids viscosity variation with temperature.

Figure 3.10 shows the variation curves of the viscosity of the fluids. Once again, like the density and the surface tension, the viscosity decreases with the temperature. Although, contrary to what was observed in the previous properties, the decreasing rate of the N-Decane is higher than the N-Heptane in the same temperature interval. The N-Decance demonstrates a clear faster decreasing rate than the N-Heptane.

3.3 Methodology

In order to perform this work, planning the methodology was a necessary step. This section will be dedicated to explaining how the experiments were performed in a rather detailed way.

This thesis has the main goal to investigate the dynamics of an isolated droplet impacting on a heated liquid film and evaluate if the correlations created for droplet impact onto non-heated films can be applied in this regime. In order to achieve that, several experiments were performed, and a work plan was devised based on the previous works in isothermal film and heated dry surfaces since research related to droplets impacting on heated liquid films is scarce at the moment.

In the first stages of studies, the camera was kept parallel to the droplet falling plane. The objective at this point was to determine the impact velocity and droplet diameter. In order to achieve the former, the fall of the droplet was recorded until the moment of impact, leaving the following frames after the impact out of consideration.

The purpose of this work is to determine the applicability and validation of the current isothermal spread/splash and bubble encapsulation thresholds for heated films. For that, several droplet falling heights were established, ranging between $y = 100\ mm$ and $y = 2250\ mm$. In every test, it was taken an image of the background and one with the reference, so it was possible to determine the pixel size. The images obtained in this first part were necessary to determine the droplet diameter and impact velocity for each fluid. These results were essential to define the liquid film thickness and determine the non-dimensional numbers with which it was possible to determine the optimal starting points to investigate the influence of the temperature in the dynamics of a droplet impinging upon a heated liquid film.

The second part consisted in recording multiple experiments with constant initial impact conditions, at least ten, in order to obtain a large enough sample of the impacts, so the probabilistic results could have an acceptable validity. During the tests, the camera was positioned with a slight angle, between $5° - 10°$, in order to improve the visualisation of the outcome of the droplet impacting the liquid film. Moreover, the liquid film temperature initiated at room temperature $(20°\mathrm{C})$ and was gradually increased up to $70°\mathrm{C}$ for the N-Heptane and $120°\mathrm{C}$ for the N-Decane, the reason for these temperature intervals is explained later in section 4.1.1. The implementation of the angle in the camera was due to the higher temperatures. In these temperatures, the fluid of the liquid film started to accumulate a thin layer in the glass of the container (Marangoni effect), this made difficult the image acquisition since it would cause a blur effect on the image. Giving the camera a slight angle allowed capturing the images from a point-of-view (POV). Where it was possible to reduce significantly the blurring effect or in some cases avoid it since the line-of-sight was above the thin layer of fluid.

Since the droplets were impinging into a liquid film, it was of utmost importance to define h^* in accordance with d_{drop}. The chosen relative film thickness was $h^* = 1$. The liquid film

thickness h was calculated in accordance with the droplet diameter obtained during the first part, and as explained in section 3.1. The method implemented to produce the liquid films consisted in determining the necessary volume of fluid. Then, the mass was calculated in accordance with the volume and the fluid density at a specific temperature. During the experiments, the thickness of the liquid film was kept constant by weighting the container to ensure the correct mass, and by using a second syringe pump to compensate for the fluid evaporated. The error associated with this method was of $\pm 0.01\ g$, which corresponds to approximately $\pm 1\ \mu m$ in the height of the fluid in the container. With this information, it is possible to consider this method precise.

During these experiments, one of the goals was to observe different outcomes. With these tests, it was possible to observe the different dynamic behaviours of the droplet impact and assess the influence of the liquid film temperature.

3.4 Data Processing Methods and Measurements Techniques

The use of high-speed cameras in engineering and scientific research has facilitated the visualization of experiments. As shown in chapter 2, to analyse and evaluate the outcomes and recur to the already created thresholds criteria one must first know not only the fluids properties but also the droplet parameters such as its diameter and impact velocity, in order to be able to calculate the non-dimensional numbers. Besides the non-dimensional numbers, the droplet diameter will also be used to determine the height of the liquid film. This information was acquired through the use of image data processing. Recurring to the software MATLAB, multiple algorithms were developed and with these codes and the use of the Image Processing Toolbox, it was possible to process, analyse and visualise the data.

This section will be, therefore, dedicated to presenting and explaining the methodologies used to process the data including image treatment, binarization, pixel sizing, etc.

3.4.1 Droplet Diameter

As mentioned before, obtaining the diameter of the droplets was a crucial step, since these results are needed to determine the liquid film thickness that should be present in the container. Since it is intended to evaluate how the properties of the fluids affect the dynamics of the impact, the droplet diameter between fluids was approximately identical. The camera was placed parallel to the droplet falling plane to obtain the necessary frames to determine the droplet diameter. For the sake of improving precision, it was made a minimum of five tests for each fluid.

To begin, the frames that were going to be analysed in MATLAB were selected (≈ 100 frames). The selection of the frames was made in order to get all the frames of the droplet completely isolated and after the major oscillations that the drop has immediately after leaving the needle until the last frame before leaving the field-of-view. A background image without any

droplet was also necessary, this would be used posteriorly, subtracting it from the droplet frames, allowing for more easy processing and analysis. Figure 3.11a shows an image of the background, while figure 3.11b displays an image of the droplet.

(a) (b)

Figure 3.11: Droplet diameter process:(a) Background image (b) Droplet frame.

Shortly, the algorithm takes the background image and subtracts it from the frames of the droplet falling. This way, the images are only left with the droplet, figure 3.12a. After the subtraction, it is possible to see in the needle some residual fluid is present. To avoid that in the analysis, the image is cut to remove it, figure 3.12b. The last step is the binarization of the images with the application of a binary filter to eliminate possible errors and noise associated with imaging processing. This way pixels would be removed below a specific threshold, outside the droplet perimeter, figure 3.12c. These errors can appear due to possible dust particles or even small reflexes.

(a) (b) (c)

Figure 3.12: Data processing steps to obtain the droplet diameter: (a) Subtraction of the background to a droplet frame; (b) Image cutting; (c) Binarization of the image with a filter.

With this process completed, the images are ready to be analysed and calculate the values of the droplet diameter. In order to perform such a task, two measurements were made, the vertical and the horizontal maximum length. The reason for such a decision is due to the oscillation of the droplet along its fall. As said before, the frame selection is made in order to remove the initial ones immediately after the drop leaves the needle due to a rapid oscillation of its form, after this during the rest of the fall the droplet still has a small oscillation. These small oscillations are taken into account when measuring the horizontal and vertical

diameters, figure 3.13. Considering this and in order to verify the droplet spherical form, all the vertical and horizontal lengths of every droplet, from the first selected frame until the last one, were considered, and their mean values were found.

Figure 3.13: Assembly of four frames, each separated by 20 ms representing the shape-shifting of the falling droplet along the fall.

Both the vertical and horizontal maximum lengths were determined using the MATLAB algorithm, where the matrix resulting from the image conversion to binary is only composed of ones and zeros, with a white pixel representing a 1 and a black one representing a 0. Then, the code would detect the column that contained the first 1 to appear, and then detect the column where appeared the last 1, by subtracting this last column from the first, the number of horizontal pixels is obtained. With this, the algorithm could obtain the horizontal length and in a similar process, the vertical length would be the subtraction between the row with the last 1 to appear and the row that contained the first 1. This process would be repeated for each column and row, and then the algorithm outputs the highest value of each length. Obtaining this way the maximum horizontal and vertical lengths.

As said previously, a minimum of five experiments were made and the mean diameter was calculated in all of these, i.e. the average value between all the vertical and horizontal maximum lengths. With the mean diameter of each test, the algorithm would perform the average of all the mean diameters, with the resulting value being the droplet diameter. In addition to that, for each case studied the droplet diameter was also confirmed again in a way to verify if the impact height had any influence on it. These values were all measured in pixels, so it was necessary to multiply them by the pixel size, to obtain the corresponding length. The droplet was considered spherical in these experiments, on the grounds that the differences between the vertical and horizontal maximum lengths never exceed 2.5 % of the droplet diameter.

3.4.2 Impact Velocity

For this thesis, it was necessary to analyse the droplets impact on the liquid film, so it was indispensable to calculate non-dimensional factors such as the Reynolds, Weber and Ohnesorge numbers. Since the properties of the fluids were already obtained and, as shown previously, the droplet diameter also, the last parameter that is missing to determine the non-

dimensional numbers is the impact velocity of the drop.

Recurring a similar process as described previously for the droplet diameter, an algorithm on MATLAB was implemented to determine the impact velocity of the droplet.

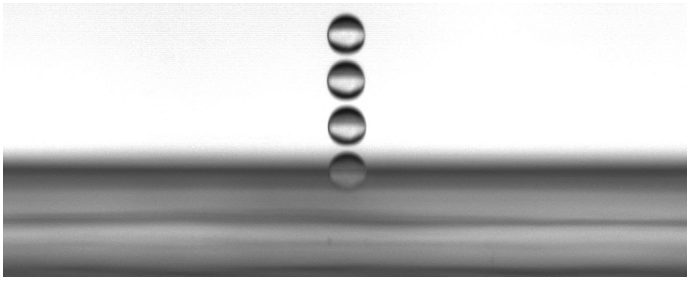

Figure 3.14: Assembly of four frames separated by $1\ ms$ of the falling droplet, including the immediate frame before impact.

In order to calculate the impact velocity, it was necessary to find the droplets centroids. To address this problem, the algorithm identified the droplet boundaries and then calculated the centroid position, as seen in figure 3.15 represented by the green cross. These images passed through processing in part identical to the droplet diameter. The algorithm would subtract the background to each frame, transform the frames into binary, and identify the droplet and its perimeter. After this, the last frame prior to impact, and the one immediately before were selected, knowing that the frame rate of the camera was $4\,000\ fps$ and as mentioned in section 3.1.1, this would imply that the time interval between frames is $0.25\ ms$. The only exception to this was to measure the impact velocities of corresponding to the highest height of the facility. For this height it was used a frame rate of $10\,000\ fps$, resulting in an interval between frames is $0.1\ ms$

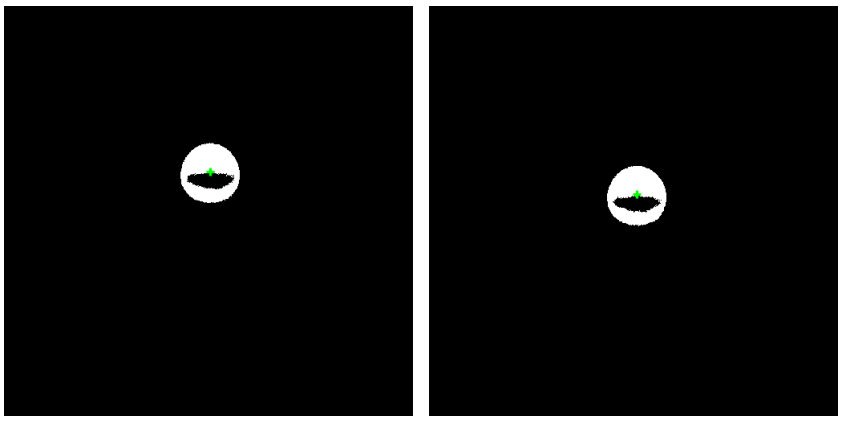

Figure 3.15: Two frames used to calculate the impact velocity, in both drops the centroid is represented by the green cross.

With this information and calculating the pixels travelled by the droplet, which when multiplied by the pixel size gives the distance travelled by the drop itself. Dividing the distance by $0.25\,ms$ the impact velocity is obtained. As in the diameter determination, a minimum of five tests were made and the mean value of them was the selected value for the impact velocity of

the drop.

3.4.3 Pixel Sizing

The measurements of this work were made through the images acquired by the high-speed camera, thus scaling them became an important step. At the beginning of each test, an image with a reference was taken to establish the proper pixel size. The reference chosen for this work was a needle with an outer diameter (D_{out}) of $1.82\ mm$. Recurring, once again, to the software MATLAB, an algorithm was written to essentially measure the number of pixels that correspond to the size of the chosen reference. Later, with the input of the reference size, the algorithm can determine the pixel size by dividing the reference size by the number of pixels in the image. The image processing is similar to the ones mentioned previously in sections 3.4.1 and 3.4.2, although in this one the background subtraction was not necessary, since no moving targets such as a droplet were present and the reference was completely isolated. The image was cut to around 20 rows of pixels and then binarized. After that, the algorithm outputs the position of the first white pixel found in the direction of the x axis and the last one. The distance between these two pixels would match the reference size. The rows chosen were to ensure the reference vertical position and to avoid any errors.

According to the *Springer Handbook of Experimental Fluid Mechanics* [77], the measurements of an object length in a digital image with pixel positions with grey values associated, can only be determined with an accuracy of ± 0.5 pixel. Since the pixel sizing in these essays varied from $0.0289\ mm/pixel$ to $0.0394\ mm/pixel$, the length measurements would have a minimum and maximum error of $\pm 0.014 mm$ and $\pm 0.017\, mm$, respectively. For the diameter measurements along this work, displayed in section 4.2.1, it was considered the maximum error, i.e., $\pm 0.017\ mm$.

The values of the impact velocities, displayed in section 4.2.2, were calculated with a minimum and maximum error of $\pm 0.058\ m/s$ and $\pm 0.152\ m/s$, respectively. This error is determined by the ratio between half a pixel and the time between the two frames ($0.25\ ms$) used to calculate the impact velocity.

Chapter 4

Results and Discussion

This chapter will be dedicated to presenting the results of the experiments performed. Firstly, it was necessary to determine the liquid film temperature depending on the aluminium block temperature, due to heat losses between the aluminium block and the liquid film. Moreover, each fluid evaporation rate and film temperature will be presented in different ranges of temperatures, adequate to the saturation temperature of each fluid. This information is needed in order to apply the correct volume of the liquid film according to the temperature, due to the variation of the thermophysical properties of the fluids, and to compensate for the losses due to evaporation.

The second section will be dedicated to the impact characterisation, where the droplets diameters and impact velocities will be determined. Having determined the droplet diameter and the variation of the thermophysical properties of each fluid presented in section 3.2, it is conceivable to define the liquid film thickness and calculate the non-dimensional numbers.

The third section will focus on the visualisation of the phenomena and evaluation of the applicability of the current thresholds for spread/splash and bubble encapsulation. This comparison allows for assessing if the liquid film temperature causes a drastic change in the dynamics of the impact, or if its influence is inconsequential when compared with the isothermal thresholds.

Finally, the last section will focus on the necessary adaptations to the current thresholds and on the graphical framing of the obtained results within the adapted correlations.

4.1 Liquid Film Characterisation

Since the thermophysical properties of the fluids varied with temperature, it was important to determine the liquid film temperature. This was a necessary step, in order to calculate the non-dimensional numbers of the liquid film and to calculate the correct mass of fluid necessary to achieve the desired liquid film thickness, as explained in section 3.2.1. Moreover, the evaporation rates for each fluid were also necessary to compensate for the variation of fluid, this way maintaining constant the liquid film thickness. The following subsections will present the results of these two measured properties.

4.1.1 Temperature Measurements

This work studied single droplet impact on a heated liquid film. One of the goals is to assess the effect of the liquid film temperature upon droplet impact dynamics. As mentioned before in section 3.2, the fluids selected were N-Heptane and N-Decane. To compare them, the non-dimensional temperature (θ) was used. This term essentially is the ratio between two differences, the film temperature (T_{film}) with the ambient temperature (T_0), and the fluid saturation temperature (T_{sat}) with the ambient temperature (T_0), equation (4.1). The range chosen was $\theta = [0, 0.6]$. Since this is an initial study, it makes sense to start with lower temperatures, and in order to avoid approaching the saturation temperature of the fluids the maximum temperature was limited to $\theta = 0.6$. As already shown in the graphics present in section 3.2, the N-Heptane and the N-Decane have a saturation temperature of $T_{sat} = 98.4°\mathrm{C}$ and $T_{sat} = 173.8°\mathrm{C}$, respectively.

$$\theta = \frac{T_{film} - T_0}{T_{sat} - T_0} \quad (4.1)$$

In order to be able to calculate the non-dimensional liquid film temperature, first was necessary to determine the temperature of the liquid film. To take these measurements, it was used a set of six thermocouples type-K. These thermocouples were submerged in the liquid film distanced $1\ cm$ between them and positioned as shown in figure 4.2. These measurements consisted of two phases. The heating phase consists in increasing the liquid film temperature until this stabilises, as can be seen in figure 4.1 between $t = [0, 1000]\ s$. The second phase is the stability phase, where the temperature of the liquid film was stable, as can be seen in figure 4.1 $t > 1000\ s$, and the measurements for the average temperature of the liquid film could begin.

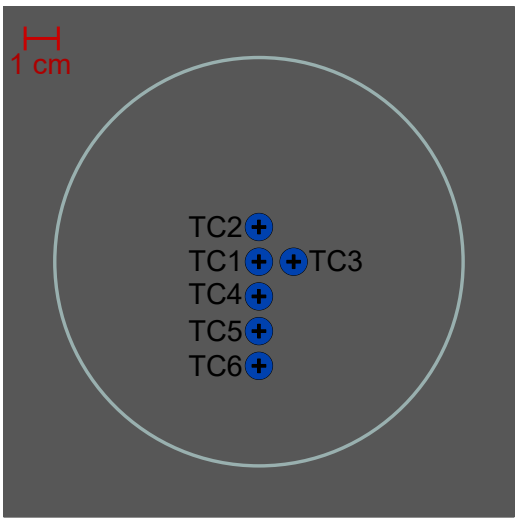

Figure 4.1: Thermocouples position in the block.

Figure 4.3 and figure 4.4 show the temperature measured in these tests, including the quadratic equation that represents the best fit to each fluid, with a coefficient of determination $R^2 \geq 0.99$.

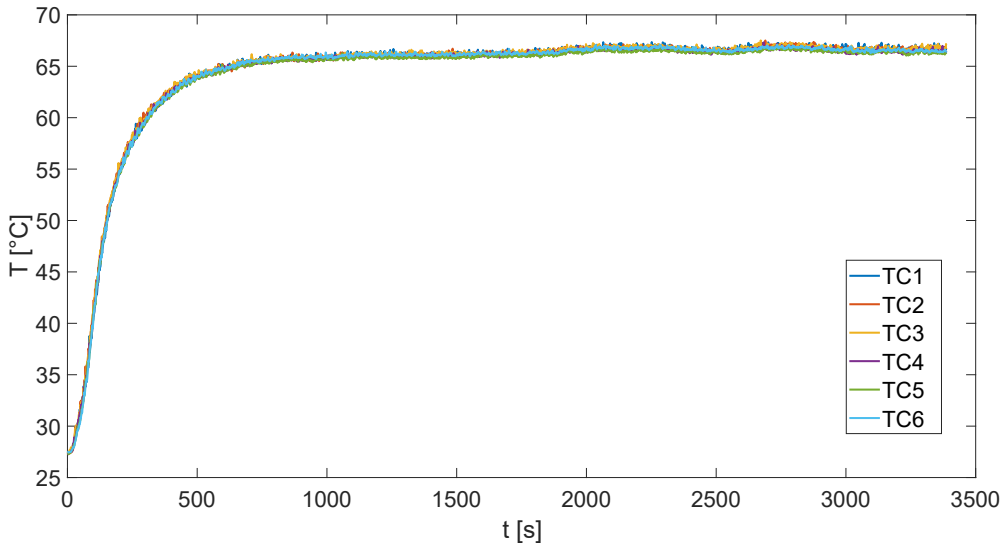

Figure 4.2: Heptane film temperature measurements of each thermocouple (TC) for $T_{block} = 70°\mathrm{C}$.

Having these measurements of the liquid film, it is possible to define the target temperatures for the desired θ in accordance with the aluminium block temperature, table 4.1. The maximum relative error associated with these temperature measurements was 0.45% for the N-Heptane and 0.43% for the N-Decane.

Table 4.1: Non-dimensional temperature interval and relation between T_{film} and T_{block} for each fluid.

Fluid	$\boldsymbol{\theta}$	$\boldsymbol{T_{film}}$ [°C]	$\boldsymbol{T_{block}}$ [°C]
C_7H_{16} (N-Heptane)	0	20	20
	0.2	36.5	37
	0.4	48.8	50
	0.6	66.6	70
$C_{10}H_{22}$ (N-Decane)	0	20	20
	0.2	49.2	50
	0.3	68.2	70
	0.4	86.9	90
	0.6	114.1	120

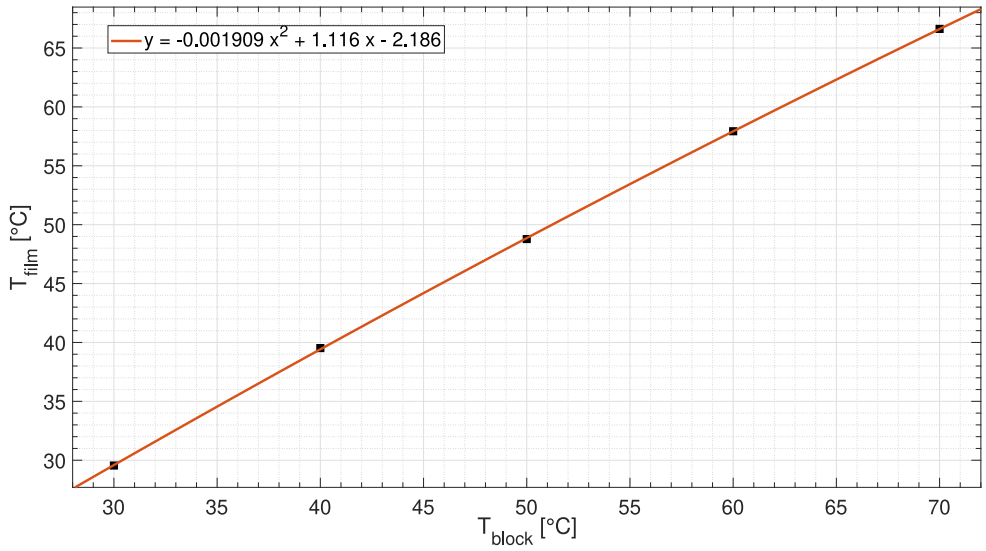

Figure 4.3: N-Heptane film temperature in relation to the temperature of the aluminium block

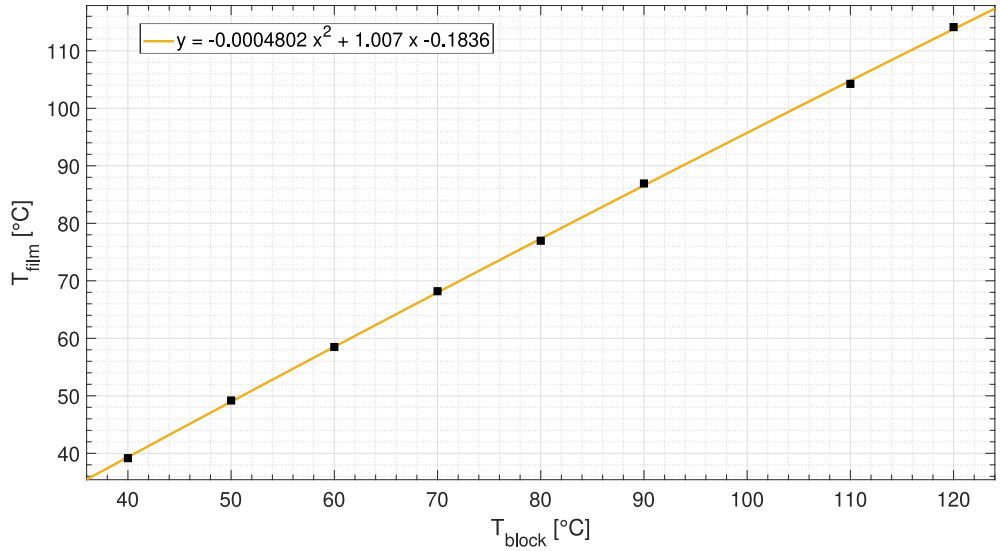

Figure 4.4: N-Decane film temperature in relation to the temperature of the aluminium block.

4.1.2 Evaporation Rate

In order to keep the liquid film thickness constant throughout the experiments, it was necessary to determine the evaporation rates of the different fluids. These consisted in filling the container with a certain amount of fluid. Afterwards, a target temperature would be set for the aluminium block. When this temperature was achieved, the container with the fluid would be set on top of it. Before starting to measure the evaporated mass, it would be necessary to wait at a minimum of ten minutes to let the temperature of the film stabilize. Subsequently, recurring to a precision scale, the mass of fluid present in the container was measured. With the initial mass obtained, the container was set again on the heated surface in order to continue the analysis. The container mass was measured in intervals of five minutes for a period of approximately one hour. This way, it was possible to determine the

evaporation rate in g/min for each fluid at specific predetermined temperatures. To minimize thermal losses, the measurements of the mass were performed as fast as possible.

Figure 4.5 and figure 4.6, represent the variation of the evaporation rate depending on the temperature of the aluminium block, in g/min. Since the fluid evaporates and causes a decrease in the mass of the liquid film, the curves were plotted to represent this loss by having negative variation values. The optimal fit found, for both fluids, was a cubic curve, with a coefficient of determination $R^2 \geq 0.99$.

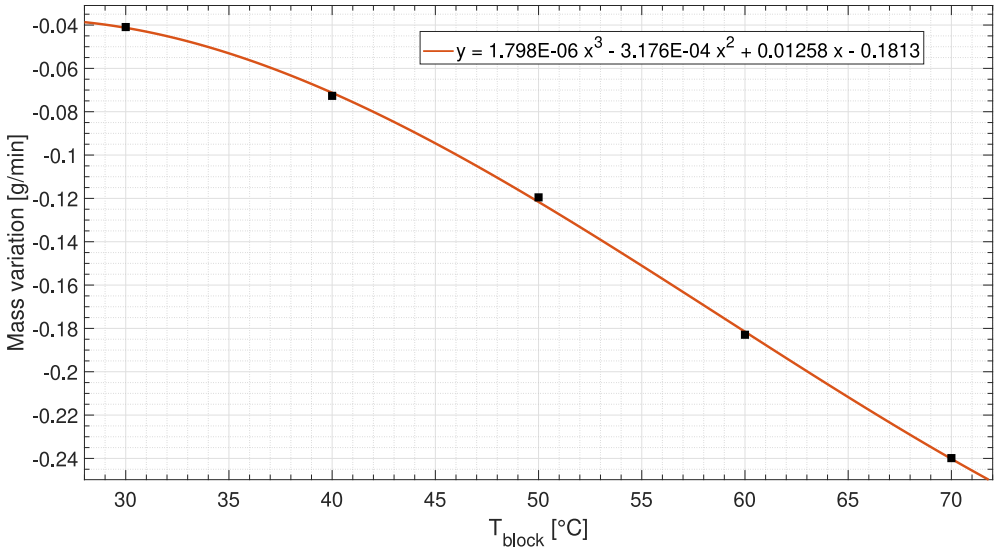

Figure 4.5: Variation of the N-Heptane evaporation rate depending on the temperature of the aluminium block.

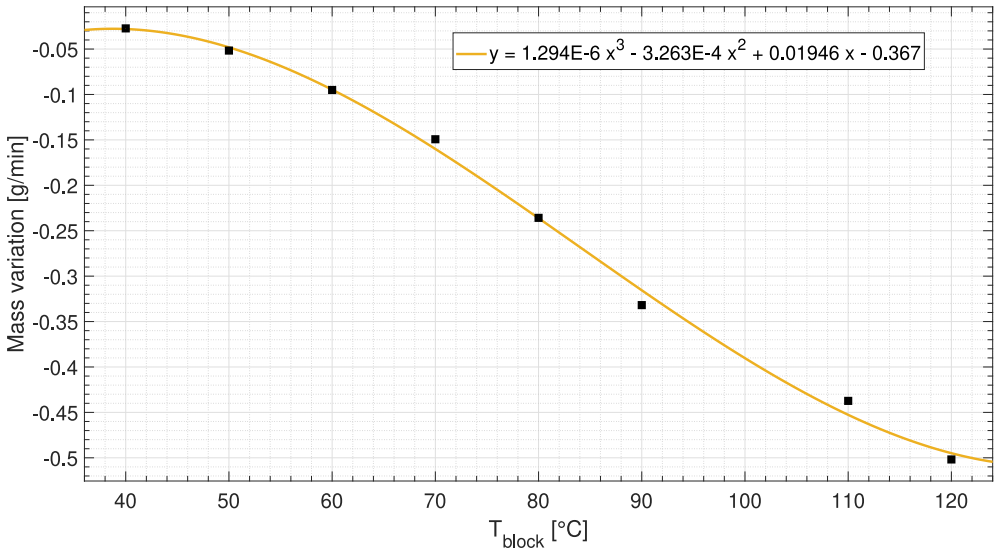

Figure 4.6: Variation of the N-Decane evaporation rate depending on the temperature of the aluminium block.

Analysing figure 4.5 and figure 4.6, it is possible to see that for the same interval range, $T_{block} = [40, 70]$, the N-Heptane was a slightly higher evaporation rate, this can be explained

due to the differences in the saturation temperature. The maximum relative error associated with these measurements was 0.59% for the N-Heptane and 1.2% for the N-Decane.

4.2 Impact Characterization

To achieve the goal of this work, it is necessary to observe the occurrence of the different phenomena although, before we can do that, it is important to determine important features. As explained in section 3.4, both the droplet diameter, d_{drop}, and its impact velocity, v_{drop}, were measured recurring to a MATLAB algorithm. The next subsection will present these values, as well as the non-dimensional numbers and the liquid film thickness, calculated in accordance with the droplet diameter and the thermophysical properties of the fluids. These parameters are crucial for a later part of the work, where they will be necessary to used and adapt the correlations.

4.2.1 Droplet Diameter

The first measurements to be obtained are the droplet diameters. Table 4.2 shows the diameters of the different fluids for all the cases studied, using a needle with an inner diameter of $D_{in} = 0.84\,mm$. As explained in subsection 3.4.1, to determine the droplet diameter five experiments were made for each fluid and the mean value was used. It was also verified that the droplet diameter does not change with the impact height. The maximum error was considered for these measurements, as explained in section 3.4.1.

Table 4.2: Droplet diameters used in the experiments.

Fluids	**Diameter** $[mm]$
C_7H_{16} (N-Heptane)	2.6 ± 0.017
$C_{10}H_{22}$ (N-Decane)	2.7 ± 0.017

As can be seen in table 4.2, the diameter of the N-Decane and the N-Heptane are similar while using the same dispensing needle diameter. During these experiments, the tip of the needle was always cleaned before every test to avoid liquid accumulation. However, no chemical treatment or substance was applied or employed to avoid wetting.

4.2.2 Impact Velocity

Recurring to the method previously explained in 3.4.2, the impact velocities were determined for all the impact heights. Table 4.3 shows the mean value of at least five tests for each case.

To determine the impact velocity, the frames were the last one before impact and the one immediately prior to it. The impact velocities vary between $1.3\,m/s$ and $5.0\,m/s$. Both fluids present similar droplet impact velocity and droplet diameter, only having a slight variation.

Table 4.3: Impact Velocities used in the experiments

Fluid	**Impact Height** $[mm]$	v_{drop} $[m/s]$
C_7H_{16} (N-Heptane)	100	1.3 ± 0.059
	130	1.5 ± 0.059
	150	1.6 ± 0.058
	190	1.7 ± 0.059
	970	3.7 ± 0.058
	1000	3.9 ± 0.069
	2250	4.9 ± 0.144
$C_{10}H_{22}$ (N-Decane)	130	1.6 ± 0.058
	150	1.7 ± 0.063
	190	1.8 ± 0.059
	970	3.8 ± 0.060
	1000	4.0 ± 0.070
	2250	5.0 ± 0.152

4.2.3 Non-dimensional Numbers

In these experiments, three non-dimensional numbers were considered, these were, Ohnesorge, Weber and Reynolds numbers. The description of these non-dimensional numbers was presented in section 2.1. Both the Weber and Reynolds numbers depend on the impact velocity, therefore these were calculated for every height. However, the Ohnesorge number is only dependent on the properties of the fluid, meaning that impact velocity differences would not affect it, as can be seen in table 4.4.

In order to study the application of the thresholds, it was necessary to provide a wide range of conditions (Table 4.4). Analysing the table, it is possible to identify the following ranges, $3402 \leq Re \leq 21227$; $149 \leq We \leq 2110$; $2.164 \times 10^{-3} \leq Oh \leq 4.277 \times 10^{-3}$.

Table 4.4: Non-dimensional numbers used in the experiments (Oh_{drop}, We_{drop} and Re_{drop})

Fluid	**Impact Velocity** $[m/s]$	$\boldsymbol{Oh_{drop}} \cdot 10^3$	$\boldsymbol{We_{drop}}$	$\boldsymbol{Re_{drop}}$
C_7H_{16} (N-Heptane)	1.3	2.164	149	5632
	1.5		198	6498
	1.6		225	6931
	1.7		254	7365
	3.7		1203	16029
	3.9		1337	16895
	4.9		2110	21227
$C_{10}H_{22}$ (N-Decane)	1.6	4.277	212	3402
	1.7		239	3615
	1.8		268	3828
	3.8		1195	8081
	4.0		1258	8293
	5.0		2068	10633

4.3 Visualisation

This section has the purpose of showing images obtained during the experiments, as a way to better understand the outcomes observed in this work. The objective of this study was to attempt to validate the existing thresholds for spread/splash and bubble encapsulation. However, it was possible to find different phenomena: spreading, prompt splash, delayed splash, jetting and bubble encapsulation. During this section, it will be presented an example of each phenomenon encountered. Keeping in mind that for the objective of this work, the most relevant outcomes were the bubble encapsulation and splash, either prompt or delayed.

Figure 4.7a, shows a droplet of N-Heptane spreading in the liquid film, also referred to as deposition. This phenomenon is associated with low-impact kinetic energy, where the impinging droplet merges with the pre-existing liquid film. In this sequence, it can be seen that the droplet impacts into the liquid film ($\tau = 0$), forming a smooth crown ($\tau = 10$), spreading slowly through the liquid film ($\tau = 22.5$) dissipating the perturbation created and stabilising the film again ($\tau = 50$).

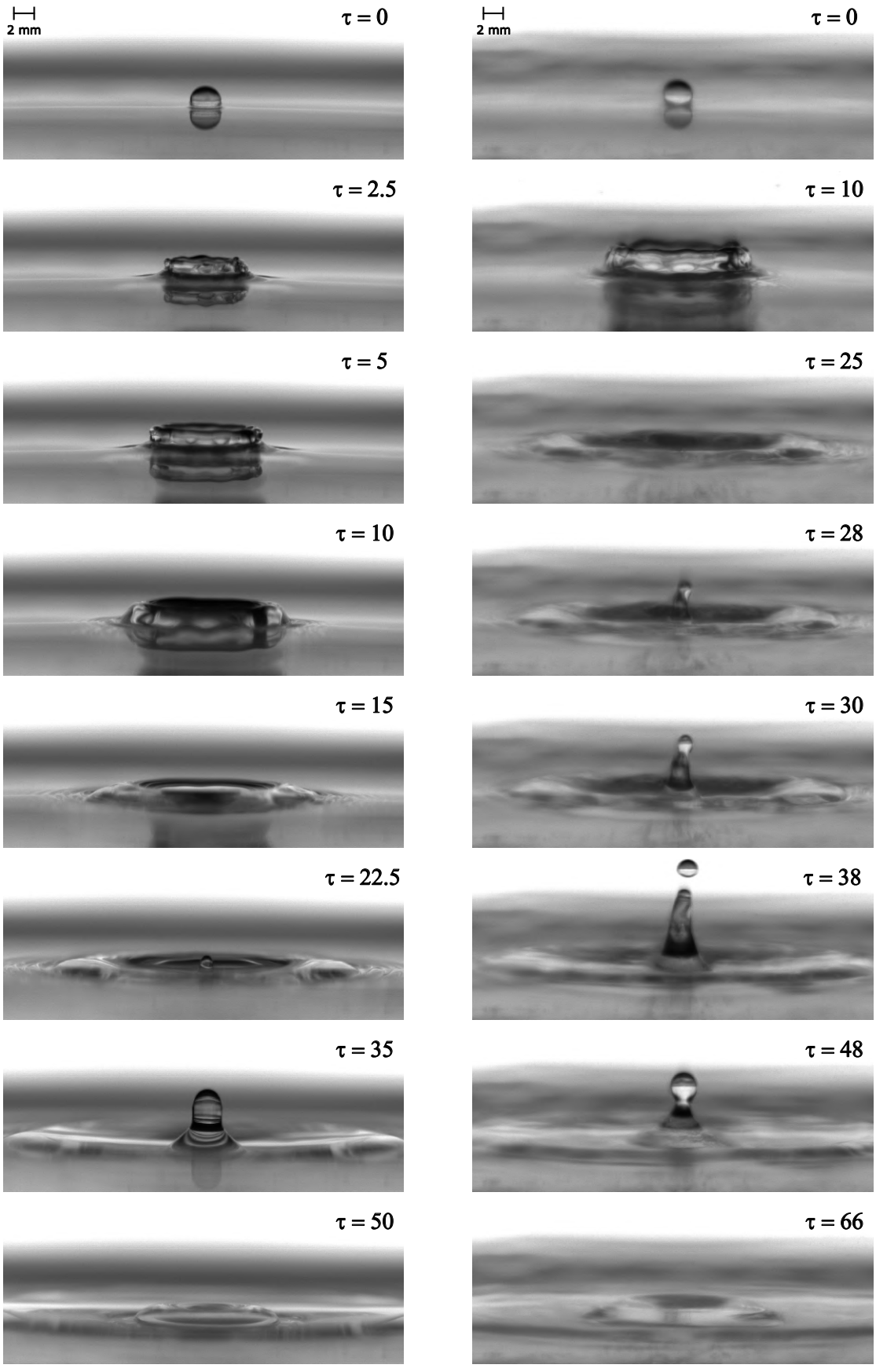

(a) (b)

Figure 4.7: Impact of a single droplet onto a heated liquid film: (a) Spreading outcome for N-Decane ($\theta = 0,\ d_{drop} = 2.7\ mm,\ h^* = 1,\ v_{drop} = 1.8\ m/s$); (b) Jetting outcome for N-Heptane ($\theta = 0.6,\ d_{drop} = 2.7\ mm,\ h^* = 1,\ v_{drop} = 1.7\ m/s$).

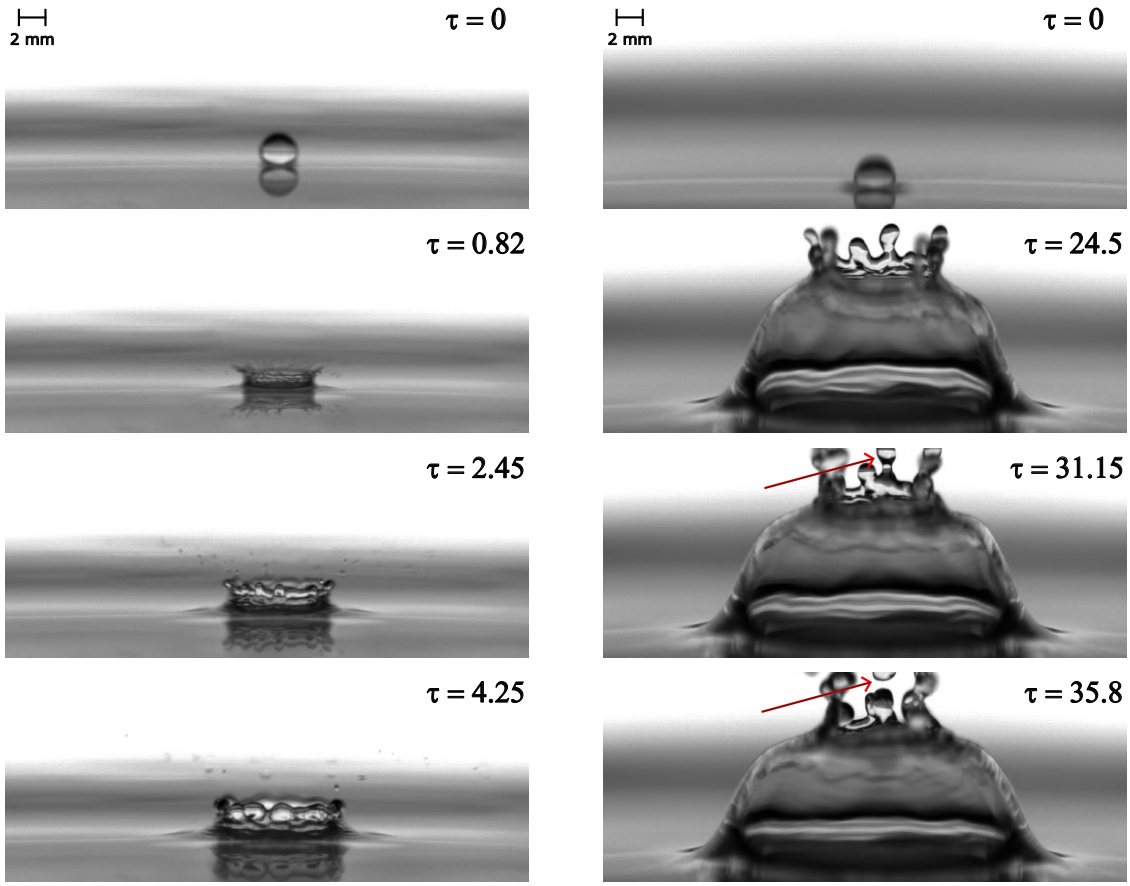

(a) (b)

Figure 4.8: Impact of a single droplet onto a heated liquid film: (a) Prompt splash for N-Heptane ($\theta = 0.6,\ d_{drop} = 2.6\ mm,\ h^* = 1, v_{drop} = 1.7\ m/s$); (b) Delayed splash for N-Heptane ($\theta = 0,\ d_{drop} = 2.6\ mm,\ h^* = 1, v_{drop} = 4.9\ m/s$).

Regarding jetting, as represented in figure 4.7b, this is present during all the tests. This vertical extension of the fluid (central jet) emerges from the centre of the impact site after the collapse of the crown, and in some cases while growing or receding ends up breaking into secondary droplets. At $\tau = 10$, a smooth crown is displayed. When it collapses ($\tau = 25$), a central jet starts to emerge ($\tau = 28$), and this jet continues to grow, eventually breaking and ejecting a secondary droplet ($\tau = 38$). This droplet continues the upward motion and then falls by gravity forces.

In figure 4.8a, it is possible to see prompt splash, where the kinetic energy of the droplet is enough to cause the ejection of droplets in the moment of impact while the crown is still growing/advancing. The phenomenon has a duration of approximately $\tau \approx 2.45$, and, after this moment, no more secondary droplets are ejected, and the crown keeps advancing. This type of phenomenon is hard to observe, due to its short duration and also due to the reduced dimensions of some ejected droplets. The example selected is one where the sheer amount of secondary droplets ejected facilitates the detection of prompt splash.

In figure 4.8b, it is possible to observe delayed splash. This phenomenon occurs after the

stage of maximum expansion, $\tau = 24.5$, of the crown liquid sheet, and it is really common in the impact with liquid films, especially for fluids with a high viscosity. Although, in this study, it had a reduced occurrence due to the range of impact conditions tested, but more importantly due to the low viscosity of the fluids used. Finger-like structures form, and due to instabilities, these break into secondary droplets, as indicated by the red arrow at $\tau = 35.8$.

The last phenomenon is bubble encapsulation. As explained previously, in section 2.2, the bubble encapsulation phenomenon is only observed in specific sets of impact conditions. Analysing figure 4.9, it is possible to see that compared with the previous phenomena, this is the most perdurable in time. From the moment at $\tau = 0$ until the total disintegration of the subsidiary formed bubble, the phenomenon has a duration of $\tau \approx 284$ for the example presented. After the impact of the droplet, it is possible to see the crown rising rapidly, followed by prompt splash at $\tau = 2.25$. The crown reaches maximum height, ejecting secondary droplets from the outer rim, at $\tau = 7.5$. Around $\tau = 12$, the jets of the crown unite at the top, closing the crown and forming a dome of liquid while encapsulating an air bubble inside. When the jets of the crown collide, they form two jets in the bubble, one upwards and the other downwards, $\tau = 22.5$. This jet starts receding due to the gravity forces, resulting in the bubble being compressed, $\tau = 90$. As soon as the fluid that composes the jet drains, the bubble starts to expand, $\tau = 210$. After this point, the liquid that constitutes the bubble continues to flow down until the bubble achieves a critical thickness, $\tau = 275.25$. When this point is reached, the bubble bursts, leading to a large ejection of secondary droplets with reduced dimensions.

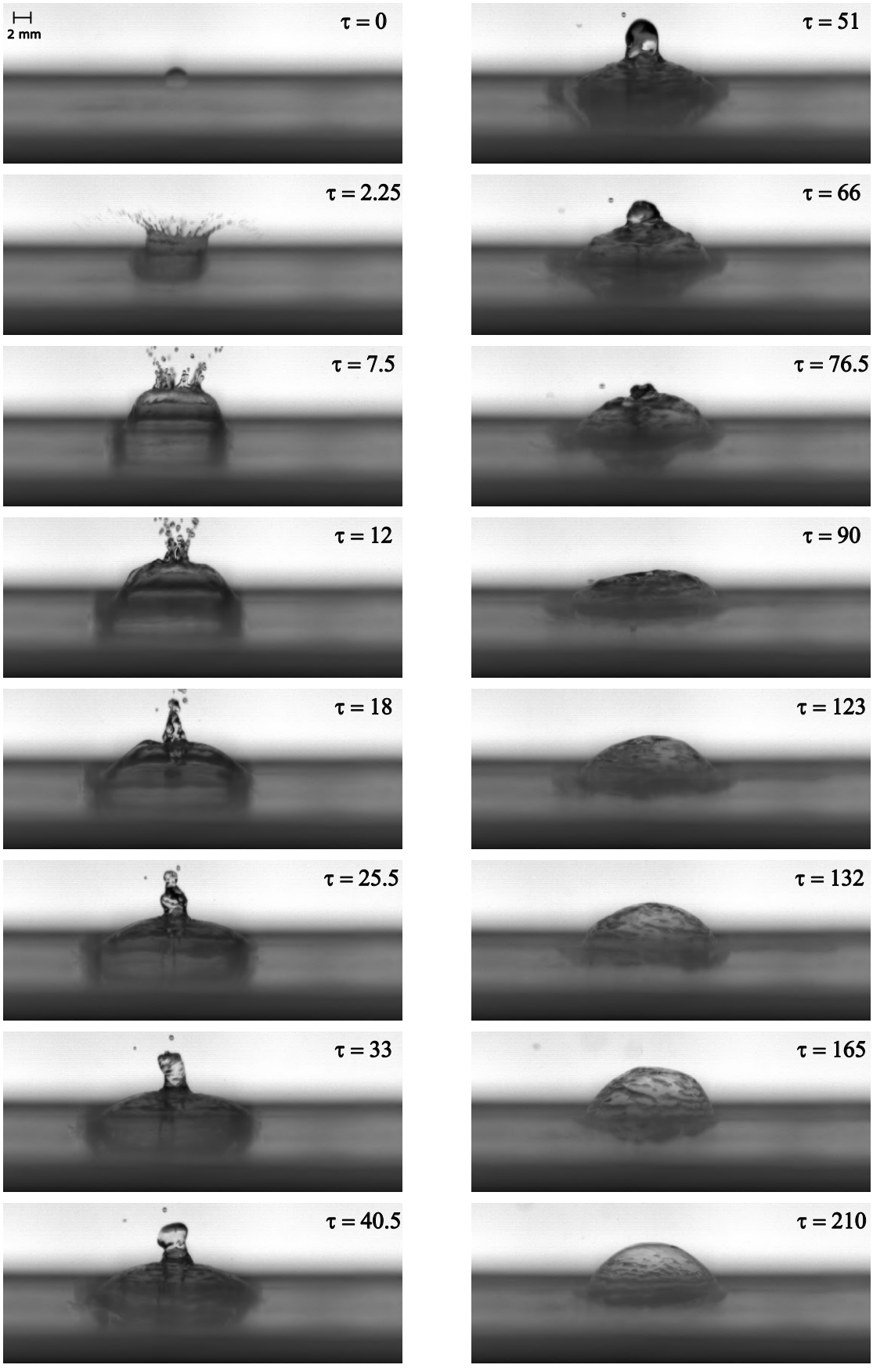
2 mm
τ = 0
τ = 2.25
τ = 7.5
τ = 12
τ = 18
τ = 25.5
τ = 33
τ = 40.5
τ = 51
τ = 66
τ = 76.5
τ = 90
τ = 123
τ = 132
τ = 165
τ = 210

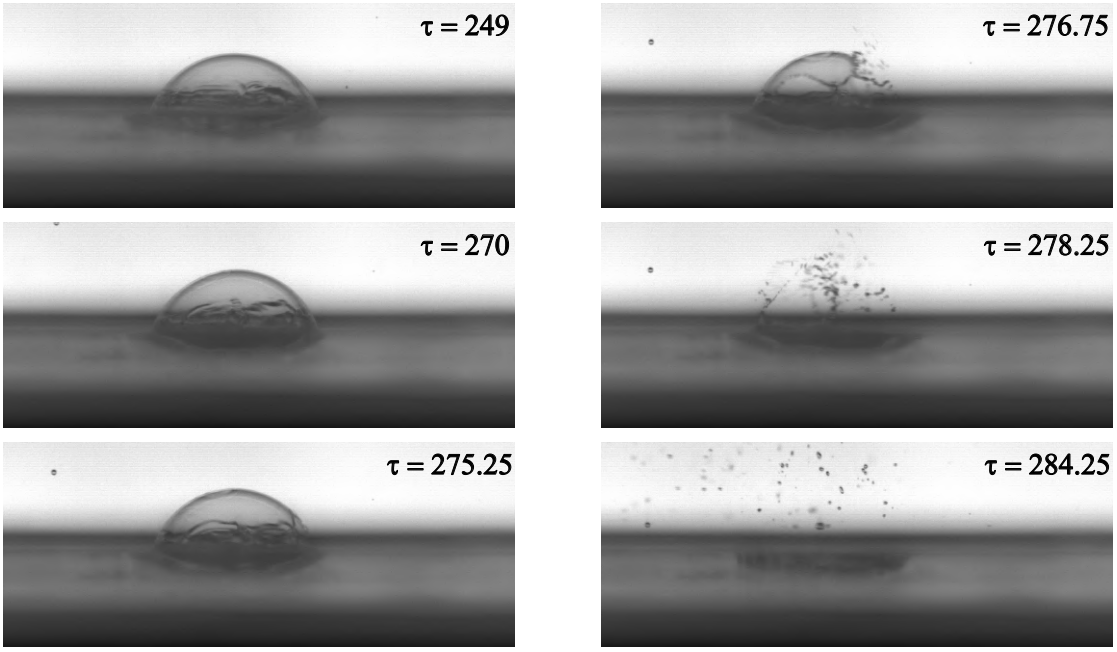

Figure 4.9: Image sequence of prompt and delayed splash followed by bubble encapsulation for N-Heptane ($\theta = 0.6,\ d_{drop} = 2.6\,mm,\ h^* = 1,\ y = 1000\,mm$).

4.4 Experimental Results

Since the objective of this work is to investigate and evaluate the application and validity of the current thresholds created for isothermal conditions, the occurrence of splash and bubble encapsulation will be presented with the corresponding probabilities of encountering the phenomenon.

4.4.1 Splash

As explained in both section 2.2 and 2.5, the phenomenon of splash is characterised by a separation of fluid from the immediate impact site.

As summarized in table 2.2, over the years, different spread/splash thresholds have been presented either for dry or wetted surfaces. These different criteria can be either to determine the existence of prompt splash [19, 50, 51, 52, 53, 54], or can be used just to determine the existence of delayed splash [55]. According to Ribeiro et al. [78], from all the criteria tested, the one presented by Vander Wal et al. [50] is the most universal inside and outside its validation regime for wetted thin films and for the conditions experimented by the authors. For this reason, this criterion was selected in order to analyse and verify its application on heated films.

The following experiments were carried out with a non-dimensional thickness of $h^* = 1$, a room temperature of $T_0 = 20°\mathrm{C}$ and relative humidity of 50%. The impact velocities in use were extrapolated based on the Vander Wal et al. [50] correlation (Eq.(4.2)), in order to

obtain the most possible similar conditions for both fluids.

$$K_c = Oh\, Re^{1.17} = 63 \quad (4.2)$$

Table 4.5 shows the probability of occurring splash for four different heights, with the corresponding impact velocity. For each height and each fluid, a minimum sample of ten impacts was made, as explained previously in section 3.3. In these tests, the objective was to obtain the point of transition between not having splash and having it at a given temperature and/or impact velocity.

Table 4.5: Splash probabilities of occurrence (percentage).

Impact Height $[mm]$		$y = 100$	$y = 130$	$y = 150$	$y = 190$
Fluid	v_{drop} $[m/s]$ / θ	**1.3**	**1.5**	**1.6**	**1.7**
C_7H_{16} **(N-Heptane)**	**0**	0	0	90	100
	0.2	0	0	10	100
	0.4	0	20	67	100
	0.6	0	58	90	100
		—	**1.6**	**1.7**	**1.8**
$C_{10}H_{22}$ **(N-Decane)**	**0**	—	0	0	50
	0.2	—	0	0	36
	0.3	—	0	0	18
	0.4	—	0	17	90
	0.6	—	0	36	100

Figure 4.10 displays the results presented in table 4.5. This allows for an easier way to assess the effect of liquid film temperature on the probability of occurrence of the phenomenon of splash. By analysing table 4.5 and figure 4.10, it is possible to detect a clear effect of the temperature on the occurrence of splash, either by suppressing or enhancing it.

Starting by describing figure 4.10a, the N-Heptane did not have any occurrence of splash at its lowest impact velocity, $1.3\ m/s$. When v_{drop} increases to $1.5\ m/s$, at $\theta = 0.4$ it is observable the occurrence of splash, showing an increase compared with $\theta = [0, 0.4[$. This effect is even more perceptible when the temperature increases to $\theta = 0.6$, where the occurrence increases beyond double the value of the previous temperature. The following v_{drop}, $1.6\,m/s$, for the N-Heptane the results show a different tendency, as follows. At $\theta = 0$, the probability of occurrence was 90%. Although, when the temperature is increased to $\theta = 0.2$, the occurrence decreases drastically, indicating that this effect almost completely suppresses the phenomenon of splash. Once again, like in the previous impact velocities, for $\theta \geq 0.4$ it is observable an augmenting effect of the occurrence of the phenomenon. At $v_{drop} = 1.7\ m/s$, the occurrence of splash stays independent of the temperature.

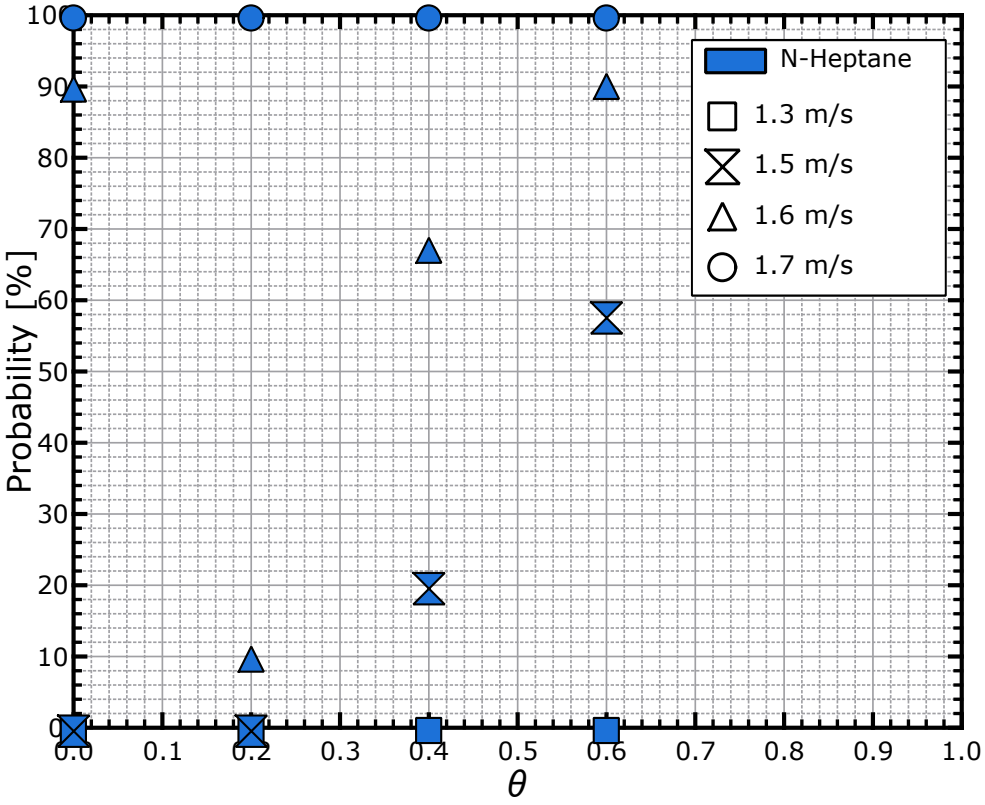

(a)

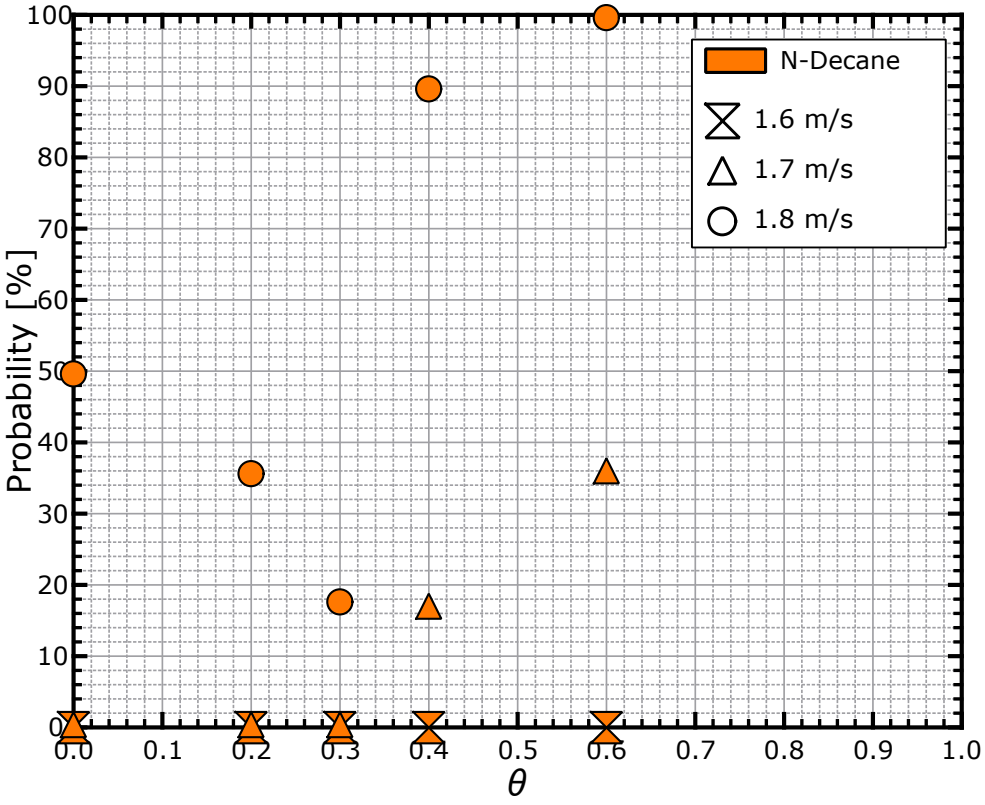

(b)

Figure 4.10: Splash occurrence probability, graphical representation: (a) N-Heptane; (b) N-Decane. The different symbols represent the distinct impact velocities.

Analysing the results of the N-Decane, figure 4.10b, similar to the N-Heptane, at its lowest impact velocity, $1.6\,m/s$, it was not possible to detect the occurrence of any splash. With the increase of v_{drop} to $1.7m/s$, the N-Decane does not create splash until it reaches $\theta = 0.4$. After this point, the occurrence of splash continues to increase with the temperature. At the highest impact velocity, $1.8m/s$, the N-Decane starts with a probability of occurrence of 50% for $\theta = 0$. Although, the same suppressing effect detected in the N-Heptane experiments is also present here. The jump between the occurrence at $\theta = 0.2$ and $\theta = 0.4$ is so drastic, that in a way to understand better what happened in that zone, an intermediate temperature was taken to assess if the occurrence would increase right after $\theta = 0.2$ or if still had a decreasing stage until reaching $\theta = 0.4$. This showed that after $\theta = 0.2$ the suppressing effect was still present, reducing even more the occurrence of splash. After reaching $\theta = 0.4$, the growing effect in the occurrence of the phenomenon is once again detected and the probability increases from 18% at $\theta = 0.3$ to $90 - 100\%$ in the interval of $\theta = [0.4; 0.6]$.

Table 4.6 and figure 4.11, allow an understanding of how the correlation proposed by Vander Wal et al. [50] fits this study. Since the Vander Wal et al. [50] correlation (Eq. 4.2), only accounts for the properties of the droplet, it does not change its result with the temperature.

Table 4.6: Critical K value, based on the correlation of Vander Wal et al. [50]. Highlighted in green are the cases where $K_c > 63$.

$v_{drop}\ [m/s]$ / **Fluid**	**1.3**	**1.5**	**1.6**	**1.7**
C_7H_{16} **(N-Heptane)**	52.9	62.6	67.5	72.4
	—	**1.6**	**1.7**	**1.8**
$C_{10}H_{22}$ **(N-Decane)**	—	58	63.4	66.6

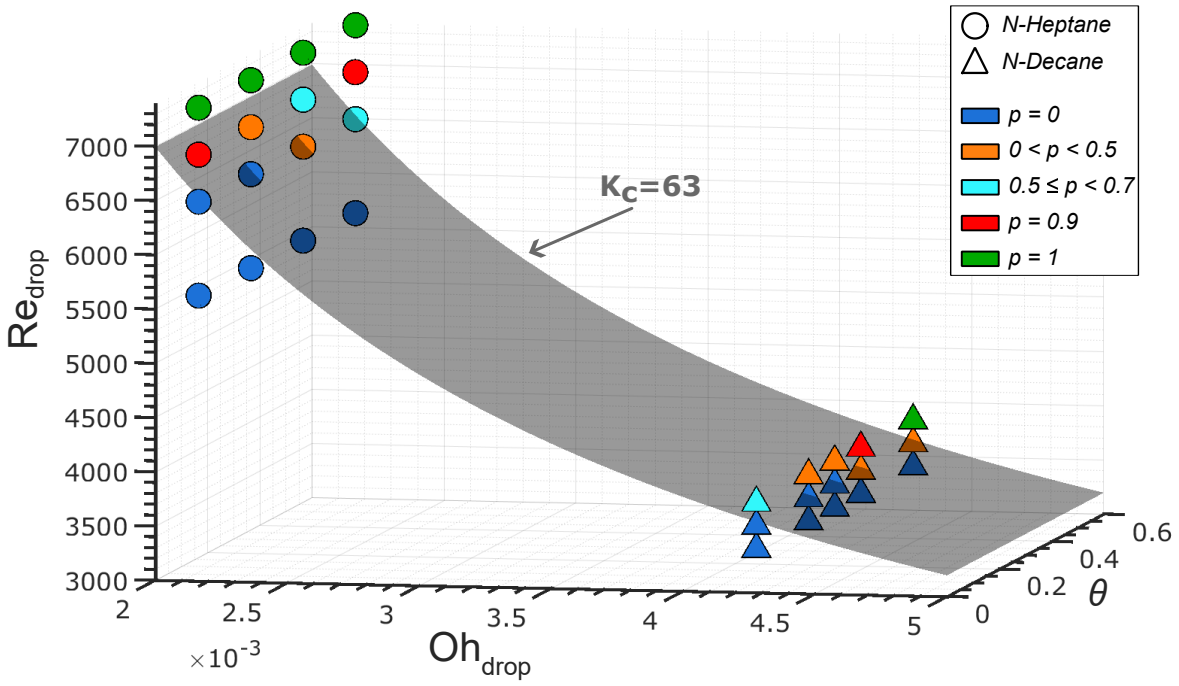

Figure 4.11: Splash events using the threshold proposed by Vander Wal et al. [50].

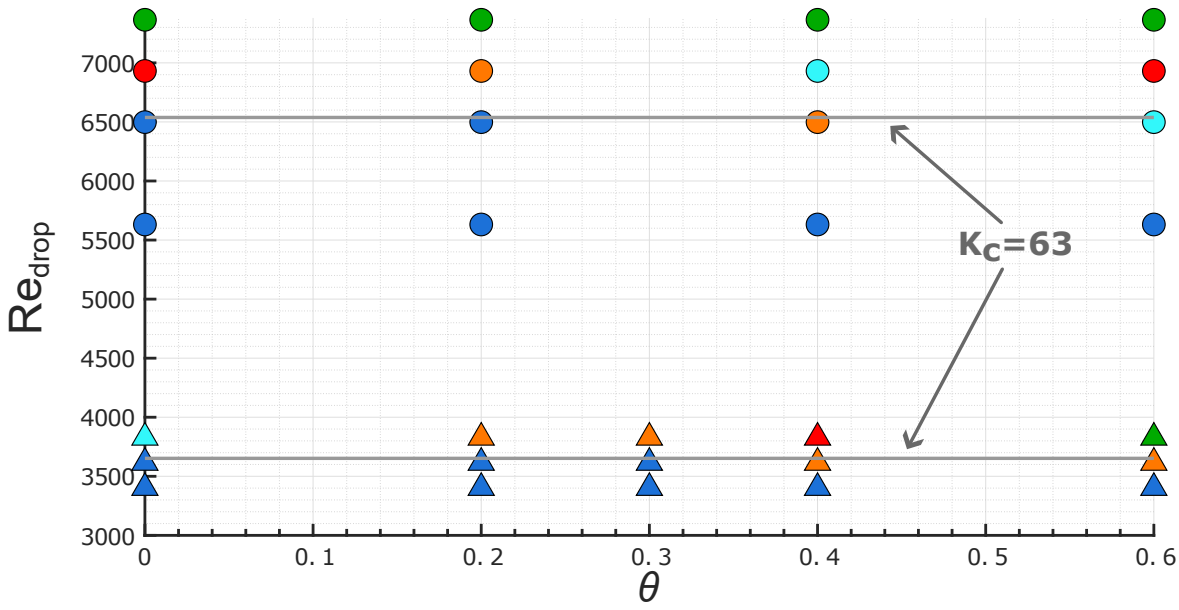

(a)

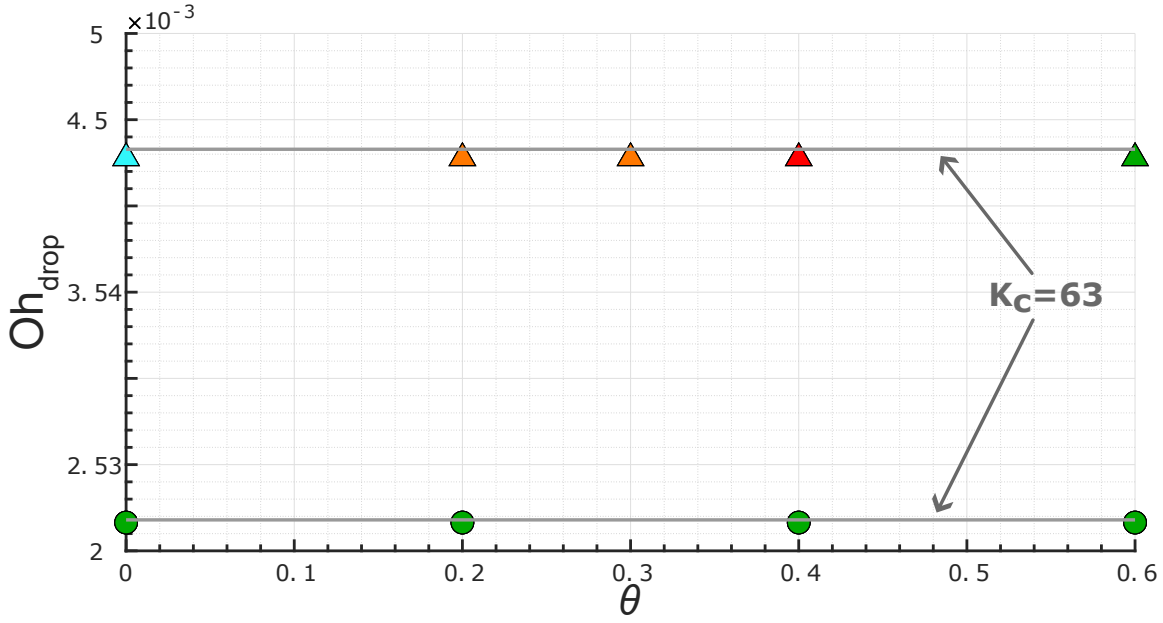

(b)

Figure 4.12: Decomposition of figure 4.11 in two graphs: (a) Re vs θ; (b) Oh vs θ

For this work, it was considered a minimum occurrence of at least 50% so that in the same conditions of Re, Oh and θ it should develop a splashing event, similar to the criterion proposed by Ribeiro et al. [62, 63] for bubble encapsulation. By analysing figure 4.11, it is possible to infer that the Vander Wal et al. [50] criterion still represents a somewhat good prediction for spread/splash. In figure 4.11, the blue symbols represent the events where no splash was detected, and as can be seen, all of these are below the threshold. The orange symbols represent events with an occurrence between $p =]0, 0.5[$, and these are located both above and below the threshold. Those that are located above the threshold represent the specific conditions where it was detected a suppressing effect with the temperature, $\theta =]0, 0.4[$. The cyan symbols show the events with an occurrence of $p = [0.5, 0.7[$, and only one of these events is below the threshold. This event corresponds to one of the conditions where the occurrence of splash increases with θ. The green and red symbols are all located above the threshold. These represent occurrences of 90% and 100%, respectively.

Although the correlation does not have into account the influence of the temperature of the liquid film, it can still predict the occurrence of splash with a certainty of 67% at or very near the transition, $K_c =]63, 68[$ table 4.6. Since the occurrence has a substantial decrease with temperature, $\theta =]0, 0.4[$, for applications near these θ, where having a significant splash occurrence is something desired, the Vander Wal et al. [50] correlation cannot predict the outcome correctly. In the account that in these θ, the correlation predicts the occurrence of splash, but in reality, the phenomenon is almost suppressed in such conditions.

4.4.1.1 Threshold Adaptation

As seen in 4.11 and table 4.6 the correlation proposed by Vander Wal et al. [50] can predict the occurrence of splash even in conditions where the liquid film is heated. Vander Wal et al. [50] do not specify a probability of occurrence of the phenomenon for the criterion proposed by them. Therefore, considering a probability of occurrence of at least 50%, similar to the criterion proposed by Ribeiro et al. [62, 63] for bubble encapsulation, it is possible to proceed to the following analysis. By analysing the results near the threshold limit, i.e., near the transition point, it is possible to see that the correlation can predict correctly $\approx 43\%$ phenomenon, confirming the results of 6 conditions out of a total of 14. Looking at the N-Decane case at $v_{drop} = 1.7\ m/s$, the critical K_c has a value of 63.4, making it practically coincident with the threshold transition point. It is possible that, since this condition is coincident with the transition point, it could be said that for the phenomenon of splash to occur it is necessary for the K_c to be a beyond the critical threshold. If we do not consider this condition in the calculations of the accuracy of the correlation, the final value increases to 6 out of 9 essays, i.e., an accuracy of $\approx 67\%$.

In order to try to adapt the correlation in a way to fit better to the experimental data, found between $\theta =]0, 0.4[$ near the transition point, two different adaptations were tested (Appendix A.3). The first uses the properties of the liquid film for the Ohnesorge number,Oh_{film}, such as implemented in the criterion proposed by Ribeiro et al. [62, 63]. The second uses the Oh_{film} and an adapted Reynolds number that combined both the properties of the droplet and the film. Unfortunately, both attempts fail to produce a suitable correlation. The first one caused the critical K_c to decrease with the temperature, which would align with the results from $\theta =]0\ ,\ 0.4[$, although it was too fast of a decrease to explain that interval and still leaving the results from $\theta \geq 0.4$ greatly below the threshold. The last one makes the critical K_c increase with the temperature, which for $\theta \geq 0.4$ matched with the observed, but it would ignore the effect of splash reduction/suppression for $\theta =]0\ ,\ 0.4[$.

This suppressing effect, experienced between $\theta =]0\,;\ 0.4[$, could be due to a very small vapour layer of fluid that may appear near the liquid film. This vapour layer would create a discontinuity between the surrounding air and the liquid film. Since the fluid present in this vapour layer would be the same as the one on the liquid film, but in a different state, recurring to the *Handbook of Aviation Fuel Properties* [76], it was observed that in the gas state, the viscosity of both these fluids would increase with temperature, therefore the vapour layer would have a much higher viscosity [34] when compared with the surrounding air, likely resulting in this suppressing effect. After passing the point of $\theta = 0.4$, the evaporation of the fluid would be much higher at a point that this layer could not be sustained.

In order to create a proper correlation or adaption of the Vander Wal et al. [50], a larger sample of tests would be necessary. It would be necessary to perform experiments with a spacing between θ smaller, i.e., increasing the non-dimensional temperature 0.1 at the time or even 0.05 in a way to achieve a more precise understanding of how the probability of occurrence

decreases and increases back. Adding to this, it would be necessary to enlarge the range of experiments, such as fluids and relative thickness, similar to the experiments of Vander Wal et al. [50].

4.4.2 Bubble Encapsulation

During these experiments, the non-dimensional thickness was kept at $h^* = 1$, the room temperature at $T_0 = 20°\mathrm{C}$ and the relative humidity in the air at 50%. To evaluate the liquid film temperature effect on the bubble encapsulation phenomenon, each fluid had a minimum sample of ten impacts for each chosen temperature, as explained previously in section 3.3. Table 4.7 shows the probabilities of occurrence of bubble encapsulation for the three different heights, with the corresponding impact velocities. The initial idea was to evaluate the superior and inferior thresholds, although that was not possible, as it will be explained later in section 4.4.2.1.

Table 4.7: Bubble Encapsulation probabilities of occurrence.

Impact Height $[mm]$		$y = 970$	$y = 1000$	$y = 2250$
Fluid	v_{drop} $[m/s]$ / θ	**3.7**	**3.9**	**4.9**
C_7H_{16} **(N-Heptane)**	**0**	0	0	50
	0.2	0	0	100
	0.4	0	0	100
	0.6	100	100	100
		3.8	**4.0**	**5.0**
$C_{10}H_{22}$ **(N-Decane)**	**0**	0	0	100
	0.2	0	0	100
	0.3	0	33	100
	0.4	0	58	100
	0.6	58	100	100

The threshold proposed by Ribeiro et al. [62, 63] (Eq. 4.3) has the novelty of using an Ohnesorge number with a characteristic length scale based on the liquid film thickness h, resulting on Oh_{film} presented in table 4.8. The correlation was created based on conditions where bubble encapsulation had a probability of occurrence of $p \geq 0.5$.

$$a = \frac{ln(34.5/Re_{drop})}{ln(Oh_{film})} \ , \ \forall\, a \in [1.022, 1.142] \quad (4.3)$$

In order to facilitate the analysis of the results, the data from table 4.7 are represented graphically in figure 4.13.

Analysing these two graphs (Fig. 4.13), it is clear that increasing the temperature of the liquid film influences the occurrence of bubble encapsulation. The N-Heptane shows an

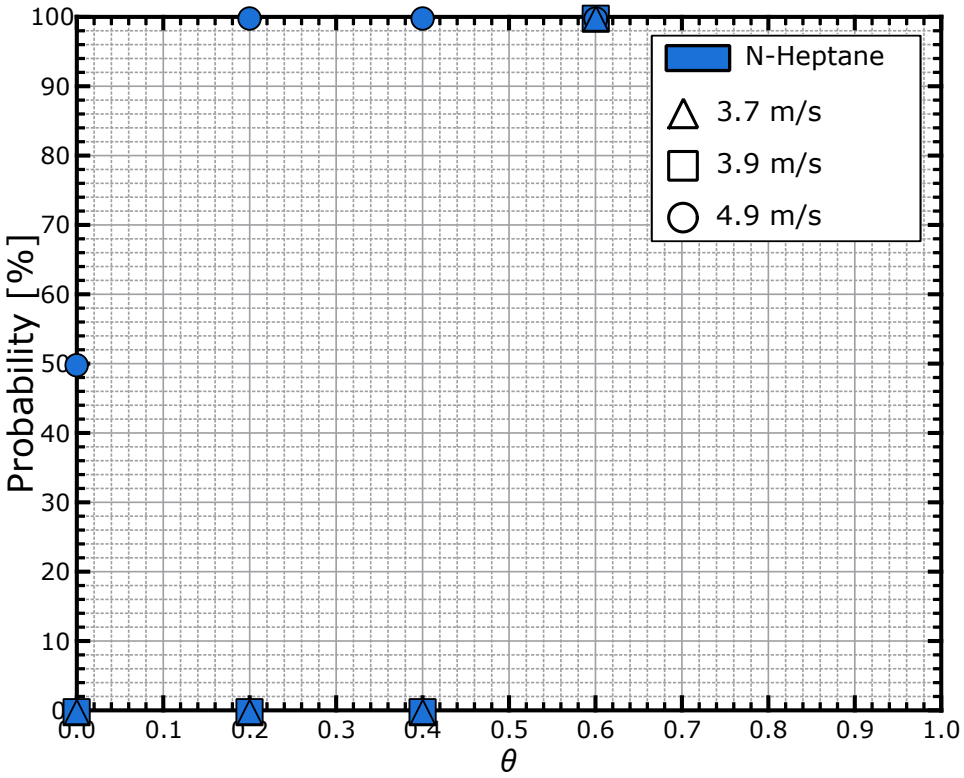

(a)

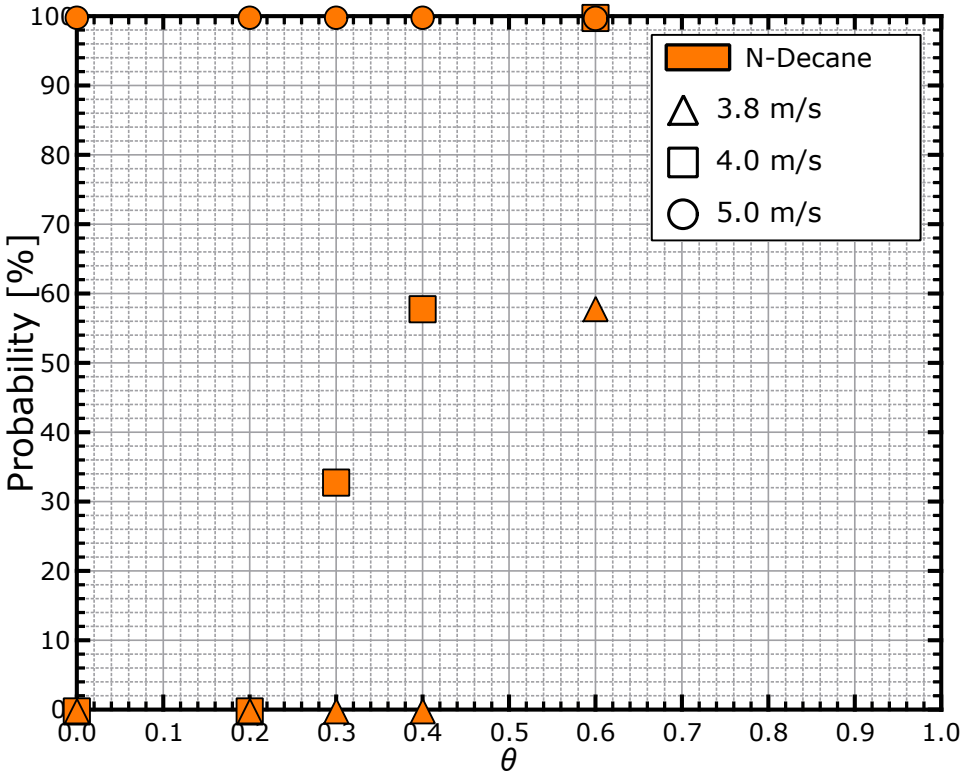

(b)

Figure 4.13: Bubble encapsulation occurrence probability, graphical representation: (a) N-Heptane; (b) N-Decane. The different symbols represent the distinct impact velocities.

abrupt increase for the first two impact velocities, $3.7\ m/s$ and $3.9\ m/s$, where for the range of $\theta = [0, 0.4]$ the probability of occurrence is 0% albeit, at $\theta = 0.6$ the occurrence value increases to 100%. The N-Decance shows results with a different tendency from the N-Heptane. The results corroborate the same increasing effect on the occurrence with the temperature, though, at a different rate. In the lowest impact velocity, $3.8\ m/s$, the phenomenon is absent between $\theta = [0; 0.4]$ however at $\theta = 0.6$ the probability increases to 58%. At $v_{drop} = 4.0\ m/s$, this augmenting effect is detected earlier at $\theta = [0.3, 0.6]$. In this interval, the occurrence goes from 33% to 100%. Once again, in the temperatures below the previous interval, i.e., between $\theta = [0, 0.3[$, the phenomenon of bubble encapsulation was not detected. Both the N-Decane and the N-Heptane show that for lower kinetic energies, at $\theta = 0$, the phenomenon was absent, although, increasing the temperature of the liquid film resulted in it appearing at $\theta = 0.6$. Both fluids present occurrences of 100%, in their highest impact velocity, with the only exception to this being the N-Heptane at $\theta = 0$. These results evidence an influence of the liquid film on the phenomenon of bubble encapsulation that will be further explained in section 4.4.2.1.

Table 4.8: Ohnesorge number of the liquid film and value of the parameter a. Highlighted in green are the a values inside the interval, $1.022 < a < 1.142$.

		$Oh_{film} \cdot 10^3$			a		
Impact Height $[mm]$		$y = 970$	$y = 1000$	$y = 2250$	$y = 970$	$y = 1000$	$y = 2250$
Fluid	v_{drop} $[m/s]$ / θ	**3.7**	**3.9**	**4.9**	**3.7**	**3.9**	**4.9**
C_7H_{16} **(N-Heptane)**	**0**	2.164			1.001	1.009	1.047
	0.2	1.928			0.982	0.991	1.027
	0.4	1.792			0.971	0.979	1.015
	0.6	1.637			0.957	0.966	1.001
		3.8	**4.0**	**5.0**	**3.8**	**4.0**	**5.0**
$C_{10}H_{22}$ **(N-Decane)**	**0**	4.277			1.000	1.010	1.051
	0.2	3.120			0.946	0.955	0.993
	0.3	2.659			0.920	0.929	0.966
	0.4	2.331			0.900	0.909	0.945
	0.6	1.993			0.878	0.886	0.922

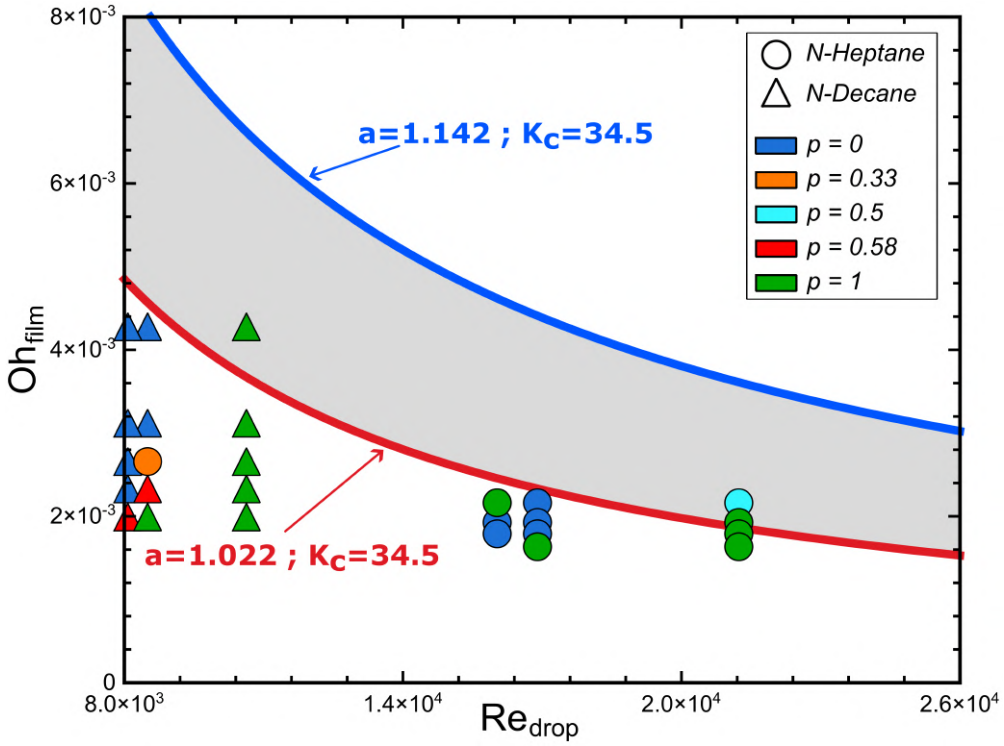

Figure 4.14: Bubble encapsulation events using the threshold proposed by Ribeiro et al. [62, 63].

The interval of the parameter a in correlation proposed by Ribeiro et al. [62, 63], was created through bubble encapsulation events with a probability of occurrence of at least 50%. Analysing table 4.8, it is possible to observe that only three situations would fit within the said interval. As figure 4.14 illustrates, most of the conditions with a probability of 50% or more are entirely off the interval, represented by the grey area. This shows that the criterion proposed by Ribeiro et al. [62, 63], suited for isothermal conditions, is unable to account for the liquid film temperature variation.

4.4.2.1 Threshold Adaptation

By analysing figure 4.14, it is possible to deduct that the current form of the correlation proposed by Ribeiro et al. [62, 63] does not fit the results for a heated liquid film. As explained previously, these results indicate that the temperature of the liquid film has a preponderant effect on the phenomenon of bubble encapsulation. The authors of the original criterion proposed it by adapting the Vander Wal et al. [50] correlation using the properties of the liquid film for the Ohnesorge number, instead of the droplet. Using a similar process of adaptation, based on the two reasons explained previously, it was used a Reynolds number but instead of using the properties of the droplet, this adapted Reynolds number would use a combination of their properties, $Re_{film,\,drop}$ (Eq. 4.4).

$$Re_{film,\,drop} = \frac{\rho_{film}\, v_{drop}\, d_{drop}}{\sigma_{film}} \quad (4.4)$$

The reasoning behind this adaptation was that the droplet volume is several orders of magnitude lower than the volume of the liquid film. Also, bubble encapsulation is an event with

a higher timescale than any event occurring at the beginning of drop impact, such as prompt splash. Therefore, physically, one expects a relatively short timescale for the heat up of the droplet material. Thus, it would be reasonable to use the thermal properties in the droplet Reynolds number at the same temperature as the liquid film. With this adaptation to the criterion, the parameter a (Eq. 4.5) and the adapted Reynolds number assume the values present in table 4.9. This hypothesis was already proposed by Mendes et al. [79], although here its validity is evaluated on a larger range of experiments.

$$a = \frac{ln(34.5/Re_{film,\,drop})}{ln(Oh_{film})}\ ,\ \forall\, a \in [1.022, 1.142] \quad (4.5)$$

Table 4.9: $Re_{film,\,drop}$ and value of the parameter a. Highlighted in green are the a values inside the interval, $1.022 < a < 1.142$.

		$Re_{film,drop}$			a		
Impact Height $[mm]$		$y = 970$	$y = 1000$	$y = 2250$	$y = 970$	$y = 1000$	$y = 2250$
Fluid	v_{drop} $[m/s]$ / θ	**3.7**	**3.9**	**4.9**	**3.7**	**3.9**	**4.9**
C_7H_{16} **(N-Heptane)**	**0**	16029	16895	21227	1.001	1.009	1.047
	0.2	18588	19592	24616	1.006	1.015	1.051
	0.4	20522	21631	27178	1.010	1.018	1.055
	0.6	23408	24674	31000	1.016	1.025	1.060
		3.8	**4.0**	**5.0**	**3.8**	**4.0**	**5.0**
$C_{10}H_{22}$ **(N-Decane)**	**0**	8081	8506	10633	1.000	1.010	1.051
	0.2	11069	12220	15275	1.008	1.017	1.056
	0.3	14084	14825	18532	1.014	1.022	1.060
	0.4	16445	17521	21901	1.019	1.028	1.065
	0.6	20597	21681	27101	1.028	1.036	1.072

With $Re_{film,\,drop}$ and Oh_{film}, it was possible to plot figure 4.15, corresponding to the adaptation of the correlation for impact onto a heated liquid film. Observing figure 4.15 and table

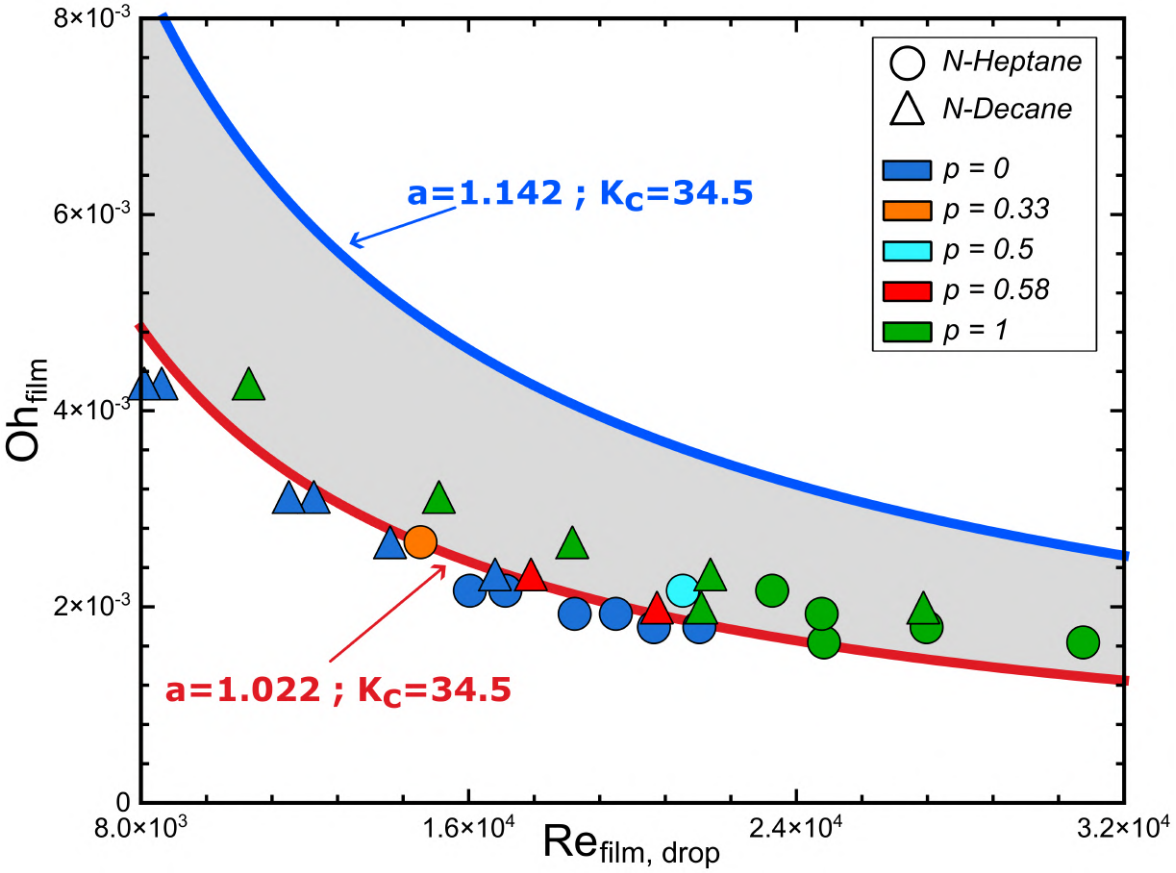

Figure 4.15: Bubble encapsulation events using the threshold adapted by from Ribeiro et al. [62, 63], Mendes et al. [79].

4.9, in combination with tables 4.7 and 4.8, it shows that every situation where the probability of occurrence of bubble encapsulation is above 50% the adaptation of the threshold resulted in all these points to be located inside the interval of the criterion. The results corroborated the hypothesis regarding the fast heating of the droplet material, and validate the adaptation of the criterion, previously developed, and the dominant role played by the liquid film in bubble encapsulation. The only result slightly outside the validation domain of the correlation is with the N-Decane at $\theta = 0.3$, where the probability of occurring bubble encapsulation 33%, lower than the predicted 50%. With the correlation adapted, it was intended to perform experiments near both thresholds. However, this was not possible since increasing the impact velocity would be required and that is not possible with the current experimental facility.

Although the proposed adaptation to the criterion developed by Ribeiro et al. [62, 63] showed to align with these experimental results, it still needs to be further studied in the future. Evaluate if the relative thickness of the liquid film influences this adaptation, and also experiment with a larger sample of fluid, similar to the original tests performed by Vander Wal et al. [50].

Chapter 5

Conclusions and Future Work

This last chapter of the thesis will be divided into two different sections. The first section concerns the conclusions achieved through this experimental study. The second section will address future work and improvements in the quality of work.

5.1 Conclusions

During the analysis the following phenomena were found, spread, prompt splash, delayed splash, jetting and bubble encapsulation. The last one was only observed for higher impact velocities, while the first one was only observed for lower ones. In order to analyse the effects of the temperature of the liquid film on the phenomena and consequently on the correlations, two were selected, spread/splash and bubble encapsulation. The correlation selected for bubble encapsulation was proposed by Ribeiro et al. [62]. This correlation was chosen for the reason that at the moment of writing this thesis, it is the only one of its type in the literature, as explained in section 2.7. Contrarily, in the current literature, exist numerous spread/splash criteria, although, for this work for comparison, the Vander Wal et al. [50] criterion was the one selected. The reason for this decision was due to a study elaborated by Ribeiro et al. [78], where the authors proved to be a universal correlation, as explained in section 4.4.1.

Firstly, the results obtained were fitted in the correlations. For the spread/splash threshold, it was possible to observe that if we consider a probability of occurrence of at least 50% for the condition to be above the threshold. Near the threshold, the correlation still can predict the existence of splash. Although the suppressing effect observed for $\theta =]0\,,\,0.4[$, cannot be predicted with this correlation. Beyond this interval, for $\theta \geq 0.4$, it was observed that the probability of occurrence would increase to the same value that was obtained at room temperature or even suppress it. In addition, it was found that the temperature also had an intensifying effect on the number of secondary droplets ejected. As explained in section 4.4.1.1, neither the attempts to adapt the Vander Wal et al. [50] correlation succeeded. A larger result sample would be necessary with refined temperature intervals in order to be able to achieve such adaptation or even propose a new criterion.

Regarding the bubble encapsulation results, it was found that the original threshold proposed by Ribeiro et al. [62] could not accommodate the results obtained while impacting a heated liquid film. It was observed that the temperature had a positive effect on the phenomenon, i.e., if the phenomenon was not present at lower temperatures, e.g. $\theta = 0$, it would have an

increase of its occurrence in higher temperatures, e.g. $\theta = 0.6$. This would indicate that the temperature of the liquid film had a preponderant effect on bubble encapsulation. Practically almost all the conditions that fulfilled the condition of having a probability of occurrence of 50% were outside the interval of the threshold. The authors that proposed this criterion had the innovativeness to adapt the spread/splash Vander Wal et al. [50] correlation by using the liquid film thickness characteristic length for the Ohnesorge number, instead of the droplet. Using a similar thought process and seeing that the phenomenon of bubble encapsulation is an event with a timescale much larger than any event occurring, it would be reasonable to use the thermal properties of the liquid film in the droplet Reynolds number, as explained before in section 4.4.2.1. With this adaptation to the correlation, all the conditions tested that fitted the condition of $p > 0.5$ were inside the threshold interval, having to report only one outline case (N-Decane at $v_{drop} = 4.0\, m/s$ and $\theta = 0.3$) where the probability of occurrence was 33% but was inside the interval.

5.2 Future Work

Throughout the development of this experimental work, several recommendations and suggestions for future works can be proposed.

Regarding the spread/splash criterion, it would be important to assess a larger sample of fluids and refine the temperature interval for experiments, i.e., perform tests incrementing the θ in intervals of 0.1 or even 0.05. This way, it would be possible to map the relevant interval $\theta =]0\,;\, 0.4[$, and create/adapt correlations that can predict this suppressing effect of splash observed. In relation to the bubble encapsulation correlation, it would also be necessary a wider range of experiments in order to corroborate the adaptation proposed and evaluate if the non-dimensional film thickness has an effect on the adaptation or if the results will align with the prediction of the correlation.

Both the splashing and bubble encapsulation phenomena, while impacting a heated liquid film, should be recorded recurring to an IR camera. This way, it would be possible to observe if the secondary droplets ejected are from the film or from the impinging droplet and to confirm the theory behind the adaptation of the bubble encapsulation correlation. With this type of imaging, it would be possible to determine the time that the droplet takes to achieve the same temperature of the liquid film and the constitution of the crown and bubble.

A work worth to explorer would be the comparison of these results with the equivalent, but with a heated impinging droplet and the liquid film in isothermal conditions with the ambient. Other works that can be developed are the measurements of crown diameter, bubble diameter and the number of secondary droplets ejected, the further study at higher temperatures to see how the intensity of the evaporation can also affect these phenomena. Of course, it would be beneficial for both analyses done here that in the future a study that could implement the use of multicomponent fuels, like the Jet-A1 and HVO, as was intended for this

work initially.

Regarding the improvement of the experimental work, a MATLAB algorithm that could adapt automatically the threshold for the binerization of the images, recurring to neural networks, would expedite the evolution of the work.

Bibliography

[1] I. Abrantes, A. F. Ferreira, A. Silva, and M. Costa, "Sustainable aviation fuels and imminent technologies-co2 emissions evolution towards 2050," *Journal of Cleaner Production*, vol. 313, p. 127937, 2021.

[2] C. M. Rodrigues, J. M. Barata, and A. R. Silva, "Liquid film dynamic on the spray impingement modeling," *Atomization and Sprays*, vol. 22, no. 9, 2012.

[3] P. Foltyn, D. Ribeiro, A. Silva, G. Lamanna, and B. Weigand, "Influence of wetting behavior on the morphology of droplet impacts onto dry smooth surfaces," *Physics of Fluids*, vol. 33, no. 6, p. 063305, 2021.

[4] ——, "Influence of wetting behavior on the morphology of droplet impacts onto dry-patterned micro-structured surfaces," *Physics of Fluids*, vol. 34, no. 12, p. 123322, 2022.

[5] A. R. Silva, C. M. Rodrigues, and J. M. Barata, "On the modeling of a spray impingement onto a hot surface," in *First Thermal and Fluids Engineering Summer Conference (TFESC), New York (NY) USA*, 2015, pp. 9–12.

[6] I. Ferrao, D. Ribeiro, J. M. Barata, and A. R. Silva, "Comparative study of droplet impact onto sloped surface versus a droplet impact onto a surface with a crossflow," in *AIAA Scitech 2019 Forum*, 2019, p. 0629.

[7] I. Ferrão, J. M. Barata, and A. Silva, "A study of a single droplet impinging onto a sloped surface: Jet-fuel and biofuel mixtures," in *ILASS 2019-29th European Conference on Liquid Atomization and Spray Systems*, 2019.

[8] I. Ferrão, D. Vasconcelos, D. Ribeiro, A. Silva, and J. Barata, "A study of droplet deformation: The effect of crossflow velocity on jet fuel and biofuel droplets impinging onto a dry smooth surface," *Fuel*, vol. 279, p. 118321, 2020.

[9] A. Silva and J. Barata, "On the modeling of a spray impinging on a surface," in *48th AIAA Aerospace Sciences Meeting Including the New Horizons Forum and Aerospace Exposition*, 2010, p. 215.

[10] C. M. Rodrigues, J. M. Barata, and A. R. Silva, "On the modelling of spray/wall impingement under crossflow conditions," in *21st AIAA Computational Fluid Dynamics Conference*, 2013, p. 2597.

[11] J. Barata and A. Silva, "Experimental study of spray dispersion and wall interaction," in *45th AIAA/ASME/SAE/ASEE Joint Propulsion Conference & Exhibit*, 2009, p. 5158.

[12] D. Ribeiro, N. Cunha, J. M. Barata, and A. Silva, "Dynamic behaviour of single droplets impinging upon liquid films with variable thickness: Jet a-1 and hvo mixtures," in *ICLASS 2018-14th International Conference on Liquid Atomization and Spray Systems 2020*. ILASS-Europe, Institute for Liquid Atomization and Spray Systems, 2018.

[13] C. Rodrigues, J. Barata, and A. Silva, "Modeling of evaporating sprays impinging onto solid surfaces," *Journal of Thermophysics and Heat Transfer*, vol. 31, no. 1, pp. 109–119, 2017.

[14] D. Vasconcelos, D. Ribeiro, J. M. Barata, and A. R. Silva, "Experimental and numerical study of single droplets impinging upon liquid films," in *ASTFE Digital Library*. Begel House Inc., 2019.

[15] R. Deegan, P. Brunet, and J. Eggers, "Complexities of splashing," *Nonlinearity*, vol. 21, no. 1, p. C1, 2007.

[16] C. Bai and A. Gosman, "Development of methodology for spray impingement simulation," *SAE transactions*, pp. 550–568, 1995.

[17] R. Rioboo, C. Tropea, and M. Marengo, "Outcomes from a drop impact on solid surfaces," *Atomization and sprays*, vol. 11, no. 2, 2001.

[18] R. L. Vander Wal, G. M. Berger, and S. D. Mozes, "Droplets splashing upon films of the same fluid of various depths," *Experiments in fluids*, vol. 40, no. 1, pp. 33–52, 2006.

[19] G. E. Cossali, A. Coghe, and M. Marengo, "The impact of a single drop on a wetted solid surface," *Experiments in fluids*, vol. 22, no. 6, pp. 463–472, 1997.

[20] G. Liang, Y. Guo, Y. Yang, N. Zhen, and S. Shen, "Spreading and splashing during a single drop impact on an inclined wetted surface," *Acta Mechanica*, vol. 224, no. 12, pp. 2993–3004, 2013.

[21] P. Foltyn, D. Ribeiro, A. Silva, G. Lamanna, and B. Weigand, "Effect of surface wettability on the droplet impact morphologies on dry smooth polycarbonate surfaces," in *International Conference on Liquid Atomization and Spray Systems (ICLASS)*, vol. 1, no. 1, 2021.

[22] G. Liang, Y. Yang, Y. Guo, N. Zhen, and S. Shen, "Rebound and spreading during a drop impact on wetted cylinders," *Experimental thermal and fluid science*, vol. 52, pp. 97–103, 2014.

[23] Z. Wang, C. Lopez, A. Hirsa, and N. Koratkar, "Impact dynamics and rebound of water droplets on superhydrophobic carbon nanotube arrays," *Applied physics letters*, vol. 91,

no. 2, p. 023105, 2007.

[24] G. Liang and I. Mudawar, "Review of mass and momentum interactions during drop impact on a liquid film," *International Journal of Heat and Mass Transfer*, vol. 101, pp. 577–599, 2016.

[25] B. Chen, R. Tian, and F. Mao, "Analysis of special phenomena of droplet impact on horizontal liquid film at low velocity," *Annals of Nuclear Energy*, vol. 136, p. 107038, 2020.

[26] G. Wang, E. Zheng, Y. Cui, Z. Shi, J. Xu, and F. Durst, "Central rebound jet of a droplet normal impact on a confined thin liquid film," *Physics of Fluids*, vol. 34, no. 11, p. 113304, 2022.

[27] K.-L. Pan, K.-R. Cheng, P.-C. Chou, and C.-H. Wang, "Collision dynamics of high-speed droplets upon layers of variable thickness," *Experiments in fluids*, vol. 45, no. 3, pp. 435–446, 2008.

[28] D. Ribeiro, M. O. Panão, J. M. Barata, and A. R. Silva, "Morphology of bubble formation on droplet impact upon thin liquid layers," in *AIAA Scitech 2020 Forum*, 2020, p. 1577.

[29] D. F. Ribeiro, M. R. Panão, J. M. Barata, and A. R. Silva, "Insights on bubble encapsulation after drop impact on thin liquid films," *International Journal of Multiphase Flow*, p. 104450, 2023.

[30] C. Tropea and M. Marengo, "The impact of drops on walls and films," *Multiphase Science and Technology*, vol. 11, no. 1, 1999.

[31] A. L. Yarin and D. A. Weiss, "Impact of drops on solid surfaces: self-similar capillary waves, and splashing as a new type of kinematic discontinuity," *Journal of fluid mechanics*, vol. 283, pp. 141–173, 1995.

[32] M. Trujillo and C.-F. Lee, "Modeling crown formation due to the splashing of a droplet," *Physics of Fluids*, vol. 13, no. 9, pp. 2503–2516, 2001.

[33] I. V. Roisman and C. Tropea, "Impact of a drop onto a wetted wall: description of crown formation and propagation," *Journal of Fluid Mechanics*, vol. 472, pp. 373–397, 2002.

[34] G. Liang, Y. Guo, and S. Shen, "Gas properties on crown behavior and drop coalescence," *Numerical Heat Transfer, Part B: Fundamentals*, vol. 65, no. 6, pp. 537–553, 2014.

[35] G. Liang, Y. Guo, Y. Yang, and S. Shen, "Liquid sheet behaviors during a drop impact on

wetted cylindrical surfaces," *International Communications in Heat and Mass Transfer*, vol. 54, pp. 67–74, 2014.

[36] G. Liang, Y. Guo, S. Shen, and Y. Yang, "Crown behavior and bubble entrainment during a drop impact on a liquid film," *Theoretical and Computational Fluid Dynamics*, vol. 28, no. 2, pp. 159–170, 2014.

[37] M. Rieber and A. Frohn, "A numerical study on the mechanism of splashing," *International Journal of Heat and Fluid Flow*, vol. 20, no. 5, pp. 455–461, 1999.

[38] G. Agbaglah and R. Deegan, "Growth and instability of the liquid rim in the crown splash regime," *Journal of fluid mechanics*, vol. 752, pp. 485–496, 2014.

[39] H. Wu, C. Liu, C. Cen, Y.-Y. Lee, and S.-L. Lin, "Study on dynamic characteristics of single droplet impact on heated liquid film," *Available at SSRN 4050276*, 2022.

[40] S. Mukherjee and J. Abraham, "Crown behavior in drop impact on wet walls," *Physics of fluids*, vol. 19, no. 5, p. 052103, 2007.

[41] G. Cossali, M. Marengo, A. Coghe, and S. Zhdanov, "The role of time in single drop splash on thin film," *Experiments in Fluids*, vol. 36, no. 6, pp. 888–900, 2004.

[42] A.-B. Wang and C.-C. Chen, "Splashing impact of a single drop onto very thin liquid films," *Physics of fluids*, vol. 12, no. 9, pp. 2155–2158, 2000.

[43] A. I. Fedorchenko and A.-B. Wang, "On some common features of drop impact on liquid surfaces," *Physics of Fluids*, vol. 16, no. 5, pp. 1349–1365, 2004.

[44] D. Ribeiro, J. M. Barata, and A. R. Silva, "The influence of liquid film thickness on crown development: Crown sheet angle," in *ASTFE Digital Library*. Begel House Inc., 2022.

[45] H. Fujimoto, T. Ogino, H. Takuda, and N. Hatta, "Collision of a droplet with a hemispherical static droplet on a solid," *International journal of multiphase flow*, vol. 27, no. 7, pp. 1227–1245, 2001.

[46] M. R. Panão and A. L. N. Moreira, "Flow characteristics of spray impingement in pfi injection systems," *Experiments in Fluids*, vol. 39, pp. 364–374, 2005.

[47] J. C. Bird, S. S. Tsai, and H. A. Stone, "Inclined to splash: triggering and inhibiting a splash with tangential velocity," *New Journal of Physics*, vol. 11, no. 6, p. 063017, 2009.

[48] R. Rioboo, C. Bauthier, J. Conti, M. Voue, and J. De Coninck, "Experimental investigation of splash and crown formation during single drop impact on wetted surfaces," *Experiments in fluids*, vol. 35, no. 6, pp. 648–652, 2003.

[49] S. Asadi and M. Passandideh-Fard, "A computational study on droplet impingement onto a thin liquid film," *Arabian Journal for Science and Engineering*, vol. 34, no. 2B, pp. 78–91, 2009.

[50] R. L. Vander Wal, G. M. Berger, and S. D. Mozes, "The splash/non-splash boundary upon a dry surface and thin fluid film," *Experiments in fluids*, vol. 40, no. 1, pp. 53–59, 2006.

[51] X. Gao and R. Li, "Impact of a single drop on a flowing liquid film," *Physical Review E*, vol. 92, no. 5, p. 053005, 2015.

[52] J. Zhu, C. Tu, T. Lu, Y. Luo, K. Zhang, and X. Chen, "Behavior of a water droplet impacting a thin water film," *Experiments in Fluids*, vol. 62, no. 7, pp. 1–13, 2021.

[53] C. Motzkus, F. Gensdarmes, and E. Géhin, "Study of the coalescence/splash threshold of droplet impact on liquid films and its relevance in assessing airborne particle release," *Journal of colloid and interface science*, vol. 362, no. 2, pp. 540–552, 2011.

[54] T. Okawa, T. Shiraishi, and T. Mori, "Production of secondary drops during the single water drop impact onto a plane water surface," *Experiments in fluids*, vol. 41, no. 6, pp. 965–974, 2006.

[55] A. Terzis, M. Kirsch, V. Vaikuntanathan, A. Geppert, G. Lamanna, and B. Weigand, "Splashing characteristics of diesel exhaust fluid (adblue) droplets impacting on urea-water solution films," *Experimental Thermal and Fluid Science*, vol. 102, pp. 152–162, 2019.

[56] C. Josserand and S. Zaleski, "Droplet splashing on a thin liquid film," *Physics of fluids*, vol. 15, no. 6, pp. 1650–1657, 2003.

[57] L. Zhang, J. Toole, K. Fezzaa, and R. Deegan, "Evolution of the ejecta sheet from the impact of a drop with a deep pool," *Journal of Fluid Mechanics*, vol. 690, pp. 5–15, 2012.

[58] O. G. Engel, "Crater depth in fluid impacts," *Journal of Applied Physics*, vol. 37, no. 4, pp. 1798–1808, 1966.

[59] C. Motzkus, F. Gensdarmes, and E. Géhin, "Parameter study of microdroplet formation by impact of millimetre-size droplets onto a liquid film," *Journal of aerosol science*, vol. 40, no. 8, pp. 680–692, 2009.

[60] A. Geppert, D. Chatzianagnostou, C. Meister, H. Gomaa, G. Lamanna, and B. Weigand, "Classification of impact morphology and splashing/deposition limit for

n-hexadecane," *Atomization and Sprays*, vol. 26, no. 10, 2016.

[61] D. Ribeiro, M. Panão, A. R. Silva, and J. M. Barata, "Insights on bubbling formation after drop impact on thin liquid films," in *ILASS 2019-29th European Conference on Liquid Atomization and Spray Systems*, 2019.

[62] D. Ribeiro, M. Panão, J. Barata, and A. Silva, "Analysis and visualization of the perturbations imposed on the liquid film by crown sheet collapse or closure," in *20th LISBON Laser Symposium 2022*. Elsevier, 2022.

[63] D. Ribeiro, A. Silva, and M. Panão, "Criterion for bubble encapsulation on drop impact onto a liquid film," *Physics of Fluids*, vol. 35, no. 3, p. 033305, 2023.

[64] P. M. M. Pinto, "Collision dynamics of a single droplet onto a heated dry surface: Jet fuel and hvo mixtures," Ph.D. dissertation, Universidade da Beira Interior (Portugal), 2021.

[65] D. Ribeiro, J. M. Barata, and A. Silva, "Experimental study of a single droplet impinging upon a heated dry surface using jet fuel and biofuel mixtures," in *ILASS–Europe 2022, 31st Conference on Liquid Atomization and Spray Systems*. ILASS-Europe, Institute for Liquid Atomization and Spray Systems.

[66] J. D. Naber and P. V. Farrell, "Hydrodynamics of droplet impingement on a heated surface," *SAE Transactions*, pp. 1346–1361, 1993.

[67] Y. Ko and S. Chung, "An experiment on the breakup of impinging droplets on a hot surface," *Experiments in fluids*, vol. 21, no. 2, pp. 118–123, 1996.

[68] L. Gangtao and M. Issam, "Review of drop impact on heat walls," *Int. J. Heat Mass Transfer*, vol. 106, pp. 103–126, 2017.

[69] J. D. Bernardin, C. J. Stebbins, and I. Mudawar, "Mapping of impact and heat transfer regimes of water drops impinging on a polished surface," *International journal of heat and mass transfer*, vol. 40, no. 2, pp. 247–267, 1997.

[70] M. Panão and A. Moreira, "Thermo-and fluid dynamics characterization of spray cooling with pulsed sprays," *Experimental Thermal and Fluid Science*, vol. 30, no. 2, pp. 79–96, 2005.

[71] D. Vasconcelos, A. Silva, and J. M. Barata, "Influence of vapour bubbles size and spacing on droplet impact outcomes under subcooled boiling regimes," in *ILASS–Europe 2022, 31st Conference on Liquid Atomization and Spray Systems*. ILASS-Europe, Institute for Liquid Atomization and Spray Systems.

[72] M. Lan, X. Wang, P. Zhu, and P. Chen, "Experimental study on the dynamic process of a water drop with additives impact upon hot liquid fuel surfaces," *Energy Procedia*, vol. 66, pp. 173–176, 2015.

[73] X. Fan, C. Wang, F. Guo, B. Chen, and M. Li, "Water droplet impact on high-temperature peanut oil surface: The effects of droplet diameter and oil temperature," *International Journal of Thermal Sciences*, vol. 159, p. 106601, 2021.

[74] D. Vasconcelos, A. Silva, and J. M. Barata, "Influence of dimensionless temperature on droplet impact onto heated liquid films for subcooled boiling regimes," in *ILASS–Europe 2022, 31st Conference on Liquid Atomization and Spray Systems*. ILASS-Europe, Institute for Liquid Atomization and Spray Systems.

[75] C. L. Yaws, *Chemical properties handbook*. McGraw-Hill Education, 1999.

[76] C. R. C. I. A. GA, *Handbook of Aviation Fuel Properties*. Society of Automotive Engineers, 1983.

[77] C. Tropea, A. L. Yarin, J. F. Foss *et al.*, *Springer handbook of experimental fluid mechanics*. Springer, 2007, vol. 1.

[78] D. F. Ribeiro, A. R. Silva, and M. R. Panão, "Insights into single droplet impact models upon liquid films using alternative fuels for aero-engines," *Applied Sciences*, vol. 10, no. 19, p. 6698, 2020.

[79] A. F. S. F. Mendes, D. A. Vasconcelos, D. F. S. Ribeiro, M. R. O. Panão, and A. R. R. Silva, "Does liquid film temperature affects single drop impact dynamics?" in *ASTFE Digital Library*. Begel House Inc., 2023.

Appendix A

Appendixs

A.1 Aluminium block technical drawing

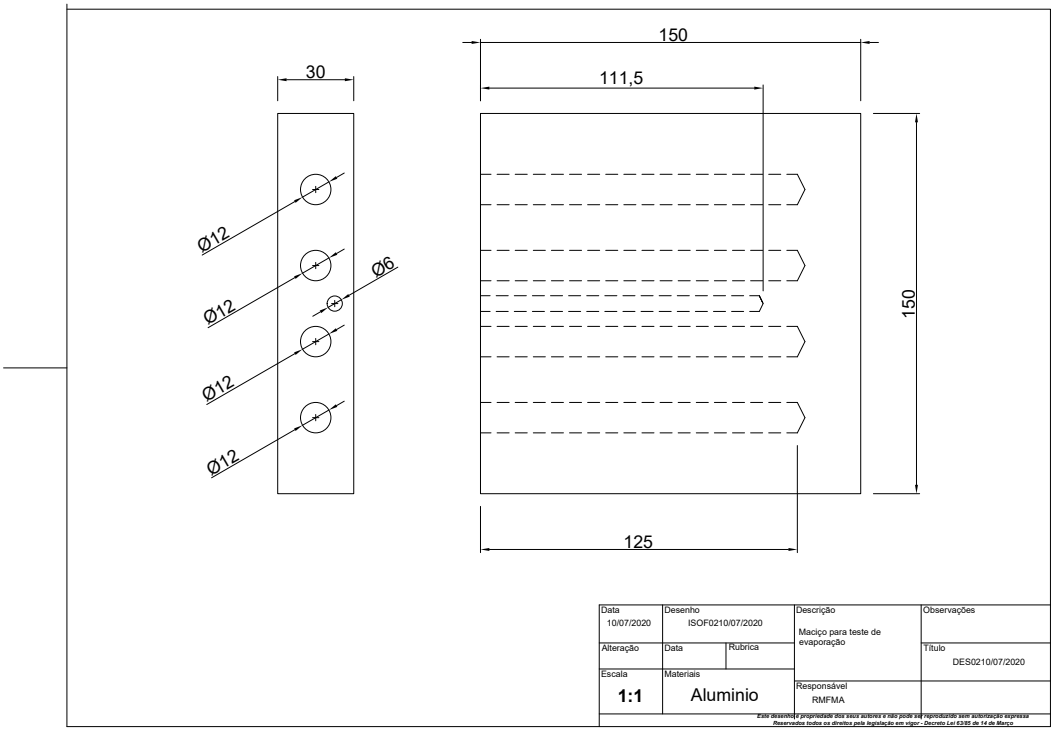

A.2 Fluids Thermophysical Properties

Table A.1: Variation of the thermophysical properties of the fluids [75] [T in K].

$\boldsymbol{\rho \cdot 10^3}$ $[\boldsymbol{kg/m^3}]$	C_7H_{16} (N-Heptane)	$0.23237 \cdot 0.26020^{-(1-T/540.26)^{0.27910}}$
	$C_{10}H_{22}$ (N-Decane)	$0.23276 \cdot 0.25240^{-(1-T/618.45)^{0.28572}}$
$\boldsymbol{\sigma \cdot 10^3}$ $[\boldsymbol{N/m}]$	C_7H_{16} (N-Heptane)	$53.640(1-T/540.26)^{1.2431}$
	$C_{10}H_{22}$ (N-Decane)	$55.777(1-T/618.45)^{1.3198}$
$\boldsymbol{\mu \cdot 10^3}$ $[\boldsymbol{Pa\ s}]$	C_7H_{16} (N-Heptane)	$10^{-5.7782+8.0587\times10^2/T+1.3355^{-2}\ T-1.4794\times10^{-5}\ T^2}$
	$C_{10}H_{22}$ (N-Decane)	$10^{-6.0716+1.0177\times10^3/T+1.2247^{-2}\ T-1.1892\times10^{-5}\ T^2}$

A.3 Splash Tests Results And Adaptations Of The Threshold Tables

mass recipiente fuels [g]	317.36
diameter recip. [cm]	12

h*	C7H16 **h [mm]**	C10H22 **h [mm]**
0.5	1.3	1.35
1	2.6	2.7

Kc igual ou superior ao threshold do VW (63) -

C7H16

d_drop [mm] 2.6
v_drop [m/s] 1.7 height [cm] 19

h*=1

T [°C]	T_film [°C]	θ	ρ [g/cm^3]	σ [mN/m]	μ [mPa s]	film mass [g]	total mass [g]	We	Re_drop	Oh_drop	Oh_film	Re_film,drop	V. Wall	V. Wall Oh film	V. Wall hot	Ocorrência
0			0.702293451	22.34645992	0.520245089	20.65115469	338.01	254.0250021	7364.615454	2.164154E-03	2.575477E-03	5966.682081	72.41920361	86.18332144	67.36978025	
10			0.694113351	21.31125867	0.46053632	20.41061633	337.77	254.0250021	7364.615454	2.164154E-03	2.348321E-03	6661.756908	72.41920361	78.58199509	69.8805536	
20			0.685799938	20.28580136	0.411594569	20.16615788	**337.53**	254.0250021	7364.615454	2.164154E-03	2.164154E-03	7364.615454	72.41920361	72.41920361	72.41920361	100.00%
30	29.55	0.121812	0.677727978	19.31585084	0.372474809	19.92879943	337.29	254.0250021	7364.615454	2.164154E-03	2.018950E-03	8042.309429	72.41920361	67.56024103	74.88953149	
37	36.51	0.210571	0.671759804	18.61501976	0.347666539	19.75330342	**337.11**	254.0250021	7364.615454	2.164154E-03	1.928135E-03	8540.305141	72.41920361	64.52129133	76.72931609	100.00%
40	39.52	0.249014	0.669151181	18.31305686	0.337737741	19.67659607	337.04	254.0250021	7364.615454	2.164154E-03	1.892127E-03	8757.233382	72.41920361	63.3163632	77.53890702	
50	48.78	0.367094	0.66104517	17.39168918	0.30987491	19.43823633	**336.80**	254.0250021	7364.615454	2.164154E-03	1.792311E-03	9429.029458	72.41920361	59.97619034	80.08287752	100.00%
60	57.93	0.483835	0.652884633	16.49004754	0.285626499	19.19827322	336.56	254.0250021	7364.615454	2.164154E-03	1.707193E-03	10103.22951	72.41920361	57.12789658	82.6991607	
70	66.62	0.594659	0.644993618	15.64293715	0.26507007	18.96623549	**336.33**	254.0250021	7364.615454	2.164154E-03	1.636580E-03	10755.16291	72.41920361	54.76495667	85.29607412	100.00%
80			0.632544626	14.35601786	0.237155864	18.60016906	335.96	254.0250021	7364.615454	2.164154E-03	1.543422E-03	11789.0707	72.41920361	51.64760661	89.56033571	
90			0.622981187	13.4085306	0.218663767	18.3189532	335.68	254.0250021	7364.615454	2.164154E-03	1.483755E-03	12592.74405	72.41920361	49.65096332	93.00427927	
95			0.618109428	12.93959786	0.210048164	18.17569763	335.54	254.0250021	7364.615454	2.164154E-03	1.456596E-03	13006.74863	72.41920361	4.874216E+01	94.82362994	

C10H22

d_drop [mm] 2.7
v_drop [m/s] 1.8 height [cm] 19

h*=1

T [°C]	T_film [°C]	θ	ρ [g/cm^3]	σ [mN/m]	μ [mPa s]	film mass [g]	total mass [g]	We	Re_drop	Oh_drop	Oh_film	Re_film,drop	V. Wall	V. Wall Oh film	V. Wall hot	Ocorrência
0			0.746637387	25.84658638	1.294752175	21.95510177	339.32	268.0765436	3827.739986	4.277470E-03	5.672158E-03	2802.588613	66.56249931	88.26549193	61.29044115	
10			0.739396498	24.86328754	1.08872396	21.74218119	339.10	268.0765436	3827.739986	4.277470E-03	4.886725E-03	3300.622667	66.56249931	76.04323244	63.94036406	
20		0	0.732072169	23.88932372	0.929496453	21.52680704	**338.89**	268.0765436	3827.739986	4.277470E-03	4.277470E-03	3827.739986	66.56249931	66.56249931	66.56249931	50%
30			0.724660179	22.9248892	0.804059381	21.30885521	338.67	268.0765436	3827.739986	4.277470E-03	3.796518E-03	4380.085044	66.56249931	59.07830983	69.17035352	
40	39.16	0.12457737	0.717789978	22.05000374	0.711156907	21.10683484	338.47	268.0765436	3827.739986	4.277470E-03	3.440175E-03	4905.329977	66.56249931	53.53319491	71.55868436	
50	49.19	0.18979194	0.710173989	21.10158688	0.627636071	20.88288435	**338.24**	268.0765436	3827.739986	4.277470E-03	3.120226E-03	5499.119232	66.56249931	48.55441386	74.18721077	36%
60	58.49	0.25026008	0.703020606	20.23132339	0.563302053	20.6725369	338.03	268.0765436	3827.739986	4.277470E-03	2.874506E-03	6065.449475	66.56249931	44.7307233	76.65014427	
70	68.19	0.313329	0.695460326	19.33319895	0.506644314	20.45022457	**337.81**	268.0765436	3827.739986	4.277470E-03	2.659091E-03	6671.222972	66.56249931	41.37860953	79.25992091	18%
80	76.97	0.37041612	0.688524964	18.52887278	0.462666695	20.24628809	337.61	268.0765436	3827.739986	4.277470E-03	2.492884E-03	7232.488015	66.56249931	38.79222162	81.67114528	
90	86.93	0.43517555	0.680545358	17.62659609	0.419496053	20.01164534	**337.37**	268.0765436	3827.739986	4.277470E-03	2.330951E-03	7884.342218	66.56249931	36.2723651	84.47901239	90%
110	104.25	0.54778934	0.666363126	16.08408452	0.357469979	19.59461245	336.95	268.0765436	3827.739986	4.277470E-03	2.101377E-03	9059.571375	66.56249931	32.69991948	89.60247231	
120	114.12	0.61196359	0.65809281	15.22063955	0.327822714	19.35142128	**336.71**	268.0765436	3827.739986	4.277470E-03	1.993412E-03	9756.282667	66.56249931	31.01985597	92.69575656	100%

C7H16

d_drop [mm] 2.6
v_drop [m/s] 1.6 height [cm] 15

h*=1

T [°C]	T_film [°C]	θ	ρ [g/cm^3]	σ [mN/m]	μ [mPa s]	film mass [g]	total mass [g]	We	Re_drop	Oh_drop	Oh_film	Re_film,drop	V. Wall	V. Wall Oh film	V. Wall hot	Ocorrência
0			0.702293451	22.34645992	0.520245089	20.65115469	338.01	225.01869	6931.40278	2.164154E-03	2.575477E-03	5615.700782	67.46039601	80.28203438	62.75672513	
10			0.694113351	21.31125867	0.46053632	20.41061633	337.77	225.01869	6931.40278	2.164154E-03	2.348321E-03	6269.888855	67.46039601	73.20119863	65.09557664	
20			0.685799938	20.28580136	0.411594569	20.16615788	**337.53**	225.01869	6931.40278	2.164154E-03	2.164154E-03	6931.40278	67.46039601	67.46039601	67.46039601	90.00%
30	29.55	0.121812	0.677727978	19.31585084	0.372474809	19.92879943	337.29	225.01869	6931.40278	2.164154E-03	2.018950E-03	7569.232404	67.46039601	62.93414436	69.76157151	
37	36.51	0.210571	0.671759804	18.61501976	0.347666539	19.75330342	**337.11**	225.01869	6931.40278	2.164154E-03	1.928135E-03	8037.934251	67.46039601	60.10328266	71.47537934	10.00%
40	39.52	0.249014	0.669151181	18.31305686	0.337737741	19.67659607	337.04	225.01869	6931.40278	2.164154E-03	1.892127E-03	8242.102006	67.46039601	58.98086036	72.22953462	
50	48.78	0.367094	0.66104517	17.39168918	0.30987491	19.43823633	**336.80**	225.01869	6931.40278	2.164154E-03	1.792311E-03	8874.380666	67.46039601	55.86940135	74.59931016	66.67%
60	57.93	0.483835	0.652884633	16.49004754	0.285626499	19.19827322	336.56	225.01869	6931.40278	2.164154E-03	1.707193E-03	9508.921889	67.46039601	53.21614067	77.03644686	
70	66.62	0.594659	0.644993618	15.64293715	0.26507007	18.96623549	**336.33**	225.01869	6931.40278	2.164154E-03	1.636580E-03	10122.50627	67.46039601	51.01499989	79.45554013	90.00%
80			0.632544626	14.35601786	0.237155864	18.60016906	335.96	225.01869	6931.40278	2.164154E-03	1.543422E-03	11095.59596	67.46039601	48.11110619	83.42781213	
90			0.622981187	13.4085306	0.218663767	18.3189532	335.68	225.01869	6931.40278	2.164154E-03	1.483755E-03	11851.9944	67.46039601	46.25118036	86.63593629	
95			0.618109428	12.93959786	0.210048164	18.17569763	335.54	225.01869	6931.40278	2.164154E-03	1.456596E-03	12241.64577	67.46039601	4.540460E+01	88.33070937	

C10H22

d_drop [mm] 2.7
v_drop [m/s] 1.7 height [cm] 15

h*=1

T [°C]	T_film [°C]	θ	ρ [g/cm^3]	σ [mN/m]	μ [mPa s]	film mass [g]	total mass [g]	We	Re_drop	Oh_drop	Oh_film	Re_film,drop	V. Wall	V. Wall Oh film	V. Wall hot	Ocorrência
0			0.746637387	25.84658638	1.294752175	21.95510177	339.32	239.11766	3615.087764	4.358953E-03	5.672158E-03	2646.889246	63.4426384	8.255575E+01	57.32567199	
10			0.739396498	24.86328754	1.08872396	21.74218119	339.10	239.11766	3615.087764	4.358953E-03	4.886725E-03	3117.254741	63.4426384	7.112413E+01	59.80417611	
20		0	0.732072169	23.88932372	0.929496453	21.52680704	**338.89**	239.11766	3615.087764	4.358953E-03	4.277470E-03	3615.087764	63.4426384	6.225669E+01	62.25669012	0%
30			0.724660179	22.9248892	0.804059381	21.30885521	338.67	239.11766	3615.087764	4.358953E-03	3.796518E-03	4136.746986	63.4426384	5.525664E+01	64.69584689	
40	39.16	0.12457737	0.717789978	22.05000374	0.711156907	21.10683484	338.47	239.11766	3615.087764	4.358953E-03	3.440175E-03	4632.811645	63.4426384	5.007023E+01	66.92968088	
50	49.19	0.18979194	0.710173989	21.10158688	0.627636071	20.88288435	**338.24**	239.11766	3615.087764	4.358953E-03	3.120226E-03	5193.612608	63.4426384	4.541352E+01	69.38817261	0%
60	58.49	0.25026008	0.703020606	20.23132339	0.563302053	20.6725369	338.03	239.11766	3615.087764	4.358953E-03	2.874506E-03	5728.48006	63.4426384	4.183717E+01	71.69178334	
70	68.19	0.313329	0.695460326	19.33319895	0.506644314	20.45022457	**337.81**	239.11766	3615.087764	4.358953E-03	2.659091E-03	6300.599473	63.4426384	3.870190E+01	74.1327382	0%
80	76.97	0.37041612	0.688524964	18.52887278	0.462666695	20.24628809	337.61	239.11766	3615.087764	4.358953E-03	2.492884E-03	6830.683125	63.4426384	3.628282E+01	76.38798477	
90	86.93	0.43517555	0.680545358	17.62659609	0.419496053	20.01164534	**337.37**	239.11766	3615.087764	4.358953E-03	2.330951E-03	7446.323206	63.4426384	3.392597E+01	79.01421597	17%
110	104.25	0.54778934	0.666363126	16.08408452	0.357469979	19.59461245	336.95	239.11766	3615.087764	4.358953E-03	2.101377E-03	8556.261854	63.4426384	3.058462E+01	83.80624842	
120	114.12	0.61196359	0.65809281	15.22063955	0.327822714	19.35142128	**336.71**	239.11766	3615.087764	4.358953E-03	1.993412E-03	9214.266963	63.4426384	2.901324E+01	86.69943363	36%

C7H16

d_drop [mm] 2.6
v_drop [m/s] 1.5 height [cm] 13

h*=1

T [°C]	T_film [°C]	θ	ρ [g/cm^3]	σ [mN/m]	μ [mPa s]	film mass [g]	total mass [g]	We	Re_drop	Oh_drop	Oh_film	Re_film,drop	V. Wall	V. Wall Oh film	V. Wall hot	Ocorrência
0			0.702293451	22.34645992	0.520245089	20.65115469	338.01	197.7703304	6498.190106	2.164154E-03	2.575477E-03	5264.719483	62.55402793	74.44315358	58.19245318	
10			0.694113351	21.31125867	0.46053632	20.41061633	337.77	197.7703304	6498.190106	2.164154E-03	2.348321E-03	5878.020801	62.55402793	67.87730423	60.36120094	
20			0.685799938	20.28580136	0.411594569	20.16615788	**337.53**	197.7703304	6498.190106	2.164154E-03	2.164154E-03	6498.190106	62.55402793	62.55402793	62.55402793	0.00%
30	29.55	0.121812	0.677727978	19.31585084	0.372474809	19.92879943	337.29	197.7703304	6498.190106	2.164154E-03	2.018950E-03	7096.155378	62.55402793	58.35696878	64.68783984	
37	36.51	0.210571	0.671759804	18.61501976	0.347666539	19.75330342	**337.11**	197.7703304	6498.190106	2.164154E-03	1.928135E-03	7535.56336	62.55402793	55.73199454	66.2770031	0.00%
40	39.52	0.249014	0.669151181	18.31305686	0.337737741	19.67659607	337.04	197.7703304	6498.190106	2.164154E-03	1.892127E-03	7726.970631	62.55402793	54.69120557	66.97630896	
50	48.78	0.367094	0.66104517	17.39168918	0.30987491	19.43823633	**336.80**	197.7703304	6498.190106	2.164154E-03	1.792311E-03	8319.731875	62.55402793	51.80604175	69.17373166	20.00%
60	57.93	0.483835	0.652884633	16.49004754	0.285626499	19.19827322	336.56	197.7703304	6498.190106	2.164154E-03	1.707193E-03	8914.61427	62.55402793	49.34575168	71.43361636	
70	66.62	0.594659	0.644993618	15.64293715	0.26507007	18.96623549	**336.33**	197.7703304	6498.190106	2.164154E-03	1.636580E-03	9489.849625	62.55402793	47.30469901	73.67676993	58.33%
80			0.632544626	14.35601786	0.237155864	18.60016906	335.96	197.7703304	6498.190106	2.164154E-03	1.543422E-03	10402.12121	62.55402793	44.61200435	77.36014015	
90			0.622981187	13.4085306	0.218663767	18.3189532	335.68	197.7703304	6498.190106	2.164154E-03	1.483755E-03	11111.24475	62.55402793	42.8873502	80.3349387	
95			0.618109428	12.93959786	0.210048164	18.17569763	335.54	197.7703304	6498.190106	2.164154E-03	1.456596E-03	11476.54291	62.55402793	4.210234E+01	81.9064516	

C10H22

d_drop [mm] 2.7
v_drop [m/s] 1.6 height [cm] 13

h*=1

T [°C]	T_film [°C]	θ	ρ [g/cm^3]	σ [mN/m]	μ [mPa s]	film mass [g]	total mass [g]	We	Re_drop	Oh_drop	Oh_film	Re_film,drop	V. Wall	V. Wall Oh film	V. Wall hot	Ocorrência
0			0.746637387	25.84658638	1.294752175	21.95510177	339.32	211.8135653	3402.435543	4.277470E-03	5.672158E-03	2491.189878	57.99374697	76.90286059	53.40037367	
10			0.739396498	24.86328754	1.08872396	21.74218119	339.10	211.8135653	3402.435543	4.277470E-03	4.886725E-03	2933.886815	57.99374697	66.25400227	55.70916556	
20		0	0.732072169	23.88932372	0.929496453	21.52680704	**338.89**	211.8135653	3402.435543	4.277470E-03	4.277470E-03	3402.435543	57.99374697	57.99374697	57.99374697	0%
30			0.724660179	22.9248892	0.804059381	21.30885521	338.67	211.8135653	3402.435543	4.277470E-03	3.796518E-03	3893.408928	57.99374697	51.47301539	60.26588576	
40	39.16	0.12457737	0.717789978	22.05000374	0.711156907	21.10683484	338.47	211.8135653	3402.435543	4.277470E-03	3.440175E-03	4360.293313	57.99374697	46.64173659	62.34676097	
50	49.19	0.18979194	0.710173989	21.10158688	0.627636071	20.88288435	**338.24**	211.8135653	3402.435543	4.277470E-03	3.120226E-03	4888.105984	57.99374697	42.30388613	64.63691079	0%
60	58.49	0.25026008	0.703020606	20.23132339	0.563302053	20.6725369	338.03	211.8135653	3402.435543	4.277470E-03	2.874506E-03	5391.510645	57.99374697	38.97242856	66.78278487	
70	68.19	0.313329	0.695460326	19.33319895	0.506644314	20.45022457	**337.81**	211.8135653	3402.435543	4.277470E-03	2.659091E-03	5929.975975	57.99374697	36.05184054	69.05659862	0%
80	76.97	0.37041612	0.688524964	18.52887278	0.462666695	20.24628809	337.61	211.8135653	3402.435543	4.277470E-03	2.492884E-03	6428.878235	57.99374697	33.79840463	71.15742022	
90	86.93	0.43517555	0.680545358	17.62659609	0.419496053	20.01164534	**337.37**	211.8135653	3402.435543	4.277470E-03	2.330951E-03	7008.304194	57.99374697	31.60293537	73.60382377	0%
110	104.25	0.54778934	0.666363126	16.08408452	0.357469979	19.59461245	336.95	211.8135653	3402.435543	4.277470E-03	2.101377E-03	8052.952333	57.99374697	28.49037936	78.06772824	
120	114.12	0.61196359	0.65809281	15.22063955	0.327822714	19.35142128	**336.71**	211.8135653	3402.435543	4.277470E-03	1.993412E-03	8672.25126	57.99374697	27.02659451	80.76280648	0%

C7H16

d_drop [mm]	2.6		
v_drop [m/s]	1.3	height [cm]	10

h*=1

T [°C]	T_film [°C]	θ	ρ [g/cm^3]	σ [mN/m]	μ [mPa s]	film mass [g]	total mass [g]	We	Re	Oh_drop	Oh_film	Re_film,drop	V. Wall	V. Wall Oh film	V. Wall hot	Ocorrência
0			0.702293451	22.34645992	0.520245089	20.65115469	338.01	148.5474926	5631.764759	2.164154E-03	2.575477E-03	4562.756886	52.91054424	62.96681288	49.22136065	
10			0.694113351	21.31125867	0.46053632	20.41061633	337.77	148.5474926	5631.764759	2.164154E-03	2.348321E-03	5094.284695	52.91054424	57.4131711	51.05576889	
20			0.685799938	20.28580136	0.411594569	20.16615788	**337.53**	148.5474926	5631.764759	2.164154E-03	2.164154E-03	5631.764759	52.91054424	52.91054424	52.91054424	0.00%
30	29.55	0.121812	0.677727978	19.31585084	0.372474809	19.92879943	337.29	148.5474926	5631.764759	2.164154E-03	2.018950E-03	6150.001328	52.91054424	49.36051412	54.71540243	
37	36.51	0.210571	0.671759804	18.61501976	0.347666539	19.75330342	**337.11**	148.5474926	5631.764759	2.164154E-03	1.928135E-03	6530.821579	52.91054424	47.1402124	56.05957635	0.00%
40	39.52	0.249014	0.669151181	18.31305686	0.337737741	19.67659607	337.04	148.5474926	5631.764759	2.164154E-03	1.892127E-03	6696.70788	52.91054424	46.25987404	56.65107549	
50	48.78	0.367094	0.66104517	17.39168918	0.30987491	19.43823633	**336.80**	148.5474926	5631.764759	2.164154E-03	1.792311E-03	7210.434291	52.91054424	43.8194942	58.50973807	0.00%
60	57.93	0.483835	0.652884633	16.49004754	0.285626499	19.19827322	336.56	148.5474926	5631.764759	2.164154E-03	1.707193E-03	7725.999034	52.91054424	41.73848854	60.42123336	
70	66.62	0.594659	0.644993618	15.64293715	0.26507007	18.96623549	**336.33**	148.5474926	5631.764759	2.164154E-03	1.636580E-03	8224.536342	52.91054424	40.01208959	62.31857683	7.14%
80			0.632544626	14.35601786	0.237155864	18.60016906	335.96	148.5474926	5631.764759	2.164154E-03	1.543422E-03	9015.171716	52.91054424	37.7345074	65.43410959	
90			0.622981187	13.4085306	0.218663767	18.3189532	335.68	148.5474926	5631.764759	2.164154E-03	1.483755E-03	9629.745448	52.91054424	36.2757302	67.95030583	
95			0.618109428	12.93959786	0.210048164	18.17569763	335.54	148.5474926	5631.764759	2.164154E-03	1.456596E-03	9946.337187	52.91054424	3.561174E+01	69.27955041	

A.4 Publications

ASTFE
American Society
of Thermal and Fluids Engineers

8th Thermal and Fluids Engineering Conference (TFEC)
May, 2023
Partially Online Virtual and at University of Maryland, MD

TFEC-2023-46327

DOES LIQUID FILM TEMPERATURE AFFECTS SINGLE DROP IMPACT DYNAMICS?

André F. S. F. Mendes,[1] Daniel A. Vasconcelos R.,[1] Daniela F. S. Ribeiro,[1] Miguel R. O. Panão,[2] André R. R. Silva[1,*]

[1]AEROG, LAETA, Aeronautics and Astronautics Research Center, University of Beira Interior, Calçada Fonte do Lameiro 6201-001 Covilhã, Portugal
[2]ADAI, LAETA, Associação para o Desenvolvimento da Aerodinâmica Industrial, University of Coimbra, 3030-788 Coimbra, Portugal

ABSTRACT

The effect of liquid film dynamics in the hydrodynamics of an isolated drop impact is a complex phenomenon and not fully understood. Therefore, in this work, an experimental setup built to characterize the impact of an isolated droplet on heated and unheated liquid films consists of a heating element made of an aluminum block with resistances to produce several impact conditions. The parametric studies include the drop impact velocity and size for different fluids to evaluate their properties effect on the phenomena. The results were compared with existing thresholds in the literature to evaluate their validity and applicability range. This comparison allows us to assess if temperature causes the limits of the thresholds to change drastically or if its influence is negligible. Regarding IC engines, thresholds like splashing and bubble encapsulation are significant since they influence the atomization of the mixture and, consequently, the pollutant emissions.

KEY WORDS: Droplet Impact, Heated Liquid Film, Bubble encapsulation

1. INTRODUCTION

The dynamics of a single droplet have been studied since Worthington (1908), the phenomena involved are complex and not completely understood. Drop and spray impact onto interposed surfaces is especially important regarding Internal Combustion (IC) engines since it affects the predicted atomization and mixture preparation, consequently, leading to higher emission of pollutant gases. In the case of a drop impacting a liquid film, this complexity includes dynamic hydrodynamic structures. For example, for high-impact kinetic energy, the droplet interacts with the liquid film and splashes, which means it forms a liquid crown with an unstable bounding rim, eventually leading to secondary atomization processes. Several authors classified splashing phenomenology as prompt splash and delayed splash (Liang and Mudawar, 2016, Vander Wal et al., 2006a), but when the drop impact occurs with a specific set of impact conditions, the crown can enfold and eventually encapsulate a bubble while remaining at the top of the liquid film.

Recently, Ribeiro et al. (2022) introduced thresholds for bubble encapsulation based on a previous spread/splash threshold from Vander Wal et al. (2006b), but the liquid droplet and film were in isothermal condition. Therefore, this work aims at analyzing how the temperature of the liquid affects the dynamics of this phenomenon and its thresholds.

*Corresponding André R. R. Silva: andre@ubi.pt

2. EXPERIMENTAL PROCEDURE

The experimental facility comprises five main sections: droplet dispensing system, image acquisition system, liquid film container, illumination of the impact site, and heating element. The droplet dispensing system comprises a medical syringe pump NE-1000 connected to a straight tip needle through a medical tube, and a second one to compensate for the amount of fluid evaporated during each test. A pumping rate of $0.3\,ml/min$ minimizes oscillations of the droplet before impact. A high-speed digital camera Photron FASTCAM mini UX50 acquired images using a macro lens Tokina AT-X M100 AF PRO D recording at $4000\ fps$ with a shutter speed of $125\ \mu s$. A transparent borosilicate glass container can withstand high temperatures without cracking. A constant liquid film thickness (h) is adjusted to the droplet diameter (D_d) depending on the dimensionless film thickness ($h^* = h/D_d$) defined for the experiments. A LED array connected to a DC power supply illuminates the impact site and a diffusive glass uniformizes the background lighting. Finally, an aluminum block with embedded cartridge heaters inside heats the liquid film.

The observation of bubble encapsulated was an unexpected finding while testing the implementation of bio-fuels in civil aviation (Ribeiro et al., 2019, 2020a,b). Following these works, adopting simpler carbon chain equivalents of fuels with well-defined thermophysical properties, the chosen fluids were heptane and decane (see table 1). In the experiments, the dimensionless film thickness was $h^* = 1$, and Table 1 also includes droplet's characteristics and corresponding Weber ($We = \rho\, U^2\, D_d/\sigma$) and Reynolds ($Re = \rho\, U\, D_d/\mu$).

Table 1 Fluid thermophysical properties at 20°C (Yaws, 1999).

Fluid	ρ	$\sigma \times 10^3$	$\mu \times 10^3$	D_d	U_d	We_d	Re_d
	$[\mathrm{kg/m^3}]$	$[\mathrm{N/m}]$	$[\mathrm{Pa \cdot s}]$	$[\mathrm{mm}]$	$[\mathrm{m/s}]$		
C_7H_{16} (Heptane)	685.8	20.3	0.41	2.6	3.9	1337	16895
$C_{10}H_{22}$ (Decane)	732.1	23.9	0.93	2.7	4.0	1323	8506

3. EXPERIMENTAL RESULTS

To evaluate the temperature's effect on the bubble encapsulation phenomenon, each fluid had a minimum sample of 10 drop impact tests for each chosen temperature. The liquid film temperature initiated at room temperature (20°C) and gradually increased up to 70°C for Heptane and 120°C for Decane. The novelty in the threshold presented by Ribeiro et al. (2022), Eq. (1), was the use of an Ohnesorge number with a characteristic length scale based on the liquid film thickness h, Oh_f, and the correlation includes the conditions where bubble encapsulation as a probability of occurrence of $p \geq 0.5$.

$$a = \frac{ln(34.5/\mathrm{Re}_d)}{ln(\mathrm{Oh}_f)}\ ,\ \forall\, a \in [1.022, 1.142] \tag{1}$$

This correlation considered experiments with a thermal equilibrium between the droplet and the liquid film, and it is reasonable to question if the thermal properties in the droplet Reynolds number should be at the initial value before the drop impact. However, the droplet volume is several orders of magnitude lower than the volume of the liquid film. Also, bubble encapsulation is an event with a higher timescale than any event occurring at the beginning of drop impact, such as prompt splash. Therefore, physically, one expects a relatively short timescale for the heat up of the droplet material. Thus, it would be reasonable to use the thermal properties in the droplet Reynolds number at the same temperature as the liquid film.

Table 2 includes the Ohnesorge, Reynolds, and the parameter a_f with the properties at the film temperature for the aforementioned reasons but also includes the value of parameter $a_{T_d(t=0)}$ where Re_d used the thermal properties at the initial temperature of the impinging drop ($T_0 = 20^\circ$C).

The results corroborated the hypothesis regarding the fast heating of the droplet material, and validate the

criterion previously developed and the dominant role played by the liquid film in bubble encapsulation. The only result slightly outside the validation domain of the correlation is with the Decane at 50°C, where the probability of occurring bubble encapsulation with 33%, lower than the predicted 50%.

Table 2 Fluids impact parameters and results of the tests. Highlighted in green are the a values inside the interval.

Fluid	T [°C]	$Oh_f \cdot 10^3$	Re_d	Occurrence	$a\,(T_d(0))$	$a\,(T_f)$
C_7H_{16} (Heptane)	20	2.164	16895	0%	1.009	1.009
	37	1.928	19592	0%	0.991	1.015
	50	1.792	21631	0%	0.979	1.018
	70	1.637	24674	100%	0.966	1.025
$C_{10}H_{22}$ (Decane)	20	4.277	8506	0%	1.010	1.010
	70	2.659	14825	33%	0.929	1.022
	90	2.331	17521	58%	0.909	1.028
	120	1.993	21681	100%	0.886	1.036

Fig. 1 shows the validation range setting the onset of bubble encapsulation and the results obtained in the experiments reported here.

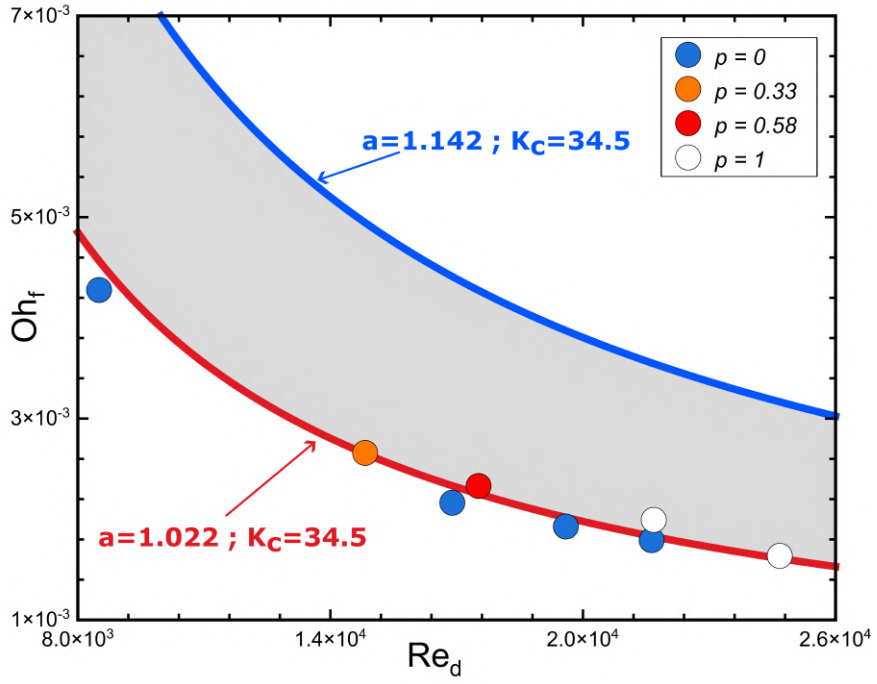

Fig. 1 Bubble encapsulation events using the threshold proposed in Ribeiro et al. (2022).

4. CONCLUSIONS

This work focused on the experimental study of the onset of bubble encapsulation and the validation of a threshold proposed by Ribeiro et al. (2022). Since previous work pointed to the dominant role of the liquid film, it did not allow to assess if this role extends to the value of the thermal properties used in the dimensionless numbers, especially the Reynolds associated with the droplet diameter as characteristic length. Experiments changing the liquid film temperature for two different fluids evidenced the dominant role of the liquid

film in the phenomenon of bubble encapsulation. Not only in terms of the characteristic length associated with the Ohnesorge number but also relative to the temperature considered in the thermal properties of both Ohnesorge and Reynolds. The physical explanation is related to the significantly lower volume of the droplet material compared to the volume of the liquid film, and the larger timescale of bubble encapsulation, leading to the short heat-up timescale of droplet material. In the conditions for bubble encapsulation, the droplet induces a relevant kinetic perturbation on the film, initiating the phenomenon, but its initial thermophysical properties before impact are not influential for predicting bubble encapsulation. Although to confirm this assessment, it is necessary to perform additional tests in the future, such as impinging a heated droplet on a non-heated liquid film.

ACKNOWLEDGMENTS

The present work was performed under the scope of Aeronautics and Astronautics Research Center (AEROG) of the Laboratório Associado em Energia, Transportes e Aeronáutica (LAETA) activities and it was supported by Fundação para a Ciência e a Tecnologia (FCT) through the project UIDB/BiOShot/ 50022 / 2022, by the Research scholarship with the reference BI 01.2022 Verão com Ciência AEROG and the Ph.D.s scholarships SFRH/BD/ 140009/ 2018 and SFRH/BD/ 143307/ 2019.

NOMENCLATURE

a	Parameter	(-)	LED	Light Emitting Diode	
$a\,(T_d)$	Parameter Using The Thermal		Oh_f	Liquid Film Ohnesorge Number	(-)
	Properties Of The Drop	(-)	p	Occurrence probability	(-)
$a_f, a\,(T_f)$	Parameter Using The Thermal		Re	Reynolds Number	(-)
	Properties Of The Film	(-)	Re_d	Droplet Reynolds Number	(-)
DC	Direct Current		T	Temperature	(°C)
D_d	Droplet Diameter	(mm)	t	Instant Time	(s)
fps	Frames Per Second		U_d	Droplet Impact Velocity	(m/s)
h	Film Thickness	(mm)	We	Weber Number	(-)
h^*	Non-dimensional Film Thickness	(-)	We_d	Droplet Weber Number	(-)
IC	Internal Combustion		μ	Viscosity	$(Pa\ s)$
K_c	Criterion between spread		ρ	Density	(kg/m^3)
	and splash	(-)	σ	Surface Tension	(N/m)

REFERENCES

Liang, G. and Mudawar, I., "Review of mass and momentum interactions during drop impact on a liquid film," *International Journal of Heat and Mass Transfer*, 101, pp. 577–599, (2016).

Ribeiro, D., Panão, M., Barata, J., and Silva, A., "Analysis and visualization of the perturbations imposed on the liquid film by crown sheet collapse or closure," *20th LISBON Laser Symposium 2022*, Elsevier, (2022).

Ribeiro, D., Panão, M., Silva, A. R., and Barata, J. M., "Insights on bubbling formation after drop impact on thin liquid films," *ILASS 2019-29th European Conference on Liquid Atomization and Spray Systems*, (2019).

Ribeiro, D., Panão, M. O., Barata, J. M., and Silva, A. R., "Morphology of bubble formation on droplet impact upon thin liquid layers," *AIAA Scitech 2020 Forum*, p. 1577, (2020).

Ribeiro, D. F., Silva, A. R., and Panão, M. R., "Insights into single droplet impact models upon liquid films using alternative fuels for aero-engines," *Applied Sciences*, 10(19), pp. 6698, (2020).

Vander Wal, R. L., Berger, G. M., and Mozes, S. D., "Droplets splashing upon films of the same fluid of various depths," *Experiments in fluids*, 40(1), pp. 33–52, (2006).

Vander Wal, R. L., Berger, G. M., and Mozes, S. D., "The splash/non-splash boundary upon a dry surface and thin fluid film," *Experiments in fluids*, 40(1), pp. 53–59, (2006).

Worthington, A. M., *A study of splashes*, Longmans, Green, and Company, (1908).

Yaws, C. L., *Chemical properties handbook*, McGraw-Hill Education, (1999).